การประเมินการใช้ไวร์ไลน์ฟอร์เมชั่นเทสเตอร์ในแหล่งกักเก็บที่มีชั้นหินบางแทรกอยู่

นางสาว วิริยา เกียรติผดุงกุล

EVALUATION OF WIRELINE FORMATION TESTERS IN THINLY LAMINATED
RESERVOIRS

Ms. Wiriya Kiatpadungkul

A Thesis Submitted in Partial Fulfillment of the Requirements

for the Degree of Master of Engineering Program in Petroleum Engineering

Department of Mining and Petroleum Engineering

Faculty of Engineering

Chulalongkorn University

Academic Year 2010

Thesis Title	EVALUATION OF WIRELINE FORMATION TESTERS IN THINLY LAMINATED RESERVOIRS
By	Ms. Wiriya Kiatpadungkul
Field of Study	Petroleum Engineering
Thesis Advisor	Assistant Professor Suwat Athichanagorn, Ph.D.
Thesis Co-Advisor	Saifon (Daungkaew) Sirimongkolkitti, Ph.D.

Accepted by the Faculty of Engineering, Chulalongkorn University in Partial Fulfillment of the Requirements for the Master's Degree

.... Dean of the Faculty of Engineering
(Associate Professor Boonsom Lerdhirunwong, Ph.D.)

THESIS COMMITTEE

.... Chairman
(Assistant Professor Sarithdej Pathanasethpong)

.... Thesis Advisor
(Assistant Professor Suwat Athichanagorn, Ph.D.)

.... Thesis Co-Advisor
(Saifon (Daungkaew) Sirimongkolkitti, Ph.D.)

.... Examiner
(Assistant Professor Jirawat Chewaroungroaj, Ph.D.)

.... External Examiner
(Witsarut Tungsunthomkhan, Ph.D.)

วิริยา เกียรติผดุงกุล : การประเมินการใช้ไวร์ไลน์ฟอร์เมชั่นเทสเตอร์ในแหล่งกักเก็บที่มีชั้นหินบางแทรก
อยู่. (EVALUATION OF WIRELINE FORMATION TESTERS IN THINLY LAMINATED
RESERVOIRS) อ.ที่ปรึกษาวิทยานิพนธ์หลัก: ผศ.ดร.สุวัฒน์ อธิชนากร, อ.ที่ปรึกษาวิทยานิพนธ์ร่วม
: ดร.สายฝน (ดวงแก้ว) สิริมังคลกิตติ 167 หน้า.

แหล่งกักเก็บมักมีลักษณะซับซ้อน ประกอบด้วยหินชนิดต่างกัน และมีความสามารถในการซึมผ่านใน
ทิศทางต่างๆไม่เท่ากัน ความสามารถในการซึมผ่านในแนวตั้งและแนวนอนที่แตกต่างกัน ณ จุดต่างๆนั้นมีผล
อย่างยิ่งต่อสมรรถภาพในการผลิตของแหล่งกักเก็บ เนื่องจากในช่วงแรกเริ่มของการผลิตนั้นความสามารถในการ
ซึมผ่านในแนวนอนจะมีผลต่อการออกแบบการผลิตของหลุมผลิต ในเวลาต่อมาความสามารถในการซึมผ่านใน
แนวตั้งจะมีผลต่อปริมาณน้ำหรือก๊าซที่ไม่ต้องการให้เกิดขึ้นจากการผลิต นอกจากนั้นความสามารถในการซึม
ผ่านในแนวตั้งยังมีผลต่อการผลิตของหลุมที่อยู่ในแนวนอนอีกด้วย นั่นจึงเป็นเหตุผลที่ทำให้มีการวัดแบบต่างๆ
เกิดขึ้นมากมายเพื่อใช้ในการหาค่าคุณสมบัติของแหล่งกักเก็บ อย่างไรก็ตามการวัดหาค่าคุณสมบัติแหล่งกักเก็บ
จากขนาดการวัดที่ไม่เท่ากัน ย่อมให้ผลลัพธ์ซึ่งคือค่าความสามารถในการซึมผ่านที่แตกต่างกัน

วิทยานิพนธ์ฉบับนี้ได้ทำการศึกษาเปรียบเทียบผลกระทบของชั้นหินบางที่แทรกอยู่ในแหล่งกักเก็บ
น้ำมันที่มีต่อการเปลี่ยนแปลงค่าความดันของแหล่งกักเก็บที่วัดได้จากไวร์ไลน์ฟอร์เมชั่นเทสเตอร์ชนิดซิงเกิลโพรบ
ชนิดดูอัลแพคเกอร์และจากการทดสอบหลุมแบบทั่วไป

โดยมีการกำหนดคุณสมบัติของชั้นหินบางที่แตกต่างกันออกไป เช่น รูปร่าง จำนวน และระยะทางจาก
ชั้นหินบางไปถึงหลุมผลิตแล้วทำการจำลองค่าความดันของแหล่งกักเก็บน้ำมันที่วัดได้การวัดที่ต่างกันทั้ง 3 ชนิด
โดยใช้โปรแกรมแบบจำลองการไหลจากนั้นใช้โปรแกรมวิเคราะห์การเปลี่ยนแปลงของค่าความดันในการหาค่า
ความสามารถในการซึมผ่านของแหล่งกักเก็บทั้งในแนวตั้งและแนวนอนพร้อมทั้งอัตราส่วนของค่าดังกล่าว
รวมทั้งค่ารัศมีในการวัดจากกราฟการเปลี่ยนแปลงของค่าความดัน

จากการศึกษาพบว่าผลกระทบจากชั้นหินบางส่งผลให้เกิดรูปเนินโค้งซึ่งสามารถเห็นได้ชัดในกราฟการ
เปลี่ยนแปลงของค่าความดันที่วัดได้จากไวร์ไลน์ฟอร์เมชั่นเทสเตอร์ชนิดซิงเกิลโพรบและชนิดดูอัลแพคเกอร์
ในขณะที่รูปคลื่นดังกล่าวมีขนาดเล็กมากจนไม่สามารถสังเกตเห็นได้จากกราฟการเปลี่ยนแปลงของค่าความดันที่
วัดได้จากการทดสอบหลุมแบบทั่วไป นอกจากนี้ระยะทางที่แตกต่างกันและรูปทรงที่แตกต่างกันของชั้นหินบาง
ล้วนมีผลต่อลักษณะของรูปคลื่นที่เกิดขึ้น ในขณะที่ปริมาณที่แตกต่างกันของชั้นหินบางกลับไม่ค่อยมีผลต่อ
ลักษณะของรูปคลื่นดังกล่าว

ภาควิชา วิศวกรรมเหมืองแร่และปิโตรเลียม   ลายมือชื่อนิสิต _____
สาขาวิชา วิศวกรรมปิโตรเลียม   ลายมือชื่ออ.ที่ปรึกษาวิทยานิพนธ์หลัก _____
ปีการศึกษา .2553   ลายมือชื่ออ.ที่ปรึกษาวิทยานิพนธ์ร่วม _____

5171615121   : MAJOR PETROLEUM ENGINEERING
KEYWORDS : PERMEABILITY / WIRELINE FORMATION TEST / LAMINATED
RESERVOIR / DUAL PACKER

WIRIYA KIATPADUNGKUL : EVALUATION OF WIRELINE FORMATION
TESTERS IN THINLY LAMINATED RESERVOIRS. THESIS ADVISOR :
ASSISTANT PROFESSOR SUWAT ATHICHANAGORN, PH.D., THESIS CO-
ADVISOR : SAIFON (DUANGKAEW) SIRIMONGKOLKITTI, PH.D., 167 pp.

Reservoir formations are complex, heterogeneous, and anisotropic. The
distribution of both horizontal and vertical permeability strongly affects reservoir
performance and the amount of hydrocarbon recovery. Early in the life of a reservoir, the
main concern is the average effective horizontal permeability to oil or gas since this
controls the productivity and completion design of individual wells. Later on, vertical
permeability becomes important because of its effect on gas and water coning as well as
the productivity of horizontal and multilateral wells. This is the reason why numbers of
measurement are needed for a full reservoir description. However, different scales of
measurement can result in different k_h, k_v and anisotropies.

This thesis studies the effect of reservoir heterogeneity, focusing on discontinued
shale barriers, on different pressure transient tests, namely, single probe WFT, dual
packer WFT, and conventional well test.

The study is done by varying shale barrier properties such as shape, amount and
distance between shale barrier and the well bore and simulating pressure responses from
the three types of pressure measurement using a reservoir simulator. Then, using pressure
transient interpretation software to estimate reservoir parameters, such as horizontal and
vertical permeability, permeability anisotropy, and radius of investigation from derivative
plots.

From the study, the effect of shale barriers can be seen as hump in derivative plots
of single probe and dual packer WFT. For well test, the scale of effect is so small and
hardly observed. Furthermore, variation in distance between shale and the well bore, and
shape of shale can result in different characteristics of hump in the derivative plot.
However, the variation in amount of shale does influence the hump in derivative plots.

Department : Mining and Petroleum Engineering.   Student's Signature _____

Field of Study : Petroleum Engineering_____   Advisor's Signature _____

Academic Year : 2010_____   Co-Advisor's Signature_____

ACKNOWLEDGEMENTS

CONTENTS

LIST OF TABLES

LIST OF FIGURES

LIST OF ABBREVIATIONS

CQG	Crystal Quartz Gauge
DST	Drill Stem Test
EFS	Effective Flow Stream model
FVF	Volume Formation Factor
GOR	Gas / Oil Ratio
IPTT	Interval Pressure Transient Testing
MDT	Modular Dynamic Formation Tester
OWC	Oil Water Contact
Pb	Bubble Point Pressure
PTA	Pressure Transient Analysis
PVT	Pressure-Volume-Temperature
RFT	Repeat Formation Tester
Rs	Solution Gas / Oil Ratio
WFT	Wireline Formation Tester

NOMENCLATURE

a	cross-section area
B	formation volume factor
c_t	total compressibility
h	reservoir thickness
h_D	dimensionless reservoir thickness
k	formation permeability
k_d	draw down permeability
k_h	horizontal permeability
k_s	spherical permeability
k_v	vertical permeability
k_{xy}	horizontal permeability
k_z	vertical permeability
k_{xyz}	spherical permeability
k_v/k_h	vertical to horizontal permeability ratio
k_h/k_v	horizontal to vertical permeability ratio
q	flow rate
p	pressure
p'_D	dimensionless pressure derivative
R_{inv}	radius of investigation
r_s	probe radius
r_{sD}	dimensionless probe radius
r_w	wellbore radius
S_p	probe skin factor
S	skin
S_{pp}	partial penetration skin factor
t	time
$t_{deviation}$	time of deviation
t_D	dimensionless time
t_p	production time

GREEK LETTERS

μ fluid viscosity

ϕ porosity

Δ difference operator

θ theta

CHAPTER I
INTRODUCTION

Reservoir management would be much simpler if permeability were distributed uniformly, but, in practice, formations are complex and heterogeneous. The number of measurements needed for a full description of heterogeneous rock is impossibly high; moreover, the result of each measurement depends on its scale. For example, for an idealized reservoir comprising isotropic sand with randomly distributed isotropic shales, measurements at different scales and in different locations will find different values for both k_h and k_v and hence different anisotropies. Whether in sandstone or carbonate, as heterogeneity increases, the distribution of permeability becomes as important as its average value. Early in the life of a reservoir, the main concern is the average horizontal effective permeability to oil or gas since this controls the productivity and completion design of individual wells. Later on, vertical permeability becomes important because of its effect on gas and water coning, as well as the productivity of horizontal and multilateral wells. The distribution of both horizontal and vertical permeability strongly affects reservoir performance and the amount of hydrocarbon recovery while also determining the viability of secondary and tertiary-recovery processes.

Formations are usually anisotropic, meaning that their properties depend on the direction in which they are measured. For fluid-flow properties, we usually consider transversely isotropic formations, meaning that formations in which the two horizontal permeabilities are the same and equal to k_h while the vertical permeability, k_v, may be different. Although more complicated formations exist, there are typically not enough measurements to quantify more than these two quantities. Permeability anisotropy can be defined as k_v/k_h, k_h/k_v, or the ratio of the lowest to the highest permeability.

Two geological features in particular account for anisotropy are cross-bedding and shales. Crossbedding is the alternated layering of sand of different grain sizes or textures at anacute angle to the major depositional features. Shales have small grain size and usually low permeability. Dispersed shale would block pore space, reduces the permeability of most formations, but does not contribute significantly to

anisotropy. On the other hand, shale layers reduce or eliminate flow to adjacent formations and therefore contribute significantly to the anisotropy at some scale.

Anisotropy is also dependent on shale continuity. For example, continuous shale may totally isolate one zone from another, in which case permeability anisotropy measured across the shale will be zero. If, on the other hand, the shale extends only a short distance from the well, the two zones will not be isolated. Fluid will follow a long tortuous path around the shale, effectively decreasing the permeability measured across it. So the extent of the shale controls the permeability across it.

There are several different methods of obtaining permeability anisotropy, such as core analysis, well testing technique, and wireline formation tester (WFT) measurements. Generally, wireline formation tester is a critical tool for petroleum reservoir evaluation. Basically, pressure measurements have become the main WFT application as well as reservoir downhole parameters measurement and sample collection. Permeability can be estimated from both the drawdown and the buildup during a pre-test. Since a reliable pressure gradient required pretests at several depths, much more permeability data become available. New generation formation testing tools that extend the range of pretest rates and volumes have greatly improved the quality of WFT data acquired in low permeability reservoirs.

However, the different types of WFT tool do not deliver the same pressure response, and this would also affect its interpretation depending on its flow area and flow geometry. Understanding pressure response obtained from different scales of WFT measurement still remains challenging, especially in laminated reservoirs. The aim of this work is to study the effect of reservoir heterogeneity on pressure response, focusing on discontinued shale barrier, for different scales of pressure transient data using pressure transient analysis method.

1.1 Methodology

A simple reservoir model was used to study the effect of discontinued shale barrier as follows:

1. Gather information of reservoir properties to be used as a base case for simulation

models.

2. Design grid block to be used as base case which characterizes reservoir properties, such as reservoir boundary, porosity, permeability, reservoir pressure, and other necessary information.

3. Build the simulation model for

   i)   single probe with the smallest grid cell size equal to single probe's flow area

   ii) dual packer with a group of grid cells' size equal to dual packer's flow area

   iii) full scale well test with a group of grid cells' size equal to well test's flow area

4. Simulate base case for each model and then compare the simulated results with analytical solution.

5. Run simulation software, ECLIPSE, to simulate pressure response for single well model in laminated reservoir by introducing discontinued shale barriers into the three different models and compare results. Various types of discontinued shale barrier are created by

   i)   Varying the distance of discontinued shale barrier from the wellbore.

   ii) Varying the amount of discontinued shale barrier.

   iii) Varying the shape of discontinued shale barrier.

All simulated pressure transient will be analyzed using Ecrin software (Saphir).

The pressure transient application in Ecrin is called Saphir software.

6. Estimate permeability and radius of investigation for different cases from all results. Compare the estimated permeability with the clean sand's effective permeability and average permeability.

7. Compare derivative plots and estimated permeability among 3 test types (single probe, dual packer, and well test)

8. Compare the result obtained from actual field sample to justify if the result provides satisfying information.

1.2 Thesis Outline

This thesis paper consists of nine chapters and the outlines of each chapter are listed below.

Chapter II reviews literatures on the effects of discontinued impermeable

barrier in pressure transient analysis for wireline formation tester and well testing.

Chapter III describes theory and concepts related to this study such as permeability measurement, buildup pressure test, pressure transient analysis, etc.

Chapter IV shows reservoir parameters and reservoir grid models of single probe WFT, dual packer WFT and well test.

Chapter V examines and analyzes the simulation results of the single well model reservoir when different distances, amounts and shapes of shale barriers that are included in the simulation models.

Chapter VI provides conclusions of this study and recommendations for further studies based on this study point of view.

CHAPTER II
LITERATURE REVIEW

2.1 Effects of discontinued impermeable barrier on well test

Bixel et al.[1] obtained solutions for the pressure behavior of a well located near a linear discontinuity, where the reservoir properties are uniform on either side. The discontinuities could be a fluid-fluid contact or a sudden change in rock characteristics such as thickness, permeability, or porosity. By using overlay technique on type-curve, the authors observed that the deviation from the infinite solution usually occurred at dimensionless times equal to 0.4. The authors also used numerical solution to estimate the distance to a discontinuity as $(0.0002636 k_1 t / t_D \Phi_1 \mu_1 c_1)^{1/2}$ where $k_1 / \Phi_1 \mu_1 c_1$ is the diffusivity near the well. In all cases, the authors used superposition to study buildup curves; they concluded that correct values of kh/μ for the region that contains the well are obtained from early shut-in times.

Bixel and Van Poollen[2] studied pressure buildup and drawdown in the presence of a radial discontinuity and reached the same conclusions as their previous work, except that they observed the deviation of the straight line from the infinite solution in this case at $t_{DL} = 0.25$ when the mobility ratio, M, is between 0.5 and 100. The authors suggested that although heterogeneity may be detected from single-well tests, in most cases the behavior of an equivalent homogeneous reservoir will be deduced. When a sharp discontinuity exists such as a well near a sealing fault, single-well tests can provide a powerful tool for detecting reservoir heterogeneity.

Douglas and Van Poollen[3] studied the influence of short flow time prior to buildup of reservoirs discontinuities on the shape of pressure buildup curves. They demonstrated the existence of several slope changes in the pressure buildup semilog plots which is affected by the duration status of drawdown prior to shut-in. The time at which the first effect of a discontinuity is observed at well, deviation from a straight line, or $t_{deviation}$ is calculated as 39.2 $\Phi \mu c a^2 /k$. Whenever flow times is less than $t_{deviation}$, problem occurs in analyzing discontinuities with pressure buildup curve.

Richardson et al.[4] studied the oil recovery from complex distributions of permeable and impermeable intervals by creating a mathematical equation of oil drainage from barrier and using a fine-grid computer model to validate mathematical model. The authors described the effect of small, discontinuous barriers to vertical flow. Also, the time required for oil drainage from a barrier was found to be proportional to its width squared and viscosity, and inversely proportional to the horizontal permeability and density difference. Lateral drainage of small barriers could be rapid and recoveries might be reduced only slightly.

Azari and Ershaghi[5] proposed an analytical solution for the effect of a slanted flow barrier on pressure buildup and drawdown behavior of a single well. The authors mentioned that, for the vertical fault, after the boundary is felt, the Horner plot is a straight line with a slope of twice the early portion. For the slanted boundary, the effect of multiple imaging caused more pressure drop and showed a straight line followed by an ever increasing slope which was not necessarily indicative of lateral changes in mobility or multi layering. The authors also concluded that it was not possible to estimate the angle of fault neither from pressure drawdown nor buildup, but the distance to a slanted fault could be determined by use of type curves.

Martinez-Romero and Cinco-Ley[6] presented a method to detect a linear impermeable barrier by analysis of pressure transient data based on desuperposition method (negative superposition) with pressure versus time semilog plot, as well as type curves. The technique was applicable for both drawdown and buildup, and it was an extension of the method presented by Gray[7].

Sageev and Horne[8] presented a pressure transient analysis method for estimating the size of and the distance to an impermeable circular subregion using semilog type curves matching of drawdown data. The authors showed that drawdown data for a well near a no-flow impermeable subregion exhibited an infinite acting radial flow period, a transition period and a second infinite acting radial flow period. The two semilog straight lines had same slope but were displaced by a constant pressure drop.

Britto and Grader[9] studied the effect of the shape, size and orientation of an impermeable reservoir region on transient pressure testing on semilog plots. The authors mentioned the more the boundary resembled a linear impermeable barrier, the greater deviation of pressure response from the line-source solution. Also,

impermeable regions must be relatively large with respect to their distance from the production well to be detected. Furthermore, the orientation of an impermeable region with respect to the production well had a great influence on the transient pressure response.

Kamal and Pan[10] proposed a method to calculate absolute permeability and average fluid saturation in homogeneous reservoir from pressure transient data. The proposed method was verified with numerical simulation as well as field examples.

Al-Harbi et al.[11] studied pressure transient analysis of well test in a reservoir with complex nature in terms of heterogeneity and fluid properties to understand the reservoir and help fine-tune development strategy. The authors determined the behavior of a tight permeability layer whether it acted as a flow barrier or not using pressure transient analysis for pressure response from different perforation intervals. The authors pointed out that, if the well test interval was across the flow barrier layer, the partial penetration effect representing spherical flow regime would not have developed on the derivative plot due to poor communication of the layer.

2.2 Pressure Transient Analysis (PTA) for Wireline Formation Tester

Stewart and Wittmann[12] have developed the analytical theory of the buildup pressure response associated with the pretest stage of the repeat formation tester operation on infinite system and the case of a reservoir layer bounded above and below by impermeable barriers. The authors showed that the spherical flow analysis method for the infinite acting case yields the equivalent spherical permeability which is influenced by formation anisotropy. Also, the authors presented a relation between gauge resolution and measurable permeability as an upper limit of measurable permeability from buildup.

Yildiz and Langlinais[13] have developed a 3D analytical model for the convergent flow geometry of the WFT tool to evaluate the validity of interpretation techniques on pressure versus spherical/radial time function in buildup plot and drawdown equation. First, the authors revealed that wellbore size did not significantly

affect pressure behavior during WFT. Second, the authors indicated that buildup plots of pressure versus both spherical and radial time functions may result in a straight line which could be used for determining permeability. But, the straight lines identified on the mentioned buildup plots were usually false straight lines as a result of inflection points from pressure derivative analysis. The permeability interpreted from buildup plots was underestimated by a factor of 0.7 and 0.4 for spherical and radial time function, respectively. In the other hand, the permeability interpreted from drawdown equation was overestimated by a factor of 2.

Da Prat et al.[14] presented an approach to evaluate layer productivity before well completion using dual packer WFT to obtain layer pressure, reservoir permeability, and formation damage. While layer anisotropy obtained was valid on a layer scale. The authors mentioned that the lack of partial penetration effects observed in many of the tested layers reflected the highly laminated nature of the layers.

Siswantoro et al.[15] studied the ability of the dual packer in the conditions, such as thin and laminated formations or formations with very low permeability, that was difficult for conventional technique like single probe. Under these conditions, the small packer might not be able to isolate the zone, might miss a thin zone or in a formation with very low permeability, the contact area with the packer might be too small to let the fluid flow. The mobility estimation from MDT dual packer measurement showed that the formation had very poor fluid mobility. The result was later on confirmed by cased hole DST, and the well was plugged and abandoned.

Whittle et al.[16] compared information that can be obtained from pressure transient recorded during a wireline formation tester with the one from well test. The authors suggested that, in lower permeability reservoirs (mobility less than about 100 mD/cp), the quality of data recorded by wireline formation test tools was suitable for pressure transient interpretation. In addition, pressure transient analysis of wireline formation tests provided estimates of spherical permeability. In thin beds of known thickness or in cases where an observation gauge is used to measure vertical interference, there was also the possibility to evaluate permeability anisotropy.

Daungkaew et al.[17] illustrated the wide range of information that could be obtained from WFT pressure response, that was obtained from actual field examples in Asia Pacific region, using an advanced well test analysis technique. The result was confirmed by analytical solution of pressure transient response generated from a

single well model numerical simulation. The obtainable information was spherical permeability, vertical to horizontal permeability ration, tool compressibility and storage, formation skin factor and radius of investigation. In addition, the detailed observation of pressure transient response could provide additional understanding of reservoir even though the radius of investigation of the WFT was very small, i.e. to monitor the pump-out data gas reservoir, to indicate an increasing fluid mobility away from the probe, and to confirm oil-water contact (OWC). Also, the shapes of pressure derivatives could be used to identify between valid and invalid tests.

Gok et al.[18] studied the effect of heterogeneities in the near-well formation region (about 40 to 60 feet) on IPTTs (Interval Pressure Transient Tests) and proposed a methodology within the Bayesian estimation framework incorporating a geostatistical model of reservoir parameters to estimate the distribution of heterogeneities in the vertical and lateral directions by history matching the dual-packer and probe pressure data sets. The authors also presented sensitivity coefficient map of the dual packer and probe pressures with respect to grid block values of horizontal and vertical permeability and porosity.

Daungkaew et al.[19] presented a systematic pressure transient analysis (PTA) method using information obtained from mini-DSTs in thinly laminated deep water reservoirs and cross-checked with other static and dynamic reservoir information such as DST, core data and single probe WFT. The authors mentioned that the dual packer increased the success rate of pretesting and sampling in formations with mobility as low as 0.1 md/cp. A log-log plot of pressure and pressure derivative showed three main flow periods; the first radial flow, which was normally, dominated by wellbore storage effect, spherical flow, and the second radial flow. The authors pointed out that with the medium scale of pressure transient response obtained from a WFT with dual packer, a more detailed pressure transient response can be seen compared to a larger scale well test where properties derived represent the average reservoir behavior.

Jackson et al.[20] compared pressure drawdown among several WFT probe size and dual packer with different interval length in unconsolidated formation. The drawdown rate was 10 cc/s and the fluid mobility was 100 mD/cp. The result showed drawdown pressure equal to 1000, 242, 76, 8, 6, 3 psi for conventional probe, extra-large diameter probe, elliptical probe, 3.2 ft packer interval length, 5.2 ft packer

interval length, 11.2 ft packer interval length, respectively.

Bertolini et al.[21] proposed an approach for mini-DST design to estimate the effective drawdown and buildup durations that were feasible for given scenario which could be applied to any other hydrocarbon environment. The authors provided equations for calculating minimum and maximum buildup period, as well as dimensionless charts of buildup period versus mobility for different net pay, anisotropy. The equation also accounted for fluid type (oil/gas), gauge resolution, and pumping rate.

CHAPTER III
THEORIES AND CONCEPTS

3.1 Permeability

Permeability determines reservoir and well performance but the term can refer to many types of measurements. For example, permeability can be absolute or effective, horizontal or vertical. Permeability is defined as a formation property, independent of the fluid. When a single fluid flows through the formation, we can measure an absolute permeability that is more or less independent of the fluid. However, when two or more fluids are present, each reduces the ability of the other to flow. The effective permeability is the permeability of each fluid in the presence of the others, and the relative permeability is the ratio of effective to absolute permeability. In a producing reservoir, we are most interested in effective permeability, initially of oil or gas in the presence of irreducible water, and later of oil, gas and water at different saturations. To further complicate matters, effective and absolute permeability can be significantly different.

3.2 Permeability Anisotropy

The anisotropic nature of permeability can affect any process in which a density difference exists between fluids, for example primary production below the bubblepoint, gas cycling, gas or water coning, waterflood and many steam processes. It can also influence injection and production rates if the anisotropy is severe. Completion and treatment strategies must also take anisotropy into account, for instance, placing perforations near oil-water or oil-gas contacts.

3.3 High/Low Permeability Barrier

The magnitude of permeability contrast becomes increasingly important with prolonged production. Thin layers, faults and fractures can have a dramatic effect on the movement of a gas cap, aquifer, and injected gas and water. For example, a low-permeability layer, or baffle, will impede the movement of gas downwards. A high-permeability layer, or conduit, will quickly bring unwanted water to a production well. Both can significantly affect the sweep efficiency and require a change in completion practices. Reasonable reservoir management depends on knowing not only the average horizontal permeability but also the permeability distribution laterally and vertically, and the conductivity of baffles and conduits.[22] Figure 3.1 shows permeability baffles and conduits at different length scales. In each case, reservoir management can be improved by quantifying the effects of these features.
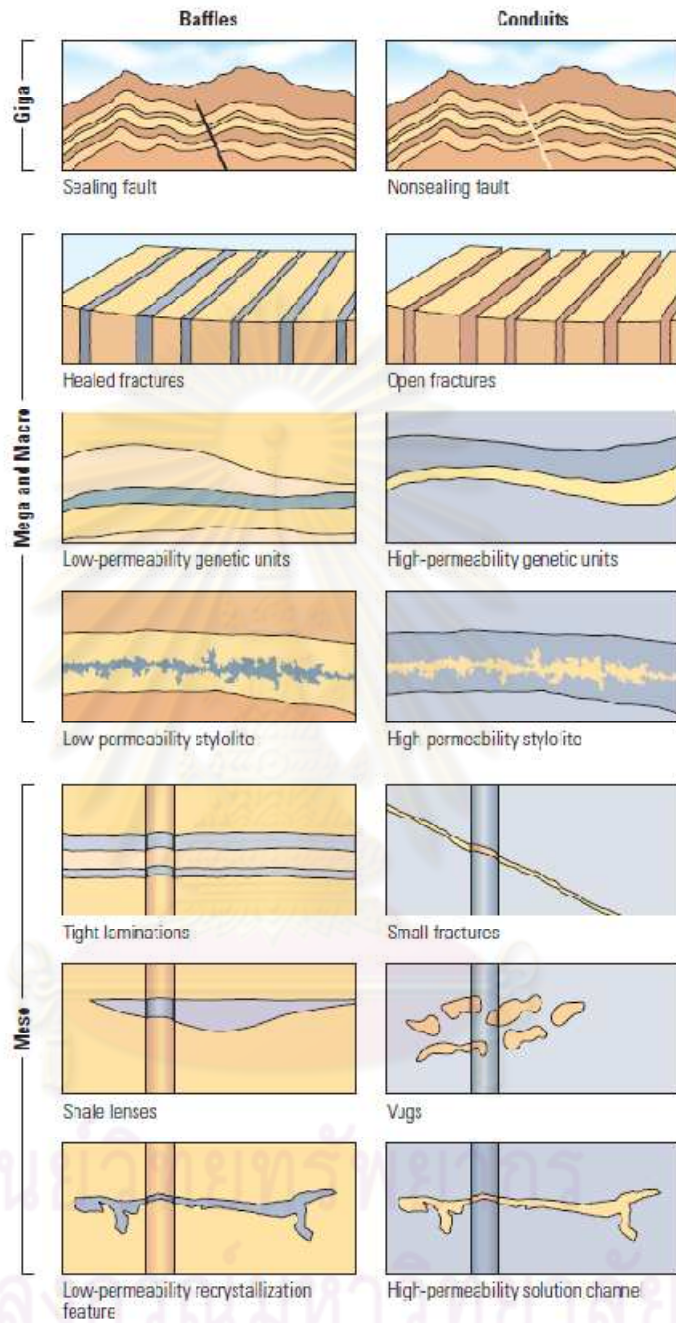
Figure 3.1: Permeability baffles and conduits at different length scales[22]

3.4 Permeability Measurement

In normal reservoir-engineering practice, the main sources of average effective permeability are pressure-transient well testing and production tests. These are usually good indicators of overall well performance. Once a reservoir has been on production, conventional history matching gives information on average permeability, but cannot resolve its distribution. The presence of high- or low-permeability streaks and their distributions are inferred from cores and logs but this information is qualitative rather than quantitative. Wireline formation testers have stepped into this gap, providing various measurements of permeability from simple drawdown with a single probe to multilayer analyses with multiple probes. The latter was originally used mainly to determine anisotropy. With recently developed analytical techniques and further experience, multilayer analyses now provide quantitative information about permeability distribution. With tens of test points in a single well, it became easier to establish a permeability profile and compare results with core and other sources.

3.5 Drawdown Pressure Test

Pretests continue to be an important feature of modern tools, although the reliability of the permeability estimate varies. Since pretests sample a small volume, typically 5 to 20 cm^3 [0.3 to 1.2 in.^{3}] depending on tool, the drawdown permeability, k_d, can be overly influenced by formation damage and other near-wellbore features. Detailed analysis shows that k_d is closest to k_h, although it is influenced by k_v.[22] The volume of investigation is significantly larger than that of a core plug, but of the same order of magnitude. However, k_d is typically the effective permeability to mud filtrate in the invaded zone rather than the absolute permeability as obtained from core. Although some good correlations between the two have been found, k_d is generally considered to be the minimum likely permeability. Nevertheless, it can be computed automatically at the wellsite, and is still used regularly as a qualitative indicator of productivity. The following equation is used for calculating drawdown mobility.

$$\frac{k_d}{\mu} = 2338 \, \frac{C' \cdot q}{r_e \Delta p} \qquad (3.1)$$

The magnitude of the pressure drop recorded during a probe pretest is used to provide a mobility estimate (the "drawdown" mobility). This value includes near-wellbore damage effects, and is not expected to be equivalent to a permeability derived from a well test. It has been shown that this drawdown mobility bears a close relationship to the core permeability. Analysis of the pressure build-up following the pretest drawdown can also provide estimates of spherical and radial permeability. However, the pressure response during this period can be affected by local changes in fluid properties and by small variations in formation properties, damage to the formation resulting from the mechanical setting of the tool, mudcake blocking the probe, and non-Darcy flow near the probe.

3.6 Buildup Pressure Test

Pretest buildups investigate further into the formation than drawdowns, several feet if the gauge resolution is sufficiently high and the buildup is recorded long enough. Except in low permeability formations, the buildup time is short. So, the tool may be measuring the permeability of either the invaded zone, the non-invaded zone, or some combination of the two[31]. As the slope eventually approaches that of the native reservoir but seldom achieves it in a time sufficient for interpretation. And in the interpretation of any pressure-transient data, flow regimes are identified by looking for characteristic gradients in the rate of change of pressure with time (pressure derivative, Bourdet et al 1983). For pretest buildups in which the flow regimes are spherical and occasionally radial, consistent gradients often prove hard to find, and even then may be affected by small changes in the pretest sampling volume (not quite if rate history is taken into account). For reliable results, each pretest must be analyzed—a time-consuming process. Previously, the analysis of short pretest buildups for permeability is rare mainly because there is no analytical solution, i.e. no software to analyze. Now, the process is started to use to be real time.

3.7 Fluid Sampling and Fluid Analyzer

Openhole wireline formation tester samples are important to the early evaluation of a reservoir. These samples are commonly used for fluid identification, preliminary reservoir evaluation, and PVT analysis. In addition, the formation tester can be used to evaluate multiple formation intervals in the same wellbore without the completion restrictions and expense imposed by full production flow tests. In the conventional procedure, the tool is set at a specific depth in the formation interval; a pretest is performed in which 20 cc of fluid (usually mud filtrate) is drawn into the tool; formation permeability at that set depth is calculated from the drawdown; and a sample chamber (maximum of two sample chambers) is opened to allow 1-12 gallons of fluid to be taken. In the sandstone/shale formations, the standard sampling configuration is a 1-gallon upper chamber and a 2 3/4-gallon lower chamber with each connected to a water cushion chamber designed to minimize the fluid pressure drop inside the tool as the sample chamber is filled. In addition, segregated samples can be obtained by initially flowing into one sample chamber (2 3/4-gallon) until formation fluids are flowing, and then switching to the second sample chamber (I-gallon). Where the mud filtrate invasion is small (high porosity formations), this technique usually insures a good hydrocarbon sample with little filtrate contamination. The quantity of mud filtrate can be determined so that the true volumes of formation water and hydrocarbon can be calculated. Wellsite evaluation of the sample can include fluid volumes recovered, API gravity of the oil, water cut, and GOR. [32]

Fluid analyzer has a visible and near-infrared absorption spectrometer for fluid discrimination and a refractometer for free gas detection. The Effective Flow Sream (EFS) model has been developed to interpret the measured data and to estimate the volume fraction of water and oil in the tool's flowline for biphasic flow. For triphasic flow, the technique can give a quantitative estimate of water, along with a qualitative evaluation of the amount of oil and gas. To obtain samples that truly representative of the reservoir fluid, it is necessary to ensure that sufficient invaded fluid has been displaced before opening a sample chamber and to maintain the sampling pressure above the bubble point to avoid the evolution of gas. Recent developments in

formation fluid sampling technology include the provision of straddle packers and pumpout capacity in a modular formation test tool string. Downhole fluid analysis in real time enhances the usefulness of these new technique.[33]

3.8 Conventional Well Test

Pressure transient analysis of well tests gives the average in-situ, effective permeability of the reservoir. However, the results have to be interpreted from the change of pressure with time. Interpreters use several techniques, including the analysis of specific flow regimes and matching the transient to type curves or a formation model. In conventional tests, the well is produced long enough for the pressure response to reach the reservoir boundaries. Impulse tests produce for a short time and are useful for wells that do not flow to surface. In both cases, especially for impulse tests, there is not necessarily any unique solution for permeability.

In most conventional tests, the goal is to measure the transmissibility ($k_h h/\mu$) during radial flow. The reservoir thickness, h, can be estimated at the borehole, but it is not always the same tens and hundreds of feet throughout the reservoir where the pressure changes are taking place. In practice, other information such as geological models and seismic data helps improve results. With conventional well tests, the degree of heterogeneity can be detected but the permeability distribution cannot be determined, and there is no vertical resolution.

Economically, well tests are expensive from the point of view of both equipment and rig time. Well tests are also undertaken to obtain a fluid sample so that the incremental cost of determining permeability may be small. However, obtaining high-quality permeability data often requires long shut-in times and extra equipment such as downhole valves, gauges and flowmeters.[22]

3.9 Wireline Formation Tester (WFT)

In developed reservoirs, wireline formation testers are used to

- Characterize vertical and horizontal barriers
- Assess vertical permeability

- Detect potential of thief zones

- Determine hydraulic communication between wells

- Detect fluid contact movement.

Wireline formation testers are also used to collect formation fluid samples. In particular, the WFT tool attempts to improve the quality of samples by using techniques for downhole fluid analysis – a system to discard contaminated fluids before taking samples and to limit the drawdown pressure by using precision flow control methods.

Tests from single probe wireline formation testers provide mobility profiles that help to pinpoint zones of better productivity. The recorded transient pressure response at each station can be analyzed to estimate permeability. In homogeneous formations, the multi-probe tester can estimate horizontal and vertical mobility; in laminated formations, this tool enables the study of potential permeability barriers and their effect on vertical fluid movement.[25] To estimate permeability of zone, definition of fluid properties, together with knowledge of the net pay thickness, permits the estimation of formation radial permeability, k_r, from the permeability thickness product, k_h. An estimate of openhole skin, a combined skin caused by limited entry, mechanical damage and rate dependency, is also obtained in the analysis. If a spherical flow is identified prior to the radial flow, it is possible to estimate vertical permeability, k_v, in addition to the radial permeability, k_r, and obtain the k_v/k_r ratio.

3.10 Single Probe WFT

Figure 3.2 depicts single probe WFT. The left picture represent a packer. The right picture presents the probe module containing a probe assembly with packer and telescoping back-up pistons. It also houses the pressure gauges, fluid resistivity and temperature sensors and the pre-test facility.

Figure 3.2: Single probe WFT[25]

Figure 3.3 exhibits the flow geometry from top view and side view of the single probe WFT.

Top view

Side view
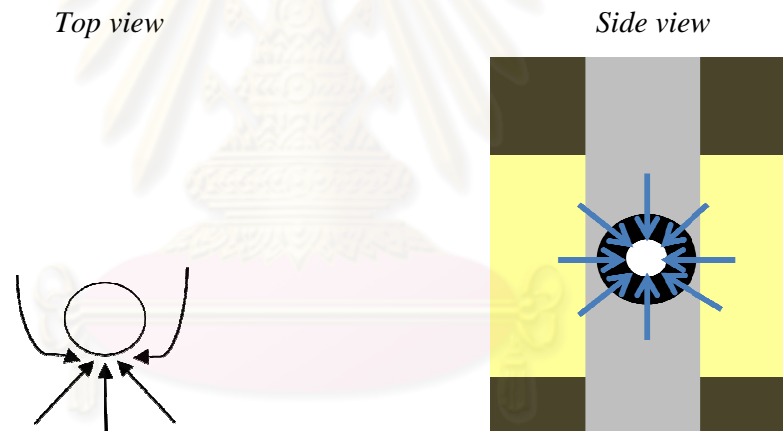
Figure 3.3: Flow geometry of single probe WFT

The single probe WFT obtains pressure and fluid samples by setting a rubber packer and small diameter probe. The packer hydraulically isolates a small part of the formation from the hydrostatic pressure while the probe enables communication between the tool and formation. There are two types of single probe. One contains only a strain gauge. The other has both a strain and quartz gauge (CQG). The strain gauge is made up of a cylinder where the bottom section contains a cylindrical pressure cavity. A passive (i.e., reference) winding is wound around the solid part of the cylinder and an active winding is wound around the pressure cavity. The outside of the gauge is at atmospheric pressure. When pressure is applied to the pressure

cavity, the outer cylindrical section of the cavity expands. This expansion stretches the active winding, slightly increasing its resistance proportionally to the applied pressure. The CQG (Crystal Quartz Gauge) is a high accuracy, high stability permanent gauge. The CQG design implements pressure and temperature measurements made at the very same location. This location is within the quartz resonator, and by doing this the errors caused by thermal lag under transient pressure or temperature conditions, are eliminated. There is a fluid resistivity and temperature cell mounted close to the probe. The resistivity measurement helps to identify the nature of the fluid flowing while sampling. There is one pretest chamber with a maximum volume of 20 cc depending on tool. The pretest is programmable from surface. During drawdown, the piston motion can be stopped by specifying the volume of the pretest or the pressure in the flowline. In addition, the pretest rate can be changed.

There is an isolation valve which reduces the volume of the flowline during a pre-test. This is needed since the complete flowline bus in a long string has a significant volume and can distort the pressure test profile due to "storage effect" which is caused by the finite compressibility of the flowline fluid. The isolation valve also serves to isolate specific probes in a tool string with more than one probe as shown in Figure 3.4.
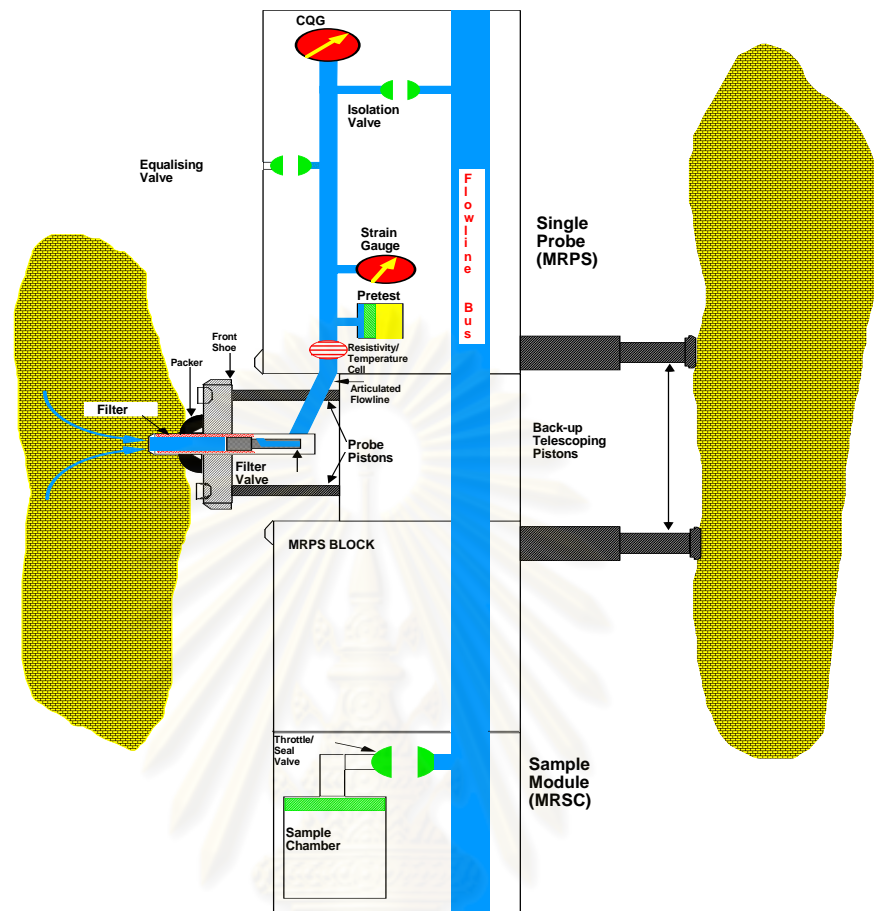
Figure 3.4: Flowline volume[34]

However, for difficult conditions such as fractured limestone, thin and laminated formations or formations with very low permeability, the application of a single probe technique is limited. Under these conditions, the small packer may not be able to isolate the zone and may miss a thin zone or in a formation with very low permeability, the contact area with the packer may be too small to let the fluid flow. To identify formation fluids under any of these conditions, a dual packer WFT and cased hole DST is usually run but it is time consuming and costly.

3.11 Dual Packer WFT

Figure 3.5 depicted dual packer WFT. Two inflatable packers are mounted on this module. When inflated, they isolate an area of borehole wall.
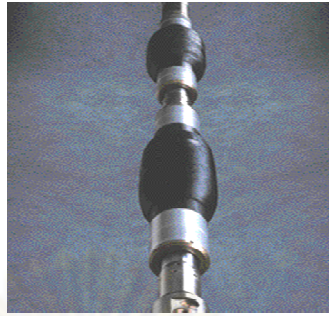
Figure 3.5: Dual packer WFT[25]

Figure 3.6 exhibits the flow geometry from top view and side view of the dual packer WFT.

Top view   *Side view*

Figure 3.6: Flow geometry of dual packer WFT

The dual packer module is used in a multi-probe configuration with the single probe module to make anisotropic permeability estimates. It consists of two probes mounted diametrically opposite each other. One probe is connected to the flowline and is called the "sink" probe. The other is called the "horizontal probe" and is not connected to the flowline bus; it is used solely as a monitor probe. The sink probe is configured similar to a single probe in that it has similar features such as a resistivity cell, programmable pretest and an isolation valve. However, the sink probe can only have a strain gauge. The horizontal probe has no resistivity cell and can have both CQG and strain gauges. Therefore, there are two versions of dual packer WFT. One has only a strain gauge at the horizontal probe. The other has both CQG and strain gages at the horizontal probe.

The dual packer has the capability of hydraulically isolating a minimum of one meter of formation. The dual packer WFT provides two inflatable packer elements which seal off a 1 meter section of the borehole (can be extended to 13 feet). The elements are inflated with wellbore fluid or with water carried down-hole in a sample chamber. The whole packed off section of borehole wall is open to the formation so that the fluid flow area is several thousand times larger than with the conventional probes. This allows pressure measurements and fluid sampling in laminated, shaly, fractured, vuggy, unconsolidated, or low permeability formations where the probes usually cannot operate. For pressure measurement, enough fluid needs to be removed from the interval to drop pressure below the formation pressure. The dual packer can be set repeatedly at different locations on a single trip in the well. Using these, pressures, real-time formation fluid identification, PVT samples, permeability, and flow rate can all be evaluated in details. In difficult conditions where the single probe wireline formation tester usually cannot operate (i.e., fractured limestone, very low permeability formations, and thin and laminated formations), the dual packer WFT allows pressure measurements, sampling, and formation fluid identification. These applications of the WFT are possible due to the increased area sealed by the packers creating a flow area of 679 in^2, compared to only 0.1521 in^2 in a conventional single probe. Dual packer WFT has been applied successfully to many cases such as a fractured carbonate reservoir, a thinly-bedded reservoir and a formation with very low permeability.

3.12 Pressure Transient Analysis (PTA)

Historically, Pressure Transient Analysis was only performed during well test operations designed to acquire and interpret these data. In the last twenty years, the term has become increasingly invalid, as the same processing has been applied to pressure and rate data acquired not only from well test operation. Currently, the main sources of pressure transient data are well tests of various types, formation tests and any well shut-in monitored with permanent gauges. The principle of Pressure Transient Analysis is the gathering of pressures and rates, preferably downhole, and the focus on a period of interest, generally a shut in period (build up or fall off) to

perform diagnostic.

For WFT, pressure response measurement is normally conducted on a well drilled partially into a reservoir or one where a limited portion of the reservoir is perforated, usually the upper portion. As a result of this, the derivative plot of the pressure response basically reveals three flow regimes. Once wellbore storage subsides, radial flow around the perforations is seen. Transient analysis of this portion of the pressure derivative is used to calculate horizontal permeability, k_h, at the perforations and also skin. As the pressure wave propagates away from the well, the second regime, spherical flow, develops. The slope of the curve of pressure plotted versus the reciprocal of the square root of time curve allows calculation of spherical permeability. Spherical permeability, k_s, is the geometric mean of horizontal and vertical permeability, $\sqrt[3]{k_h^2 k_v}$. Hence, vertical permeability and anisotropy may be determined. When the third regime, radial flow, develops far from the well, another value for horizontal permeability can be calculated. If permeability anisotropy is low and vertical permeability approaches horizontal permeability, and wellbore storage effects often mask the early-time radial flow. Spherical flow can also occur earlier and may also be masked.
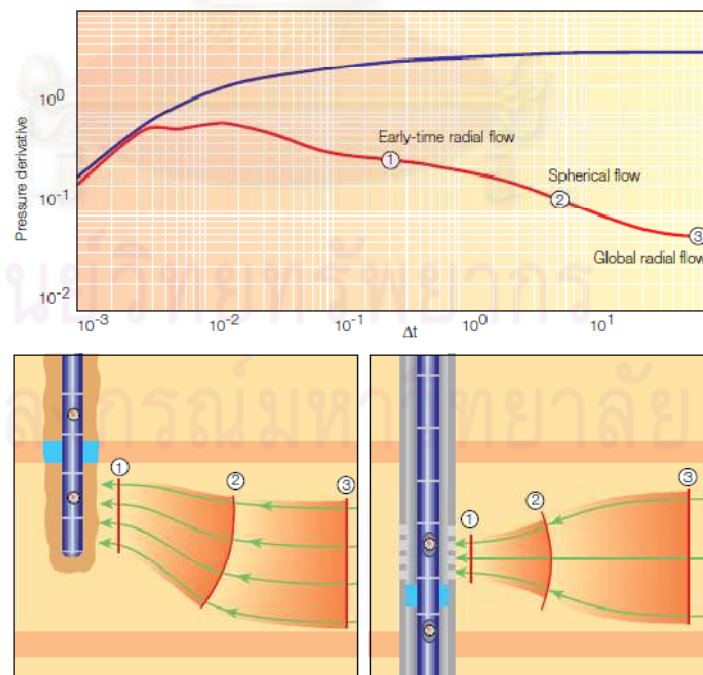
Figure 3.7: Spherical and radial flow regimes[23]
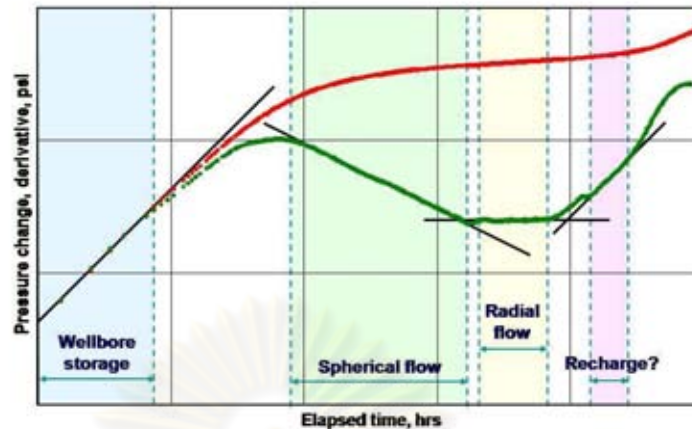
Figure 3.8: Sample of pressure transient analysis[25]

3.13 Interpretation Methodology

The objective of well test interpretation is to obtain the most self-consistent and results with available data. This can be achieved by following a systematic approach.

1. Data processing

Transient well tests are conducted as a series of dynamic events triggered by specified changes in the surface flow rate. During interpretation, it may be desirable to analyze just one particular event or all events simultaneously. In either case, the data must first be processed.

The first step in data processing is to split the entire data set into individual flow periods. The exact start and end of each flow period are specified. Because the sampling rate is usually high, each transient typically includes many more data points than are actually required. A high density of data is needed only for early-time transients. Therefore, special algorithms are usually employed to reduce the data set to a manageable size. Because of the nature of the pressure disturbance propagation, a logarithmic sampling rate is preferred.

The sequence of events should incorporate the recent flow rate history of the well with the surface flow rate changes observed during the test. This enables rigorous accounting for superposition effects. As stated previously, the shape of the pressure transient curve is affected by the production history of the reservoir. Each change in

production rate generates a new pressure transient that passes into the reservoir and merges with the previous pressure effects. The pressure trends observed at the wellbore result from the superposition of all the pressure changes.

The next step is to transform the reduced data so that they display the same identifiable features, regardless of test type. A popular transformation is the pressure. Other useful transformations are the rate-normalized pressure, sandface rate-convolved time function and convolution derivative.

After the data are transformed, the task of identifying the flow regime begins.

2. Flow regime identification

Identifying flow regimes, which appear as characteristic patterns displayed by the pressure derivative data, is important because a regime is the geometry of the flow streamlines in the tested formation. Thus, for each flow regime identified, a set of well or reservoir parameters can be computed using only the portion of the transient data that exhibits the characteristic pattern behavior.

The eight flow regime patterns commonly observed in well test data are radial, spherical, linear, bilinear, compression/expansion, steady-state, dual-porosity or -permeability, and slope-doubling.[26]

3.14 Radial flow

The most important flow regime for well test interpretation is radial flow, which is recognized as an extended constant or flat trend in the derivative. Radial flow geometry is described as flow streamlines converging to a circular cylinder (Figure 3.9). In fully completed wells, the cylinder may represent the portion of the wellbore intersecting the entire formation (Figure 3.9b). In partially penetrated formations or partially completed wells, the radial flow may be restricted in early time to only the section of the formation thickness where flow is directly into the wellbore (Figure 3.9a). When a well is stimulated (Figure 3.9c) or horizontally completed (Figure 3.9d and 3.9e), the effective radius for the radial flow may be enlarged. Horizontal wells may also exhibit early time radial flow in the vertical plane normal to the well (Figure 3.9d). If the well is located near a barrier to flow, such as a fault,

the pressure transient response may exhibit radial flow to the well, followed by radial flow to the well plus its image across the boundary (Figure 3.9f).

(a) Partial Radial Flow
Top of zone   Bottom of zone

(b) Complete Radial Flow

(c) Pseudoradial Flow to Fracture
Fracture   Fracture boundary

(d) Radial Flow to Horizontal Well

(e) Pseudoradial Flow to Horizontal Well

(f) Pseudoradial Flow to Well near Sealing Fault
Actual well   Image well
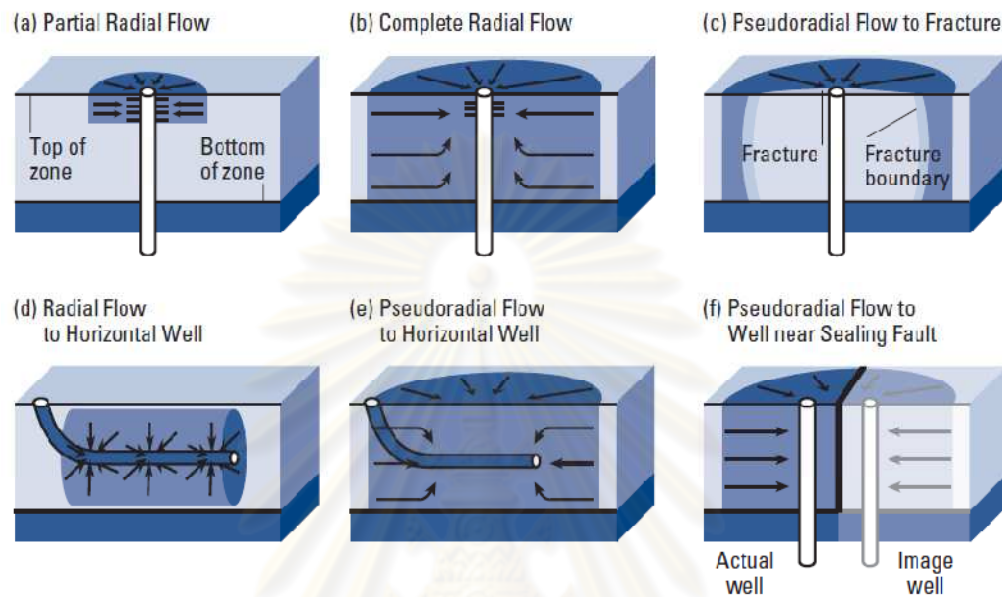
Figure 3.9: Different types of radial flow regimes, recognized as an extended flat trend in the derivative[26]

Whenever radial flow occurs, the values for k and s can be determined. When radial flow occurs in late time, the extrapolated reservoir pressure p^* can also be computed. For well A in Figure 3.10, radial flow occurs in late time, so k, s and p^* can be quantified.
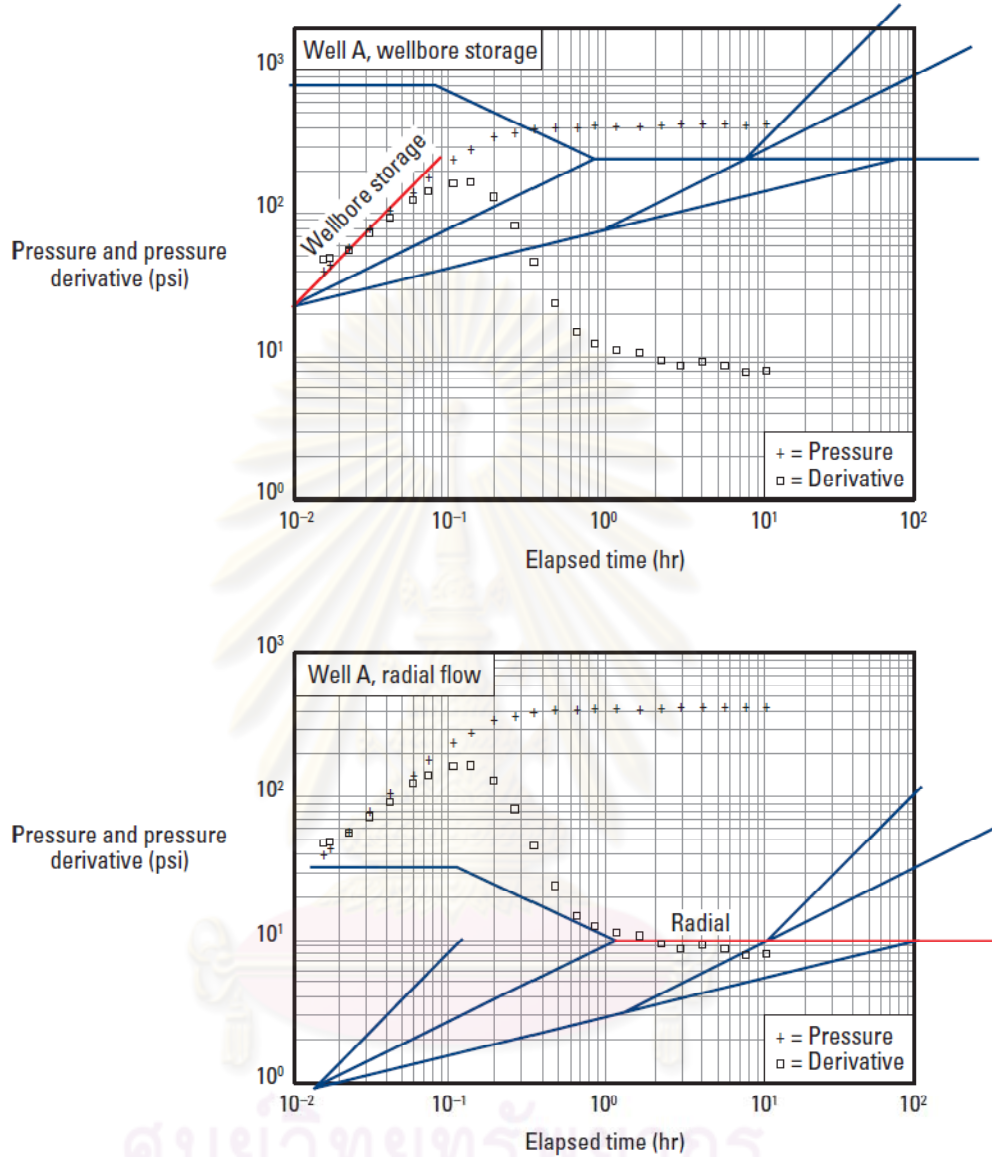
Figure 3.10: Radial flow occurring at late time. Values for the permeability, skin effect and extrapolated pressure to infinite shut-in can be computed[26]

3.15 Spherical flow

Spherical flow occurs when the flow streamlines converge to a point (Figure 3.11). This flow regime occurs in partially completed wells (Figure 3.11a) and partially penetrated formations (Figure 3.11b). For the case of partial completion or partial penetration near the upper or lower bed boundary, the nearest impermeable bed

imposes a hemispherical flow regime. Both spherical and hemispherical flows are seen on the derivative as a negative half-slope trend. Once the spherical permeability is determined from this pattern, it can be used with the horizontal permeability k_h quantified from a radial flow regime occurring in another portion of the data to determine the vertical permeability k_v.

The importance of k_v in predicting gas or water coning or horizontal well performance emphasizes the practical need for quantifying this parameter. A DST can be conducted when only a small portion of the formation has been drilled (or perforated) to potentially yield values for both k_v and k_h, which could be used to optimize the completion engineering or provide a rationale to drill a horizontal well.
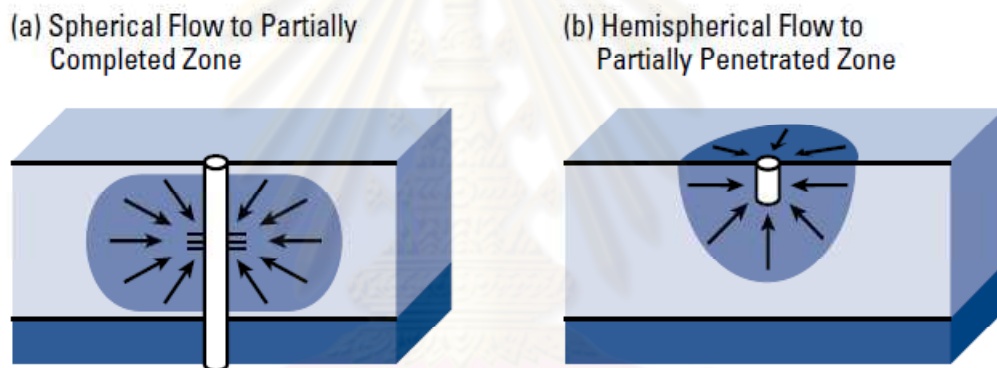
Figure 3.11: Spherical flow regime, which results from flow streamlines converging to a point[26]

Well B (Figure 3.12) is an example of a DST from which the values of k_v and k_h were determined for the lower layer. These permeabilities were derived from the portion of the data exhibiting the spherical flow regime (negative half-slope) trend (red line in Figure 3.12a). The reason why spherical flow occurs in early time is evident from the openhole log in Figure 3.12, which shows only a few feet of perforations into the middle of the lower layer (Figure 3.12a).

Negative half-slope behavior is commonly observed in well tests that indicate a high value of s. A complete analysis in these cases may provide the value of k_v and decompose the skin effect into components that indicate how much is due to the limited entry and how much to damage along the actively flowing interval. The treatable portion of the damage can then be determined, and the cost effectiveness of

damage removal and re-perforating to improve the well productivity can be evaluated.
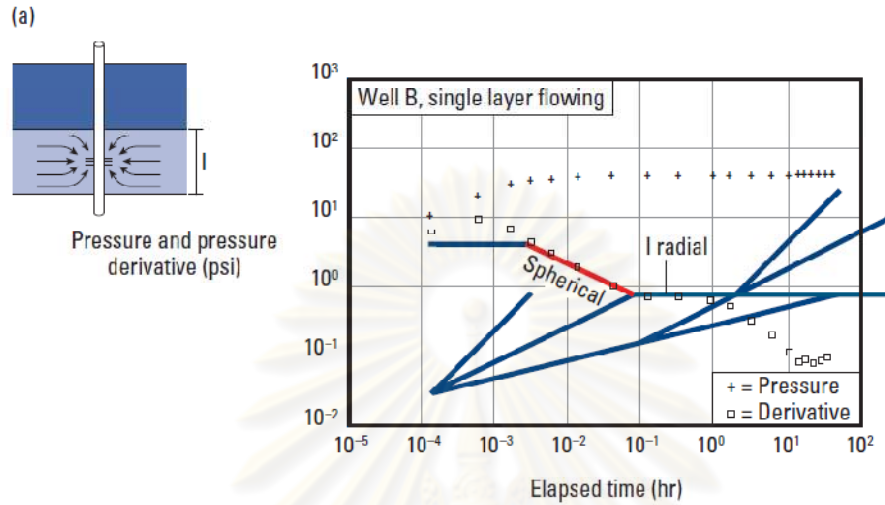
Figure 3.12-a: Spherical flow regime in the lower layer is indicated by the negative half-slope trend (red line), followed by late-time radial flow[26]
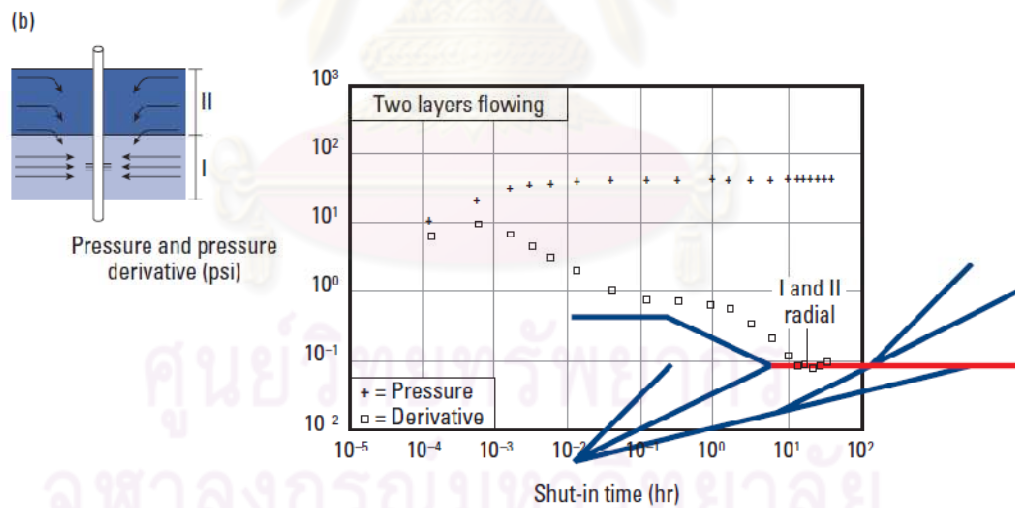
Figure 3.12-b: Following a transition period, radial flow is from the combined two layers[26]

The interpretation of horizontal permeability is based on build up following a single drawdown. So, the Horner plot is used for calculating permeability from the straight line slope, m, in the Infinite Acting Radial Flow (IARF) regime.

Pressure drop equation at IARF[29]

$$\Delta p = 162.6 \frac{q\mu B}{kh} \left[log \left(\frac{t_p \Delta t}{t_p + \Delta t} \right) + log \left(\frac{k}{\emptyset \mu C_t r_w^2} \right) - 3.23 + 0.87S \right] \quad (3.2)$$

Slope of IARF straight line in Horner plot

$$m = 162.6 \frac{q\mu B}{kh} \quad (3.3)$$

The interpretation of vertical permeability is based on spherical flow regime analysis on pressure derivative plot. The spherical permeability can be identified when a negative half-unit slope occurs in the pressure derivative plot.

Pressure drop equation in spherical flow regime[17]

$$\Delta p = \frac{q\mu B}{2(0.007082)k_{xyz}r_s} \left[1 - \sqrt{\frac{\emptyset \mu C_t r_s^2}{\pi(0.0002637)k_{xyz}}} \frac{1}{\sqrt{\Delta t}} + S_p \right] \quad (3.4)$$

The derivative of dimensionless pressure drop in spherical flow regime[16]

$$p_D' h_D = \frac{1}{2\sqrt{\pi \frac{t_D}{r_{sD}^2}}} \quad (3.5)$$

The spherical permeability equation[19]

$$k_{xyz} = \sqrt[3]{k_{xy}^2 k_z} \quad (3.6)$$

3.16 Effect of Radius of Investigation

Figure 3.13 illustrates the case of a laminated sand-shale sequence where the permeability being measured is affected by the radius of investigation. The permeability measurement on the smallest scale (smallest radius of investigation) is high representing the basic rock information. The permeability measurement on the

medium scale is low due to the impermeable barriers. Though, the permeability measurement on the large scale is moderate since the impermeable barriers are not continuous.
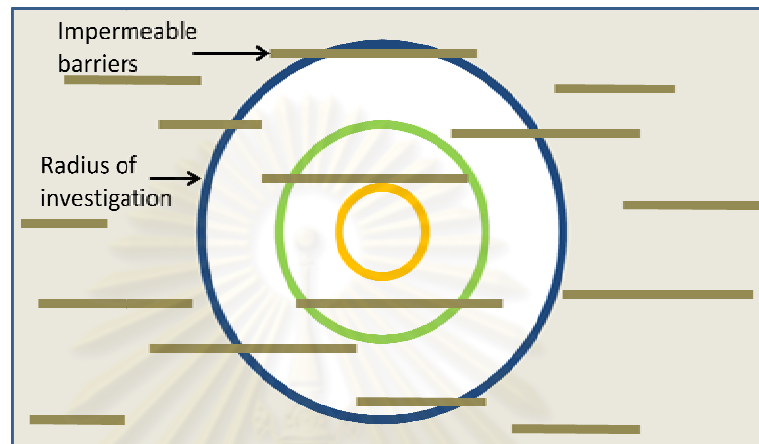
Figure 3.13: Effect of scale on permeability measurement

3.17 Reservoir Model for WFT

The flow into the WFT probe is a 3D physical phenomenon, and the flow pattern is convergent. Neither 1D spherical nor 1D radial geometry truly represents the convergent flow during the test. The formulation of the 3D convergent flow into the probe requires the assumptions that

- Darcy's law is valid
- Only one phase flow exists
- The fluid has constant and small compressibility
- The formation is homogenous
- The WFT probe is square on a cylindrical surface
- No supercharging effect exists
- The flow rates during the drawdown are constant but can be different

In the service industry, most WFT tools use circular probes. Mathematically, however, it is difficult to define a circular shape on a cylindrical surface, and the

solution for a circular probe requires an inordinate amount of computing time. Hence, the square probe assumption is made. Also, since the size of the probe is very small compared to the other dimensions in the physical problem, the assumption is reasonable.[9]

3.18 Permeability Averaging Techniques

For making zonal averages of the permeability, it should be noted that three types of average are possible: arithmetic, geometric, and harmonic.

3.18.1 Arithmetic Mean

The arithmetic mean of a set of values is the quantity commonly called the mean or the average. Given a set of samples,

$$K = \{k_1, k_2, k_3, .., k_n\} \tag{3.7}$$

and corresponding non-negative weight,

$$W = \{w_1, w_2, w_3, .., w_n\} \tag{3.8}$$

the arithmetic mean is[30]

$$\bar{k}_A = \frac{\sum_1^n k_i w_i}{\sum_1^n w_i} \tag{3.9}$$

where

$\bar{k}_A$ = arithmetic mean

k_i = values of samples i

n = number of samples

w_i = weight of sample i

It is apparent that the arithmetic average is equivalent to the effective

permeability of a completely ordered system composed of n parallel layers; each layer is continuous and homogeneous with a permeability of k_i. This is the familiar "layer-cake" or ideally stratified model that is used extensively in the prediction of waterflood performance.[27]

This average is appropriate to use if the flow in the reservoir is in the direction of the bedding plane. Small, impermeable streaks will have only very little effect on the average.[28]

3.18.2 Harmonic Mean

The harmonic average of n weighted samples is given by the following expression.[29]

$$\bar{k}_H = \frac{\sum_1^n w_i}{\sum_1^n \frac{w_i}{k_i}} \tag{3.10}$$

where

$\bar{k}_H$	=	harmonic mean
k_i	=	values of samples i
n	=	number of samples
w_i	=	weight of sample i

In this case, the average is equivalent to the effective permeability of a completely ordered system in which n samples are arranged in series; again, each sample is continuous and homogeneous with a permeability of k_i. This model is quite unrealistic since, in a radial system, it consists of a series of annular regions which are concentric with the wellbore.[27]

In effect, one takes the average of the inverse of the individual k_i, then inverts the result at the end. This average is appropriate to use if the flow in the reservoir is normal to the direction of the bedding plane. Impermeable streaks will completely dominate the zonal average.[28]

3.18.3 Geometric Mean

The geometric mean is defined by the following expression.[30]

$$\bar{k}_G = \left(\prod_1^n k_i{}^{w_i}\right)^{\frac{1}{\sum_1^n w_i}} = exp\left(\frac{\sum_1^n w_i \log(k_i)}{\sum_1^n w_i}\right) \tag{3.11}$$

where

$\bar{k}_G$	=	geometric mean
k_i	=	values of samples i
n	=	number of samples
w_i	=	weight of sample i

In effect, one takes the average of the logarithms of the individual k_i, then takes the exponential at the end. This average is appropriate to use if the flow in the reservoir is partially in the direction of the bedding plane and partly normal to it. Impermeable streaks will have some influence but not completely kill off the zonal average.[28]

CHAPTER IV
SIMULATION MODEL

4.1 Reservoir Model

A single well model is used in this study to simulate pressure response of a well located in a reservoir with thinly bedded laminated shale layers by using ECIPSE black oil simulator simulating 3 different tests (single probe WFT, dual packer WFT, and conventional well test) in different scenarios. Then, the pressure response is used for horizontal and vertical permeability interpretation using Ecrin. After that, interpreted results as well as analytical results from derivative plots are analyzed and compared among each case.

The single well model is a circular boundary, radial grid model with dimension of 100 x 20 x 31 grid blocks in the r, θ, and z direction, respectively. The size of grid blocks is increasing logarithmically, in all directions, starting from small grid at the center of well bore, which is the probe location, towards the reservoir boundary in the r-direction, the opposite side of the probe location in θ-direction, and the top/bottom of reservoir in the z-direction.

Initially, radial and theta absolute porosity and permeability for clean sand are input as 0.18 and 10 mD, respectively, with absolute permeability anisotropy (k_v/k_h) of 0.1. Therefore, vertical absolute permeability is equal to 1 mD. Thinly bedded laminated shale feature is simulated by assigning low porosity and permeability values (porosity= 0.00018, k_h=0.01 mD, and k_v=0.001 mD) to various specific grid blocks representing difference in thin bedded shale properties such as shape, size, thickness for all scenarios. In any case, there is a limitation in defining shape of laminated shale barrier in this study since shape of shale barrier can be constructed from the radial grid shape only. The other detailed reservoir parameters and conditions are depicted in Table 4.1.

Table 4.1: Reservoir parameters

Reservoir model		
Geometry	radial	-
Boundary	no flow	-
Reservoir radius	1000	feet
Datum depth	8110	feet
Thickness	20	feet
Pressure at datum depth	5000	psia
Fluid properties at surface condition		
Oil	51.457	lb/cu.ft
Gas	0.0437	lb/cu.ft
Water	63.029	lb/cu.ft
Gas/Oil ratio		
Gas/Oil ratio, Rs	0	scf/bbl
Bubble point pressure, P_b	1847.9	psia
Rock properties		
Reference pressure	3450	psia
Rock compressibility	1.05E-06	psia
Well information		
Datum depth	8120	feet
Wellbore ID	0.5	feet
Clean sand properties		
Absolute k_h	10.000	md
Absolute k_v	0.100	md
Effective k_h	8.09	md
Effective k_v	0.809	md
k_v/k_h	0.1	-

Table 4.2 shows reservoir fluid properties which are formation volume factors and viscosities versus depths that are used in this study.

Table 4.2: PVT data

Pressure (psia)	FVF (rb/stb)	Viscosity (cp)
1847.9	1.3129	0.34932
2005.6	1.3088	0.35453
2163.2	1.3053	0.36022
2320.8	1.3023	0.36636
2478.4	1.2997	0.37293
2636.0	1.2974	0.37992
2793.6	1.2954	0.38730
2951.2	1.2935	0.39507
3108.8	1.2919	0.40319
3266.4	1.2904	0.41167
3424.0	1.2891	0.42049
3581.6	1.2879	0.42964
3739.2	1.2868	0.43911
3896.8	1.2857	0.44888
4054.4	1.2848	0.45896
4212.0	1.2839	0.46932
4369.6	1.2831	0.47996
4527.2	1.2824	0.49088
4684.8	1.2816	0.50206
5000.0	1.2804	0.52515

Figure 4.1 shows sample of shale barrier grid cell assignment used in this study. The blue grid cells represent shale barriers around the well bore while the red grid cells represent clean sand.

Top view – 1 shale barrier

Side view – 1 shale barrier

Top view – 2 shale barrier

Side view – 2 shale barrier
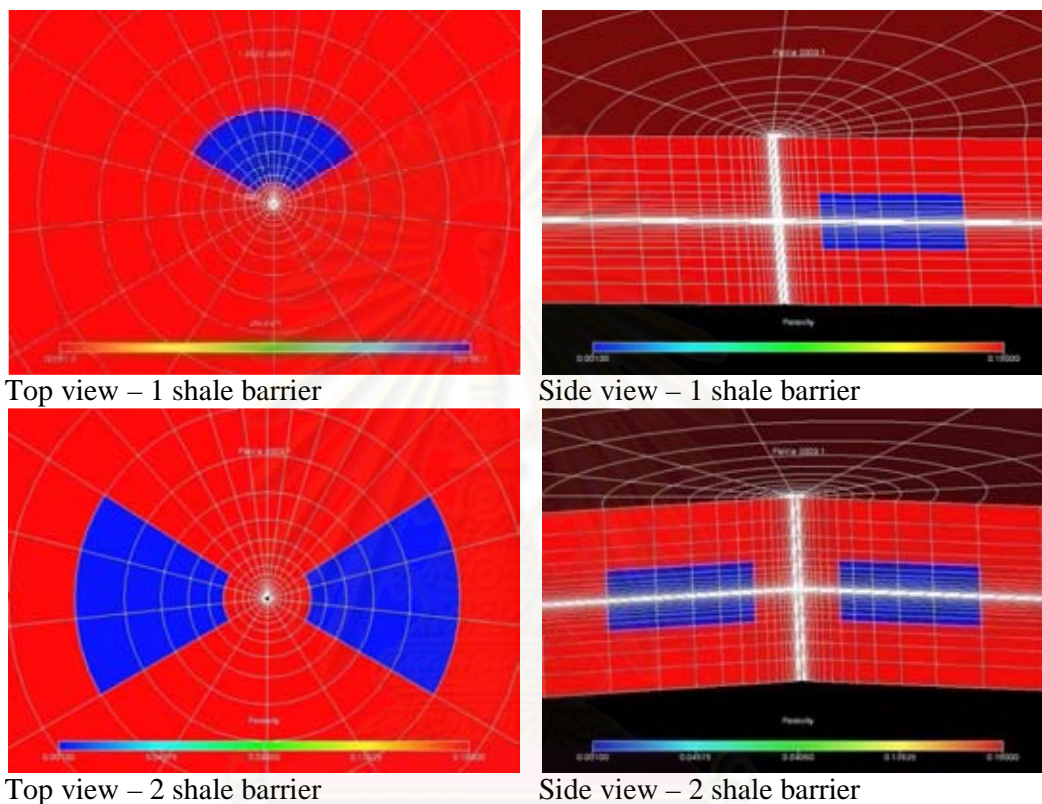
Figure 4.1: Sample of shale barrier

The fluid flow area is calculated from probe's flow area for single probe WFT. For dual packer WFT and conventional well test, the flow areas are calculated from open interval multiplying well bore circumference. The open intervals are 1 meter (3.28084 feet) for dual packer WFT and 20 feet for the conventional well test based on the assumption that the reservoir is fully perforated. The flow area and flow rate of each test type are shown in Table 4.3.

Table 4.3: Flow area

Test type	Flow area (sq.in.)	Flow rate (stb/d)
Single probe	0.15	0.5
Dual packer	679.00	15.0
Well test	4525.71	80.0

Figure 4.2 depicts the top view and side view of flow geometries for single probe WFT and dual packer WFT. For single probe WFT, the probe and the packer is connected to wellbore only at side. While for dual packer WFT, the packers are connected around wellbore, similar to conventional well test.

Single probe WFT   Dual packer WFT
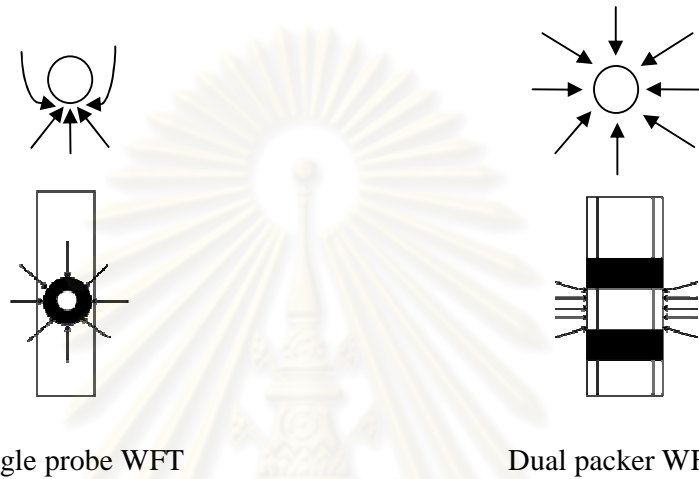
Figure 4.2: Flow geometry of single probe WFT and dual packer WFT

Table 4.4 shows the grid cell dimension in the r, θ, and z direction for single probe WFT and well test. For single probe, the grid cell that represents the single probe's flow area is represented by grid cell (1, 1, 1). For well test, the connection between the wellbore and the reservoir is represented by grid cell (1, 1-20, 1-32).

Table 4.4: Single probe wireline formation tester (WFT) and well test grid

Radial direction		Theta direction		Vertical direction	
Grid No.	Δr (ft)	Grid No.	$\Delta\theta$	Grid No.	Δz (ft)
1	0.03227	1	7.8029	1	2.394
2	0.05877	2	10.3016	2	1.829
3	0.07931	3	11.8367	3	1.398
4	0.10702	4	13.6006	4	1.068
5	0.14441	5	15.6273	5	0.816
6	0.19487	6	17.956	6	0.623
7	0.26296	7	20.6318	7	0.476
8	0.35484	8	23.7062	8	0.364
9	0.47883	9	27.2389	9	0.278
10	0.64614	10	31.2979	10	0.212
11	0.87192	11	31.2979	11	0.162
12	1.17658	12	27.2389	12	0.124
13	1.58770	13	23.7062	13	0.095
14	2.14247	14	20.6318	14	0.072
15	2.89109	15	17.956	15	0.055
16	3.90128	16	15.6273	16	0.032
17	5.26446	17	13.6006	17	0.032
18	7.10396	18	11.8367	18	0.055
19	9.58621	19	10.3016	19	0.072
20 - 100	12.93580	20	7.8029	20	0.095
Total	1084.684775	Total	359.9998	21	0.124
				22	0.162
				23	0.212
				24	0.278
				25	0.364
				26	0.476
				27	0.623
				28	0.816
				29	1.068
				30	1.398
				31	1.829
				32	2.394
				Total	20.000

Table 4.5 shows the grid cell dimension in the r, θ, and z direction for dual packer WFT. The connection between the wellbore and the reservoir is represented by grid cell (1, 1-20, 1).

Table 4.5: Dual packer wireline formation tester (WFT) grid

Radial direction		Theta direction		Vertical direction	
Grid No.	Δr (ft)	Grid No.	$\Delta\theta$	Grid No.	Δz (ft)
1	0.03227	1	7.8029	1	2.394
2	0.05877	2	10.3016	2	1.829
3	0.07931	3	11.8367	3	1.398
4	0.10702	4	13.6006	4	1.068
5	0.14441	5	15.6273	5	0.816
6	0.19487	6	17.956	6	0.623
7	0.26296	7	20.6318	7	3.267
8	0.35484	8	23.7062	8	0.476
9	0.47883	9	27.2389	9	0.623
10	0.64614	10	31.2979	10	0.816
11	0.87192	11	31.2979	11	1.068
12	1.17658	12	27.2389	12	1.398
13	1.58770	13	23.7062	13	1.829
14	2.14247	14	20.6318	14	2.394
15	2.89109	15	17.956	Total	20.000
16	3.90128	16	15.6273		
17	5.26446	17	13.6006		
18	7.10396	18	11.8367		
19	9.58621	19	10.3016		
20 - 100	12.93580	20	7.8029		
Total	1084.684775	Total	359.9998		

Figure 4.3 depicts the reservoir grid model with a single well in the middle.
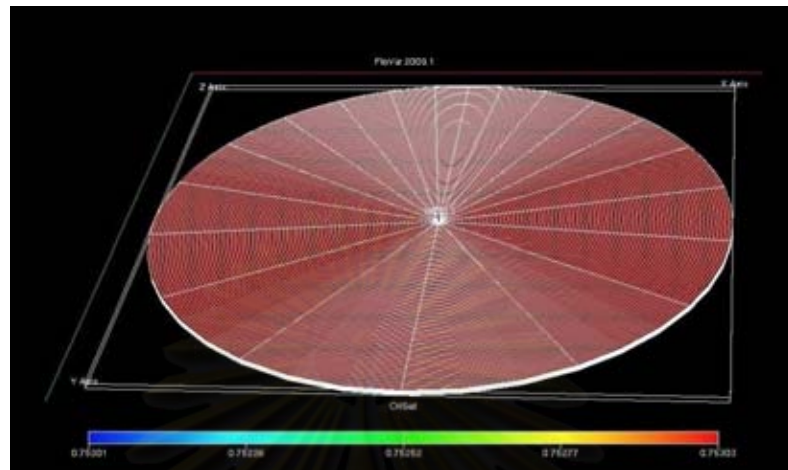
Figure 4.3: Reservoir grid model

Figure 4.4 shows the oil and water relative permeability curves at different water saturation that are used in this study. At initial, the water saturation is 0.25 and the oil relative permeability is 0.809.
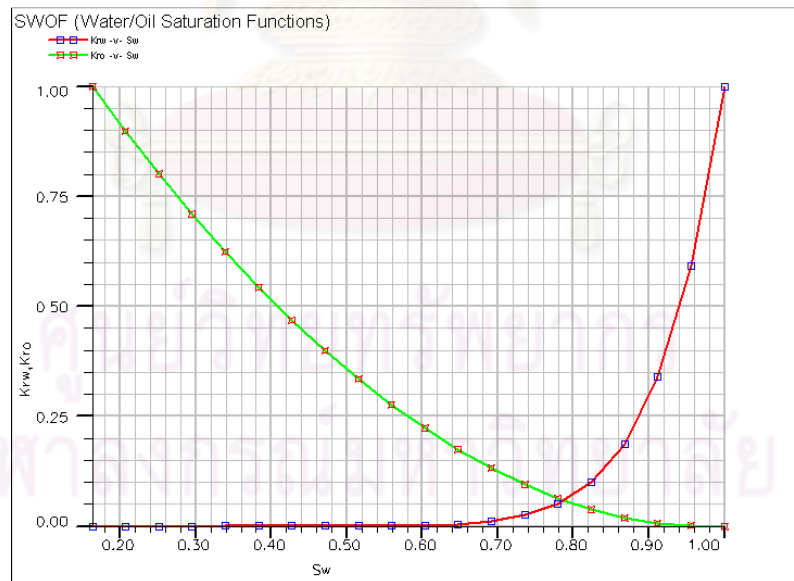
Figure 4.4: Water-oil saturation table

4.2 Average Permeability Calculation

There are different configurations of impermeable shale barrier in this study. The method used for calculating average permeability for comparison is done by combining 2 methods as following.

First, the arithmetic method is used for grid cells that have different permeabilities in the vertical direction or between layers. Second, the harmonic method is used for grid cells that have different permeabilities in the horizontal direction. The process can be described by Figure 4.5. Note that, the grid cells used in calculation are only the grid cells under radius of investigation of each test.
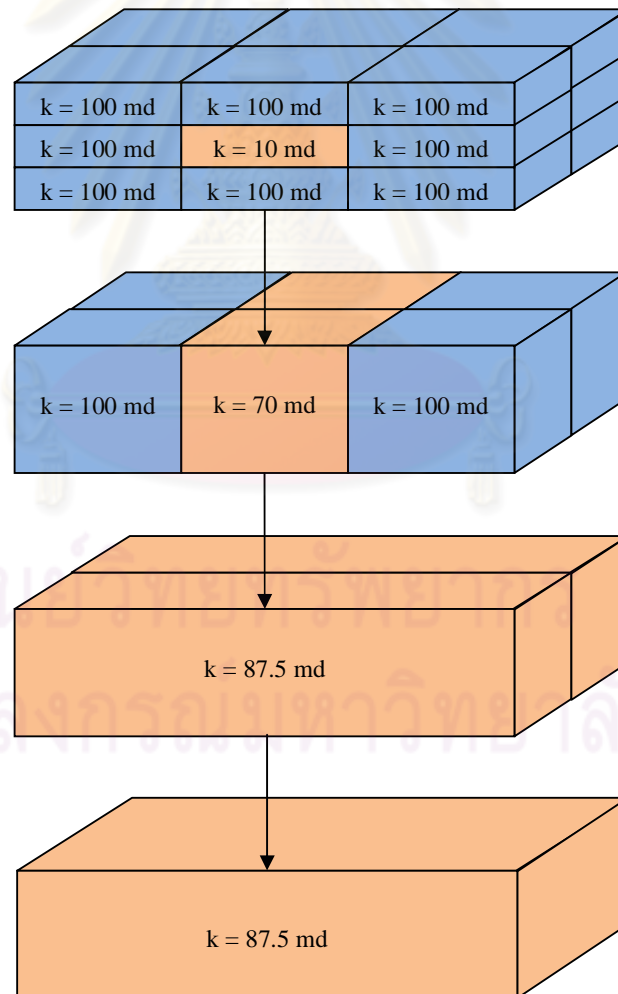
Figure 4.5: Average permeability calculation

For radial grid, the calculation in this study is a bit different since the shale barriers are not complete circles in all case. So, the θ- direction needs to be taken into account for the calculation as well. The calculation is started in the same way as the method for Cartesian block, except that each section in the θ- direction would be averaged using the harmonic method before using the harmonic method again in the r-direction.

CHAPTER V
SIMULATION RESULTS AND ANALYSIS

5.1 Base case

A base case is chosen as a reference example for the simulation of shale barrier. Additionally, the base case is used to confirm that the theoretical model can be utilized to study the effect of shale barriers on wireline formation testing performance and apply to the actual reservoir. Initially, radial and theta permeability is input as 10 mD with absolute permeability anisotropy (k_v/k_h) of 0.1. Therefore, vertical absolute permeability is equal to 1 mD. In this study, the fluid drawdown rate, buildup rate and duration are different between each type of test as single probe test takes 30 minutes drawdown with a flow rate of 0.5 stb/day. Dual packer test takes 60 minutes drawdown with a flow rate of 15 stb/day. Well test takes 240 minutes drawdown with a flow rate of 80 stb/day. The buildup period is varied for different scenarios. In fact, the testing period of an actual wireline formation test is very small, but, in our theoretical model, longer period is used in order to define all possible flow regimes as well as to allow us to see the completion of pressure response effect from laminated shale barrier. However, in most of the cases, the same buildup period is used to compare among 3 test types except for the case that buildup extension is needed. A schematic reservoir description for base case for each test type is shown in Figure 5.1, describing single probe WFT, dual packer WFT, and conventional well test, respectively from left to right.
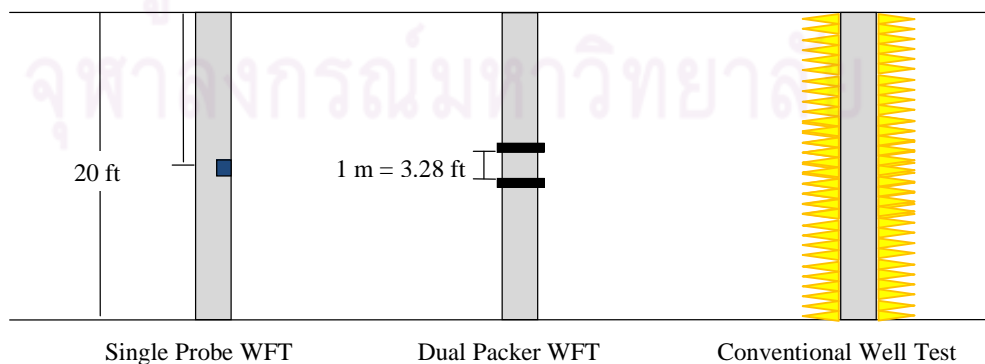
Figure 5.1: Base case (no shale barrier)

From reservoir simulation, the pressure responses during drawdown and

buildup tests of the base case are shown in Figure 5.2-a, 5.2-b, and 5.2-c. After that, the result can be interpreted by using well test interpretation software as can be seen in Figure 5.3-a, 5.3-b, and 5.3-c.
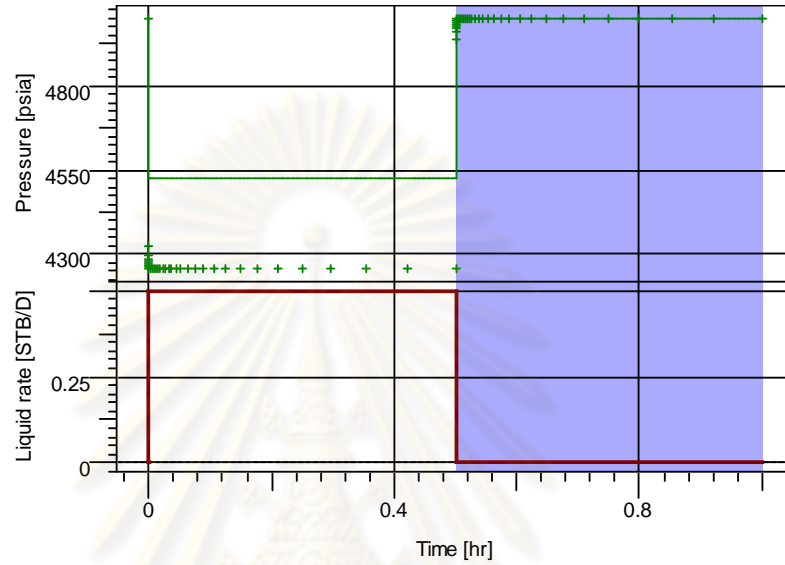
Figure 5.2-a: Pressure history of single probe WFT's base case
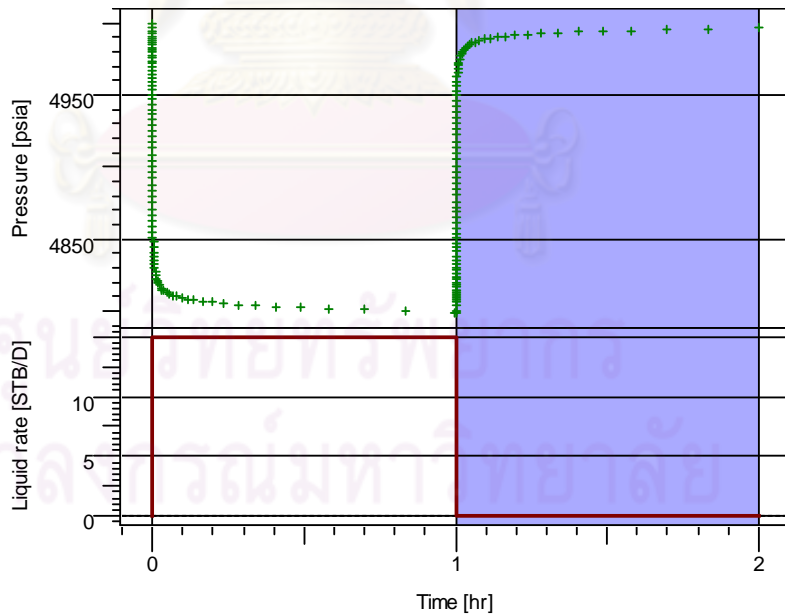
Figure 5.2-b: Pressure history of dual packer WFT's base case
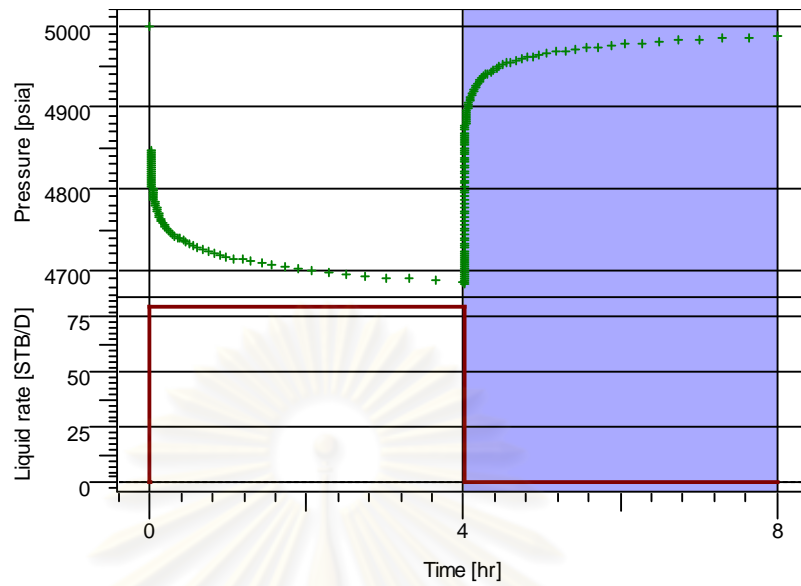
Figure 5.2-c: Pressure history of well test's base case

Single Probe
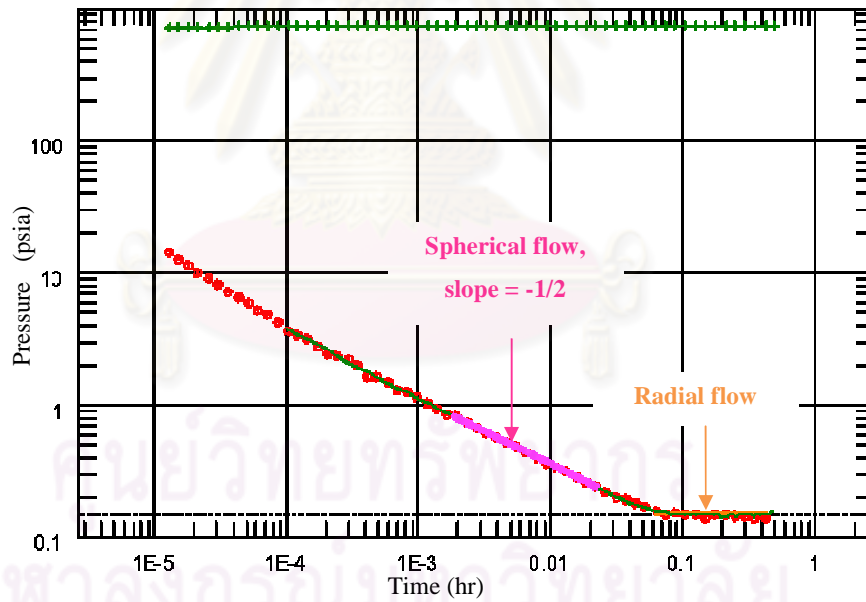
Figure 5.3-a: Single probe WFT derivative plot of base case
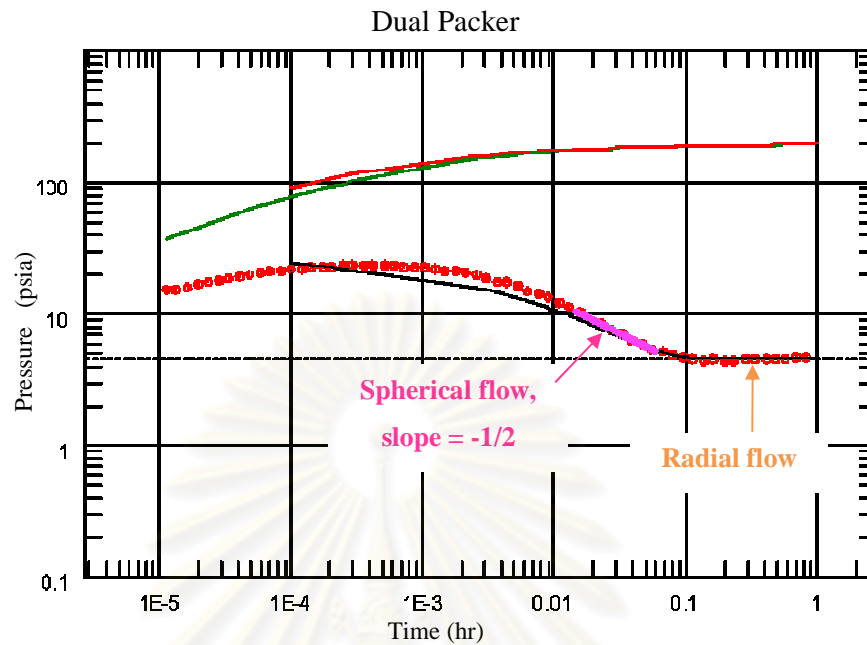
Dual Packer

Figure 5.3-b: Dual packer WFT derivative plot of base case
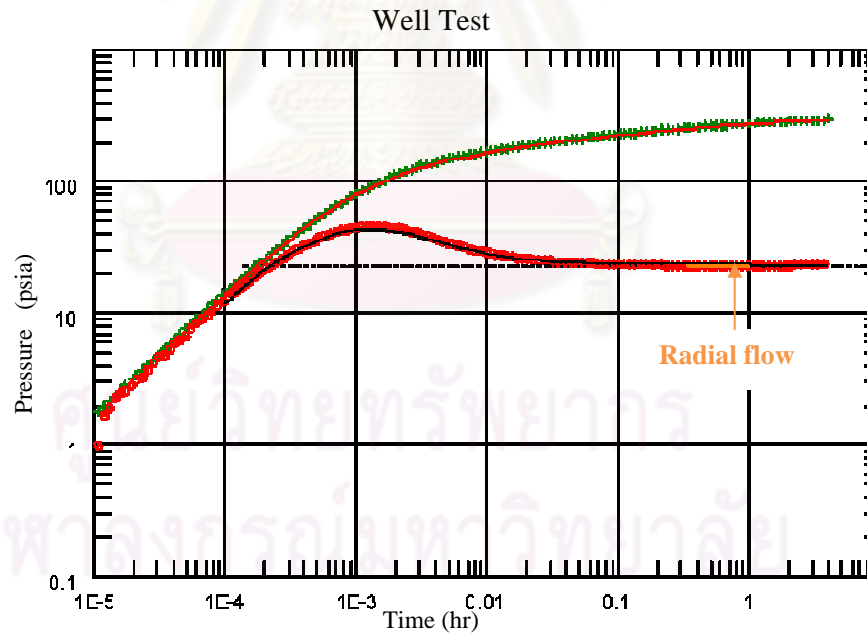
Well Test

Figure 5.3-c: Well test derivative plot of base case

As can be seen in Figure 5.3-a and 5.3-b, the spherical flow model can be matched to the curve at time between 0.01 hr to 0.1 hr. At late times, after 0.2 hr, the radial flow model can be matched to the curve. From Figure 5.3-a, 5.3-b and 5.3-c, the regression show good matched on log-log diagnostic plot.

For base case of single probe WFT and dual packer WFT, the derivative plot of single probe starts with a spherical flow, followed by infinite acting radial flow. This allows us to calculate the vertical permeability from spherical flow and horizontal permeability from the infinite acting radial flow. For well test, the flow starts without spherical flow due to full perforation; there is only infinite acting radial flow. This allows us to calculate horizontal permeability from the infinite acting radial flow only. In addition, the derivative plot of dual packer and well test shows the wellbore storage effect before the spherical flow and infinite acting radial flow. In actual test data, the wellbore storage effect also occurs in the case of single probe.

Table 5.1 shows the comparison between the clean sand's effective permeability, as the input of ECLIPSE simulator and the interpreted effective permeability as output from Ecrin. The estimated horizontal permeabilities from all tests are consistent with less than 5% deviation from the actual value. The estimated vertical permeability from dual packer WFT is also consistent with a small deviation while the estimated vertical permeability from single probe WFT is overestimated with 35.60% error.

Table 5.1: Base case's interpreted horizontal and vertical permeabilities

Test type	k_h			k_v		
	Input (md)	Interpreted (md)	Error (%)	Input (md)	Interpreted (md)	Error (%)
Single probe	8.09	7.73	-4.49	0.809	1.10	35.60
Dual packer	8.09	7.90	-2.38	0.809	0.81	0.54
Well test	8.09	8.19	1.20	0.809	N/A	N/A

The thinly laminated shale layers in this study are varied by distance from the well bore, shape, and amount. For referential purpose in this thesis, the red grid represents clean sand while the blue grid represents laminated shale layer. In all cases, we assume the laminated shale layer is in the middle of the reservoir in the same level as the probe position.

5.2 Effect of distance from wellbore to shale barrier

In this case study, the objective is to investigate the effects of distance between wellbore and shale barrier on pressure derivatives and estimated permeabilities by varying the distance and fixing other parameters such as amount of shale barrier, shape of shale barrier, and dimension of shale barrier (Δr, $\Delta \theta$, and Δz). However, when the distance between shale barrier and the wellbore is changed, it also affects the circumference of the shale barrier. As the distance increases, the total volume grid cells that are used for assigning shale barrier will be larger than those ones located near the wellbore. So, the volume of shale barrier cannot be fixed in these cases.

5.2.1 Case I: Shale distance from wellbore = 4.4 ft

Figure 5.4 exhibits the shale configuration of case I. The upper picture shows the top view and the cross-sectional view of the grid model. The lower picture depicts the side view of the reservoir model with a wellbore and a shale barrier located 4.4 ft away from the wellbore. The following is the dimension of the shale barrier.

Shale dimension: Δr = 15.8 ft, $\Delta \theta$ = 136.3 °, Δz = 5.8 ft
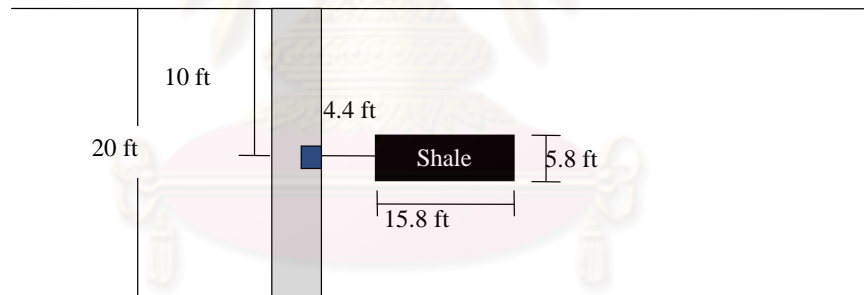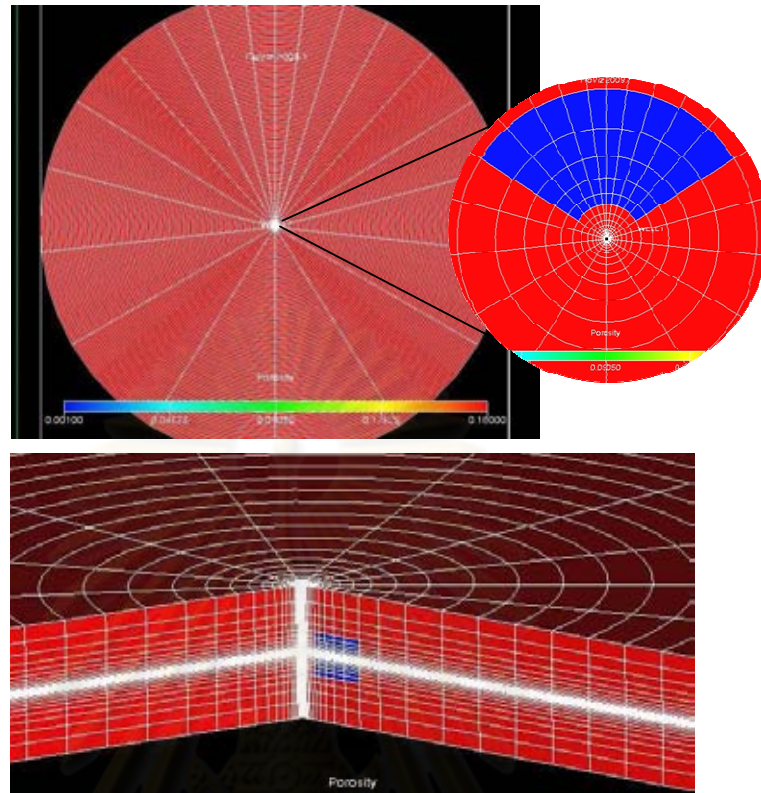
Figure 5.4: Shale configuration of case I

Figure 5.5-a, 5.5-b and 5.5-c show pressure responses simulated from a reservoir simulator for single probe, dual packer and well test, respectively.
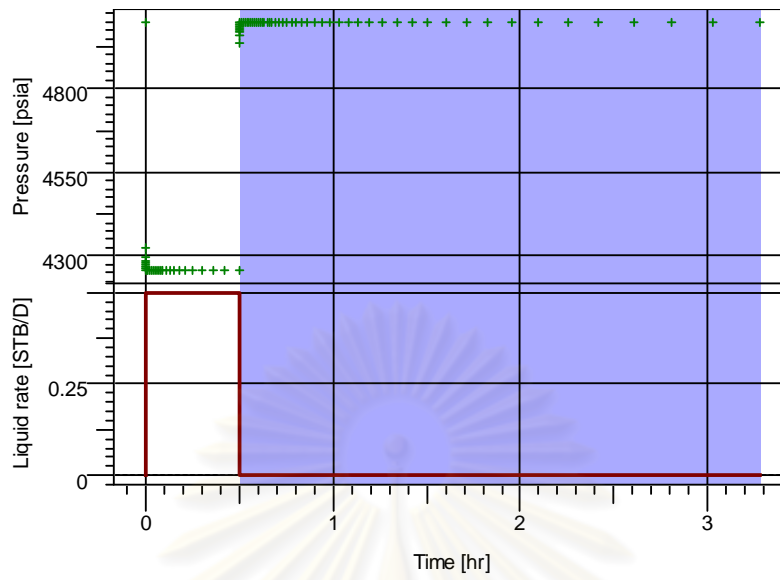
Figure 5.5-a: Pressure history of single probe WFT for case I
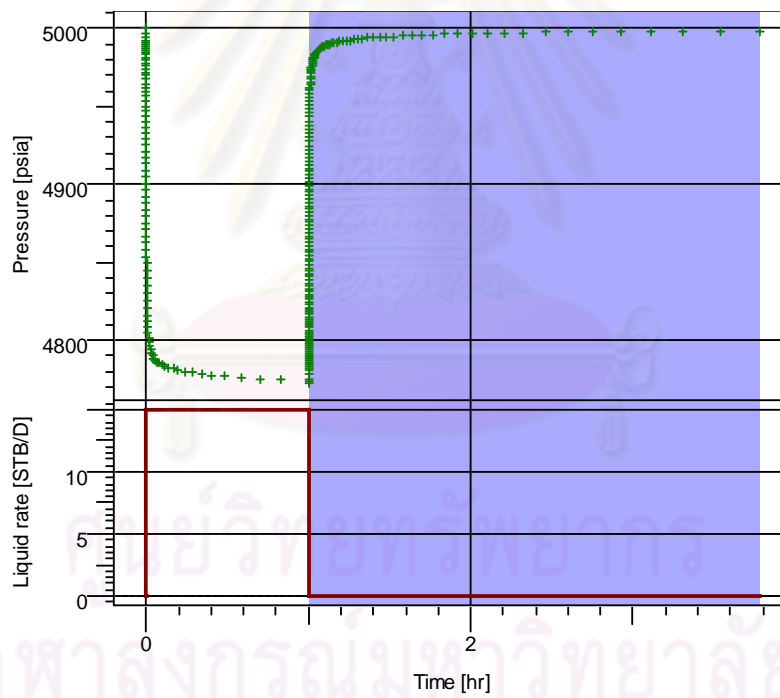
Figure 5.5-b: Pressure history of dual packer WFT for case I
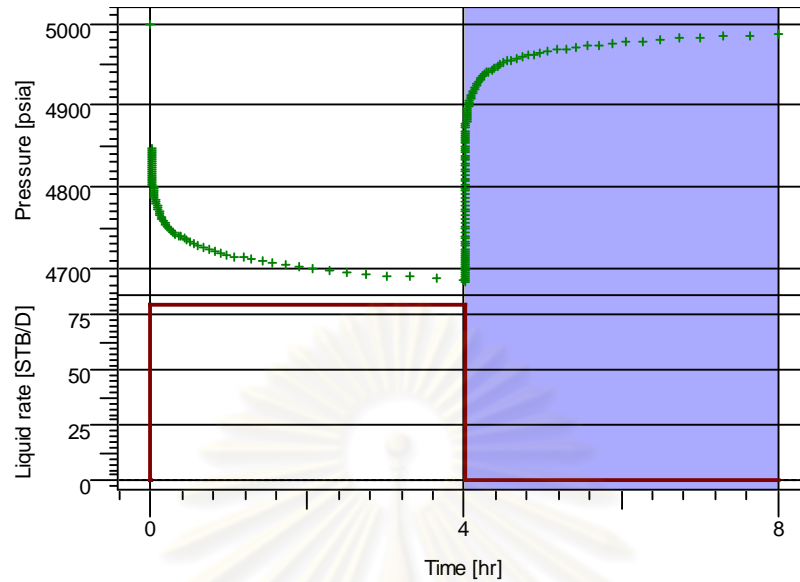
Figure 5.5-c: Pressure history of well test for case I

The draw down period for single probe WFT, dual packer WFT and well test is 30 minutes, 60 minutes, and 240 minutes, orderly. Although, the buildup period is by default the same as the draw down period, it is, sometimes, extended in order to allow us to see the whole effect of laminated shale layers on derivative plots, especially when the distance of shale from the well bore is long or when the size of the shale barrier is large.
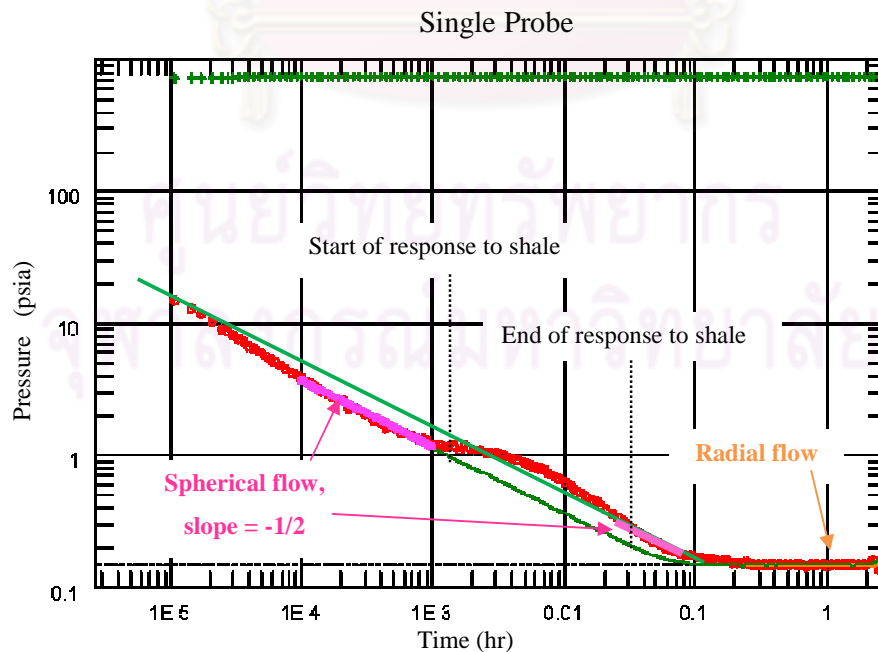
Figure 5.6-a: Single probe WFT derivative plot of case I

Dual Packer

Figure 5.6-b: Dual packer WFT derivative plot of case I

Well Test

Figure 5.6-c: Well test derivative plot of case I
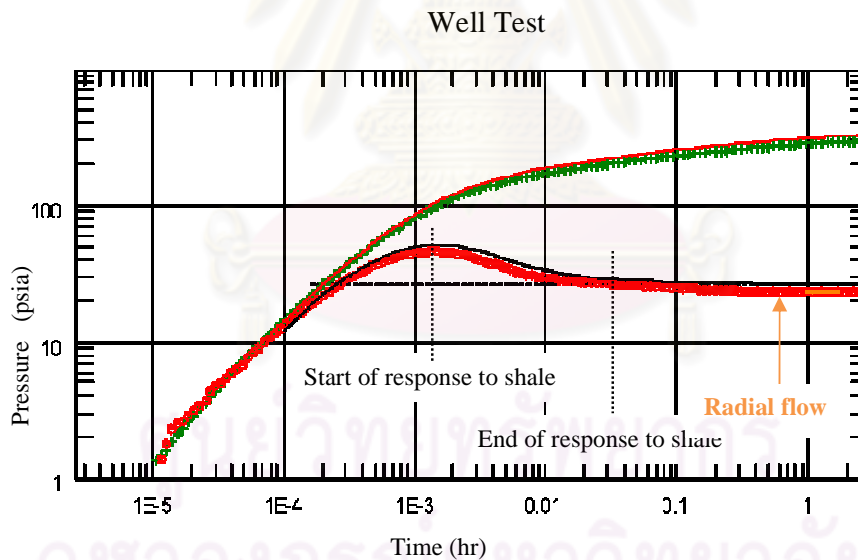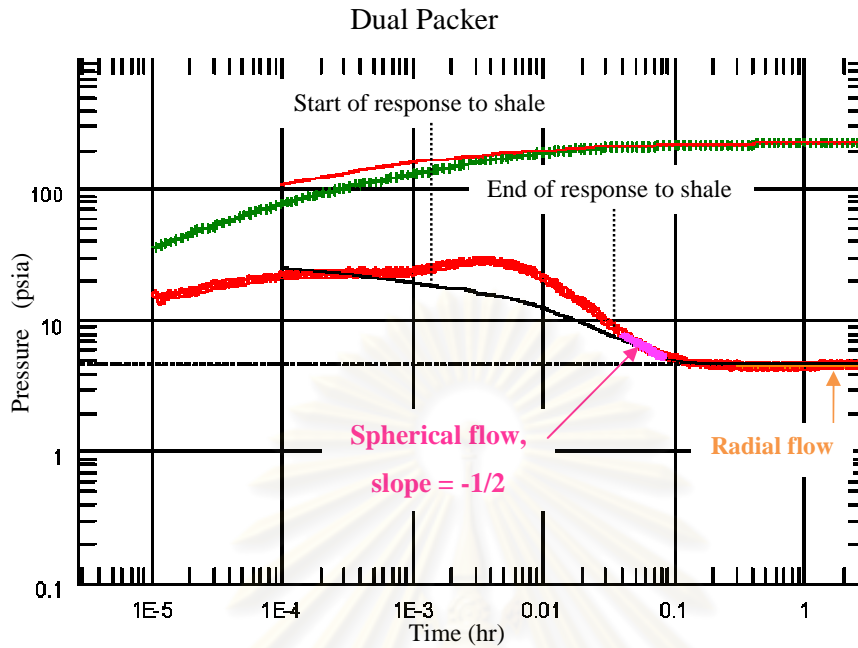
As can be seen in Figures 5.6-a, and 5.6-b, the spherical flow model can be matched to the curve at time before 0.1 hr. At late times, after 0.2 hr, the radial flow model can be matched to the curve for all plots (Figure 5.6-a, 5.6-b, and 5.6-c). The effect of the shale barrier can be seen as a hump in the derivative plots. From Figure 5.6-a and 5.6-b, the hump appears during the spherical flow regime. From Figure 5.6-

c, the hump seems to be rather between well bore storage effect and radial flow regime. For single probe WFT, it is possible to calculate the vertical permeability from 2 positions, before and after the occurrence of hump in the derivative plot as shown in Figure 5.6-a. In this study, the spherical line that is taken for estimating the vertical permeability from single probe WFT's derivative plot is always the latter one, when possible, in order to take the effect of shale barrier into account.

Among 3 derivative plots, it is possible to identify the existence of shale barrier from the occurrence of hump in the derivative plots of single probe WFT and dual packer WFT. For well test derivative plots, it is difficult to identify the existence of shale barrier as the magnitude of the hump is small and unnoticeable. Table 5.2 shows a comparison of different shale volume calculations and the average permeability, which depends on the radius of investigation of each test type.

Table 5.2: Shale volume and average permeability calculation for case I

	Single probe	Dual packer	Well test
Draw down period (min)	30	60	240
Build up period (min)	167	167	240
Radius of investigation (ft)	186	189	234
Volume of investigation (ft^3)	2,174,606	2,245,320	3,441,806
Volume of shale (ft^3)	2,729	2,729	2,729
Volume of sand (ft^3)	2,171,877	2,242,591	3,439,077
V_{sh} (%)	0.13	0.12	0.08
Average permeability, k_h (md)	7.81	7. 82	7.87

The drawdown periods are different for the three test types but the buildup periods are equal for single probe and dual packer. So, the radiuses of investigation for single probe and dual packer are about the same. This also results in almost similar volume of investigation, V_{sh} and average permeability for single probe and dual packer. However, since the buildup period of well test is longer than those of the others, the radius of investigation, V_{sh} and the average permeability of well test are slightly different.

Table 5.3: Interpreted horizontal and vertical permeabilities compared to clean sand and average permeability for case I.

| Test type | Compared with clean sand | | | | | |
| | k_h | | | k_v | | |
	Input (md)	Interpreted (md)	Error (%)	Input (md)	Interpreted (md)	Error (%)
Single probe	8.09	7.68	-5.10	0.809	0.74	-9.0
Dual packer	8.09	7.69	-4.98	0.809	0.60	-26.3
Well test	8.09	8.15	0.70	0.809	N/A	N/A
Test type	Compared with average permeability					
	k_h			k_v		
	Calculated (md)	Interpreted (md)	Error (%)	Calculated (md)	Interpreted (md)	Error (%)
Single probe	7.81	7.68	-1.71	0.78	0.74	-5.7
Dual packer	7.82	7.69	-1.63	0.78	0.60	-23.7
Well test	7.87	8.15	3.57	0.79	N/A	N/A

Table 5.3 shows the estimated horizontal and vertical permeabilities from pressure transient interpretation software, Ecrin, compared with the clean sand's effective permeability, which is input of ECLIPSE simulator, and also compared with the calculated averaged permeability from Table 5.2. The estimated horizontal permeabilities from the three tests are still consistent with the input with less than 6% error since the volume of shale is small compared to the volume of investigation and the effect of shale occurs in the spherical flow which mainly affects the vertical permeability estimation. The estimated vertical permeability from single probe WFT is not overestimated like in the base case and becomes closer to clean sand's and average permeability due to permeability reduction by shale barrier. However, the estimated vertical permeability from dual packer WFT is oppositely underestimated with almost 30% error.

5.2.2 Case II: Shale distance from wellbore = 11 ft

Figure 5.7 exhibits the shale configuration of case II. The upper picture shows the top view and the cross-sectional view of the grid model. The lower picture depicts the side view of the reservoir model with a wellbore and a shale barrier located 11 ft away from the wellbore. The following is the dimension of the shale barrier.

Shale dimension: $\Delta r = 16.3$ ft, $\Delta\theta = 136.3$ °, $\Delta z = 5.8$ ft
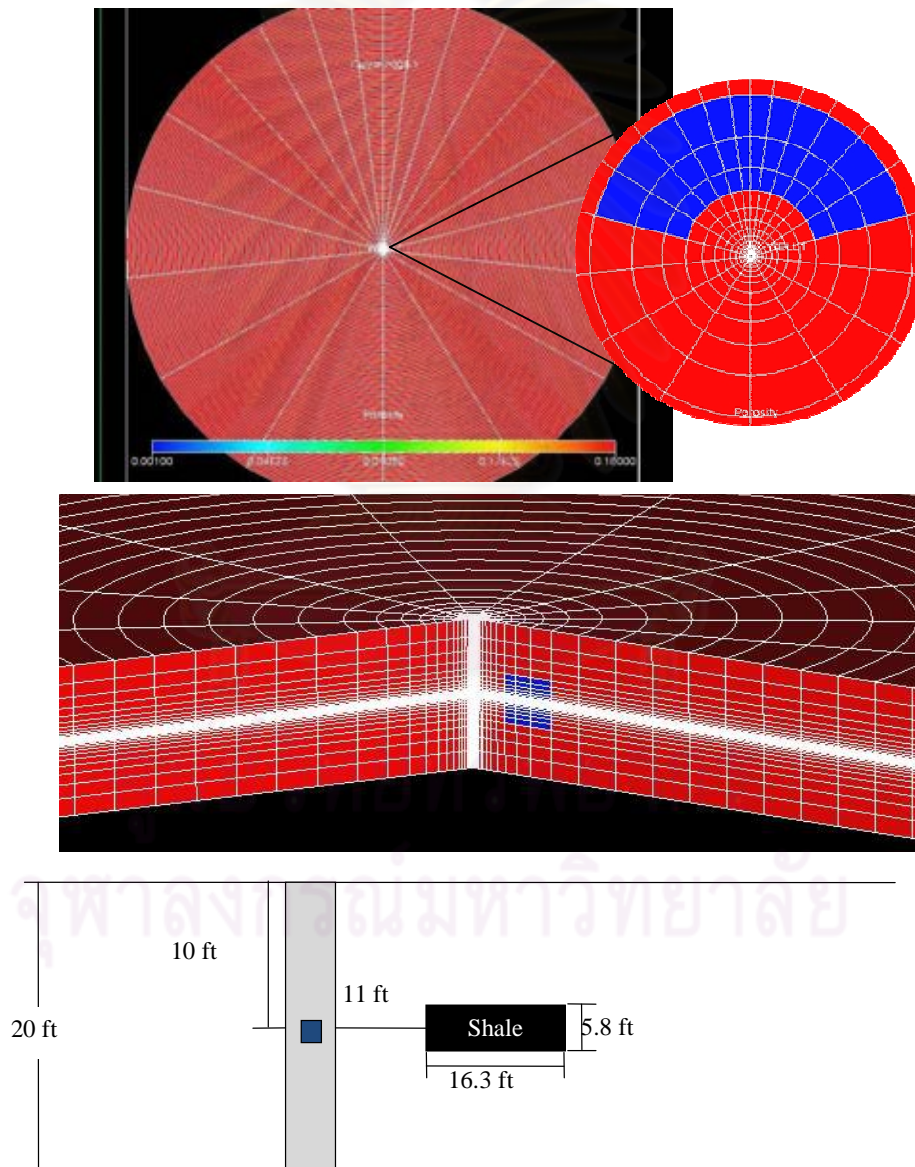
Figure 5.7: Shale configuration of case II

Figure 5.8-a, 5.8-b and 5.8-c show pressure responses simulated from a reservoir simulator for single probe, dual packer and well test, respectively.
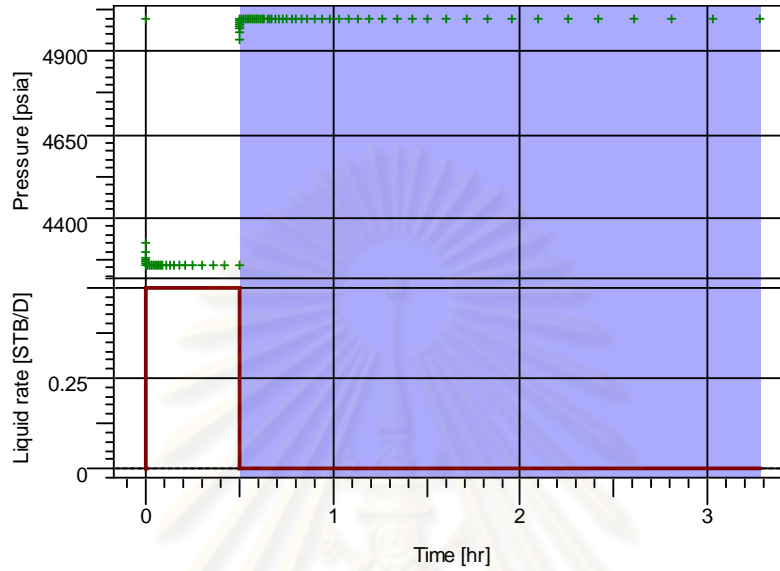
Figure 5.8-a: Pressure history of single probe for case II
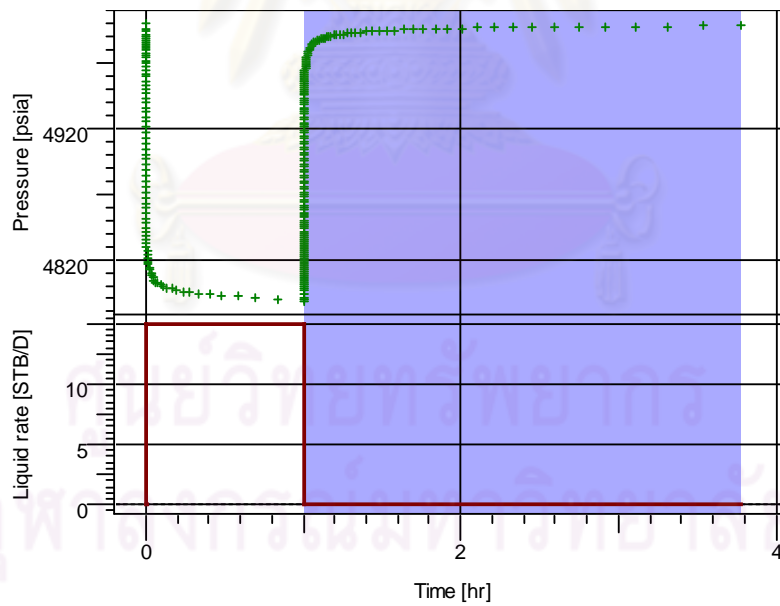
Figure 5.8-b: Pressure history of dual packer for case II
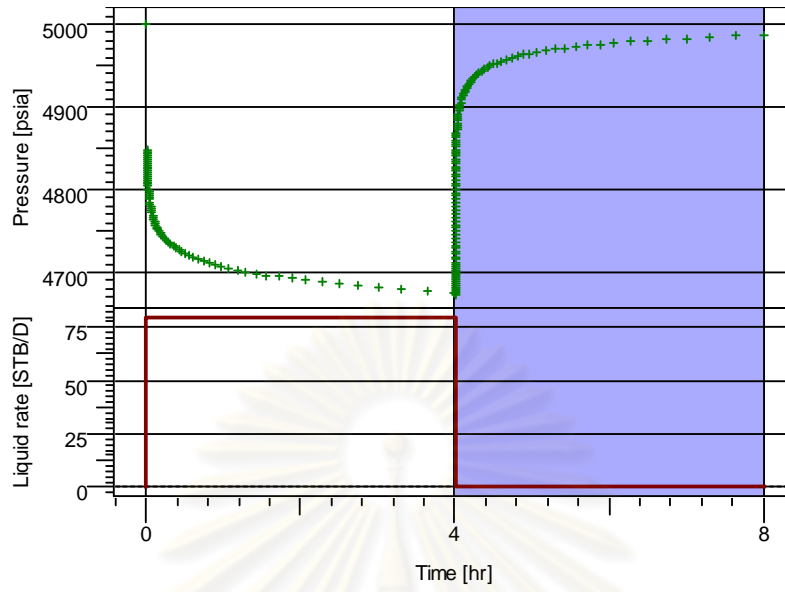
Figure 5.8-c: Pressure history of well test for case II

Single Probe
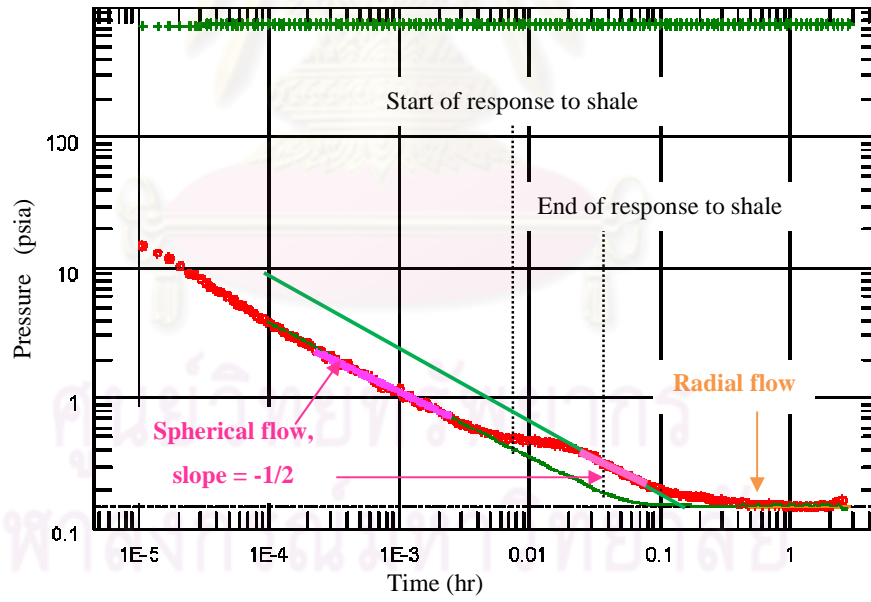
Figure 5.9-a: Single probe WFT derivative plot of case II
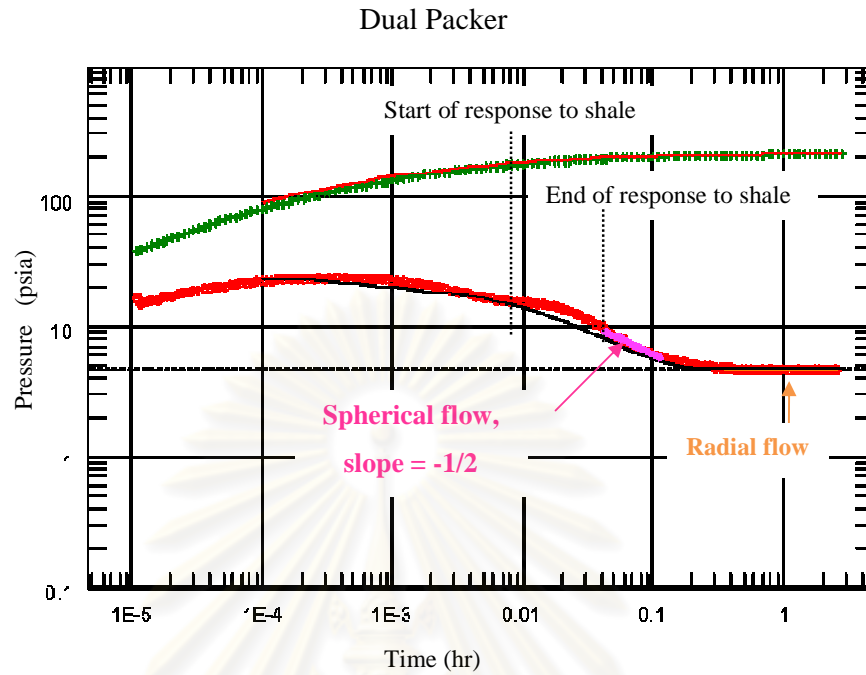
Dual Packer

Figure 5.9-b: Dual packer WFT derivative plot of case II
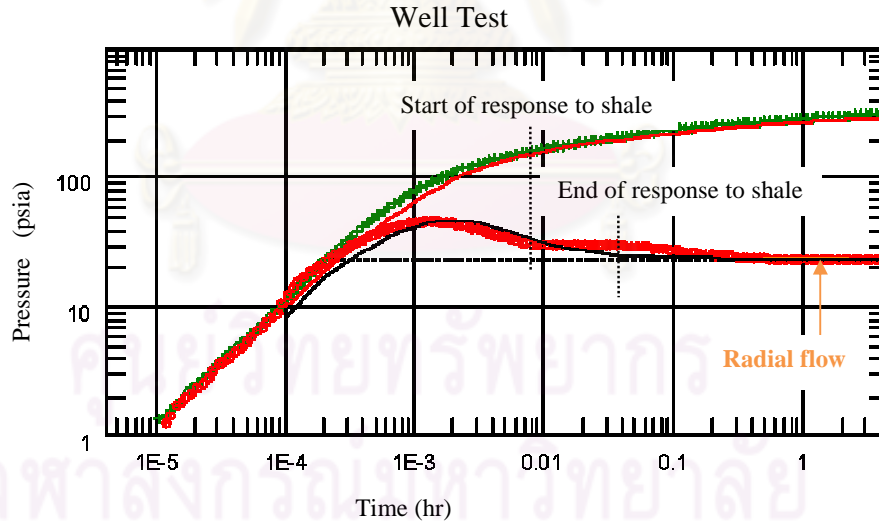
Well Test

Figure 5.9-c: Well test derivative plot of case II

As can be seen in Figure 5.9-a, and 5.9-b, the spherical flow model can be matched to the curve at time between 0.01 hr to 0.1 hr. At late times, after 0.2 hr, the radial flow model can be matched to the curve for all plots (Figure 5.9-a, 5.9-b, and 5.9-c). The regression shows good match on log-log diagnostic plots between data and

the model. For single probe WFT (Figure 5.9-a), the hump occurs at the time between the end of spherical flow and the beginning of the radial flow regime. For dual packer WFT (Figure 5.9-b), when the shale barrier moves a bit further away from the well bore, the hump still occurs during the spherical flow. For conventional well test (Figure 5.9-c), the hump seems to be between the wellbore storage effect and radial flow regime, but most of its effect occurs during radial flow regime. The magnitude of the hump in this case is smaller than that in case I due to longer distance from the well bore to shale barrier. For well test derivative plot, it is more obvious to notice the hump than in the previous case. Table 5.4 shows a comparison of different shale volumes and the average permeabilities which depend on the radius of investigation of each test type.

Table 5.4: Shale volume and average permeability calculation for case II

	Single probe	Dual packer	Well test
Draw down period (min)	30	60	240
Build up period (min)	167	167	240
Radius of investigation (ft)	184	192	233
Volume of investigation (ft^3)	2,128,091	2,221,623	3,412,451
Volume of shale (ft^3)	4,382	4,382	4,382
Volume of sand (ft^3)	2,123,710	2,217,241	3,408,070
V_{sh} (%)	0.21	0.20	0.13
Average permeability, k_h (md)	7.80	7.81	7.86

The drawdown periods are different for the three test types but the buildup periods are equal for single probe and dual packer. So, the radiuses of investigation for single probe and dual packer are about the same. This also results in almost similar volume of investigation, V_{sh} and average permeability for single probe and dual packer. However, since the buildup period of well test is longer than those of the others, the radius of investigation, V_{sh} and the average permeability of well test are slightly different.

Table 5.5: Interpreted horizontal and vertical permeabilities compared to clean sand permeability and average permeability for case II

| Test type | Compared with clean sand | | | | | |
| | k_h | | | k_v | | |
	Input (md)	Interpreted (md)	Error (%)	Input (md)	Interpreted (md)	Error (%)
Single probe	8.09	7.50	-7.33	0.809	0.47	-41.6
Dual packer	8.09	7.62	-5.84	0.809	0.43	-47.2
Well test	8.09	8.15	0.70	0.809	N/A	N/A
Test type	Compared with average permeability					
	k_h			k_v		
	Calculated (md)	Interpreted (md)	Error (%)	Calculated (md)	Interpreted (md)	Error (%)
Single probe	7.80	7.50	-3.87	0.78	0.47	-39.4
Dual packer	7.81	7.62	-2.41	0.76	0.43	-45.2
Well test	7.86	8.15	3.66	0.79	N/A	N/A

Table 5.5 shows that the estimated horizontal permeabilities are more deviated from those in case I for single probe and dual packer due to the fact that the volume of shale barrier is increased. Even though, the estimated horizontal permeabilities contain more error than the ones in case I, the estimated horizontal permeabilities are still consistent with 10% deviation. In contrast, the estimated vertical permeabilities are highly underestimated with up to 50% error. Especially for single probe, the estimation error increases highly in this case. The reason is that the estimation is affected by the effect of shale barrier occurs are detected at period closer to the spherical flow regime than that in case I.

5.2.3 Case III: Shale distance from wellbore = 27.3 ft

Figure 5.10 exhibits the shale configuration of case III. The upper picture shows the top view and the cross-sectional view of the grid model. The lower picture depicts the side view of the reservoir model with a wellbore and a shale barrier located 27.3 ft away from the wellbore. The following is the dimension of the shale barrier.

Shale dimension: Δr = 22.5 ft, $\Delta\theta$ = 136.3 °, Δz = 5.8 ft
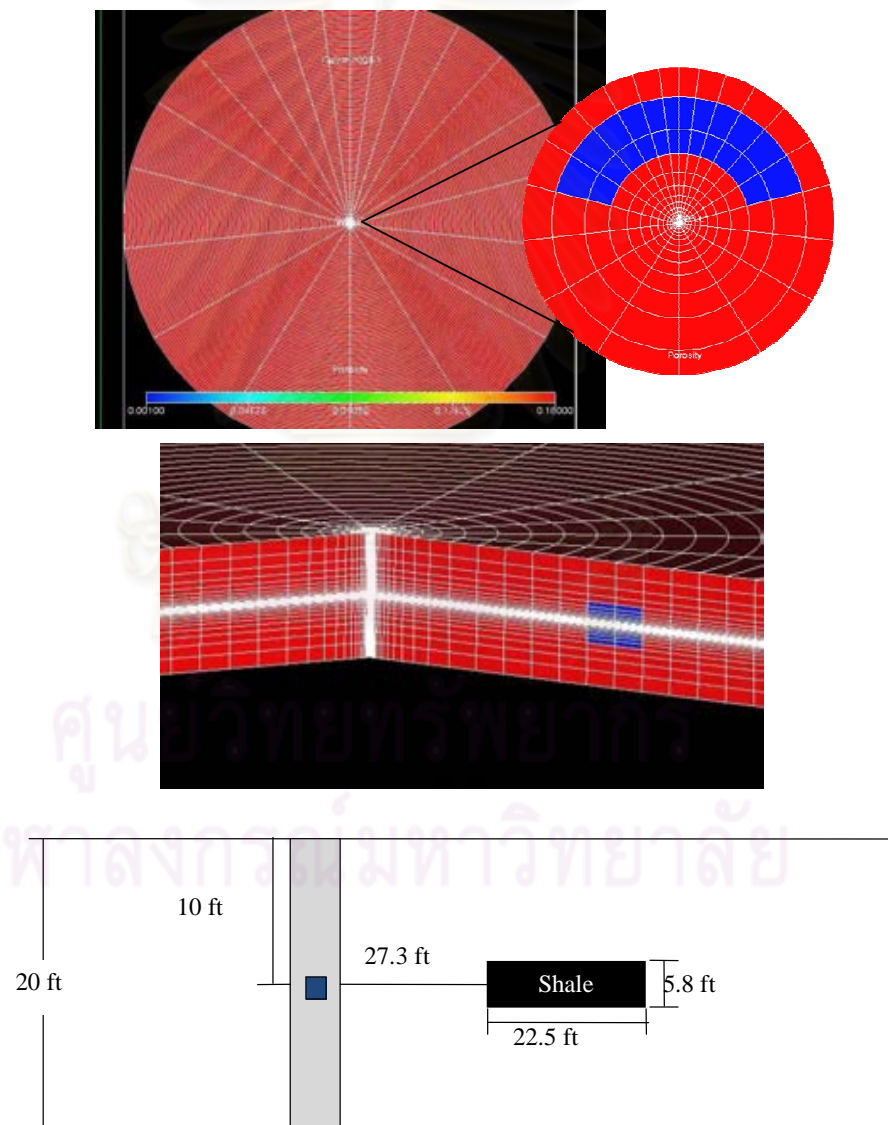
Figure 5.10: Shale configuration of case III

Figure 5.11-a, 5.11-b and 5.11-c show pressure responses simulated from a reservoir simulator for single probe, dual packer and well test, respectively.
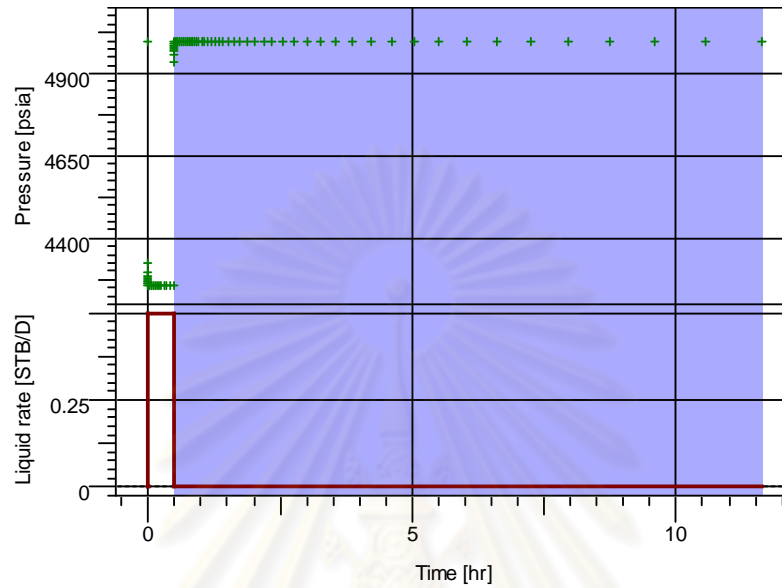
Figure 5.11-a: Pressure history of single probe for case III
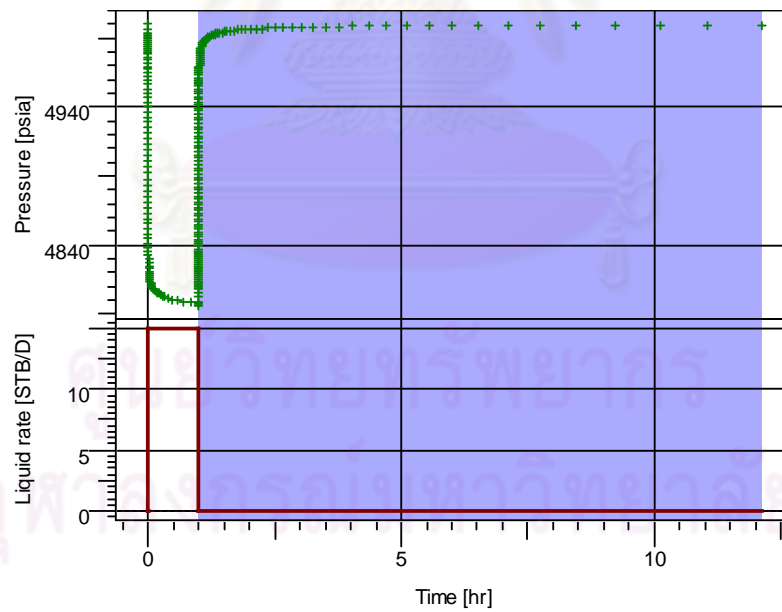
Figure 5.11-b: Pressure history of dual packer for case III
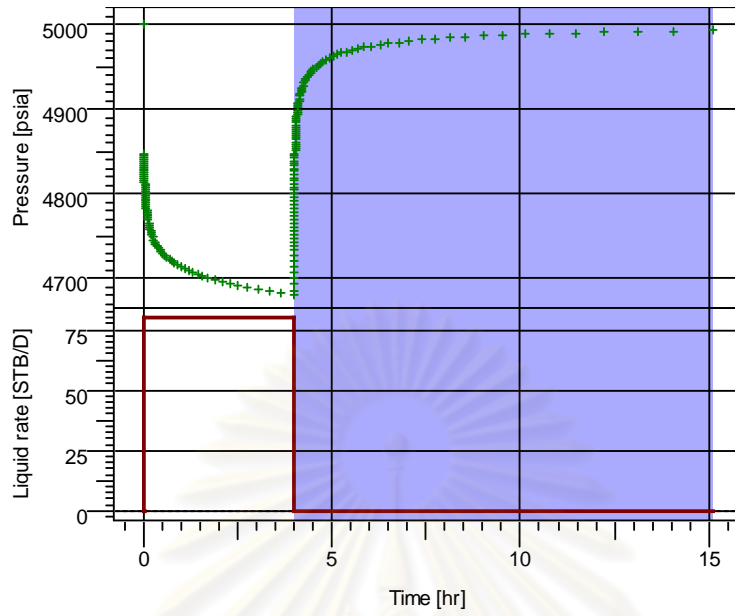
Figure 5.11-c: Pressure history of well test for case III

Single Probe
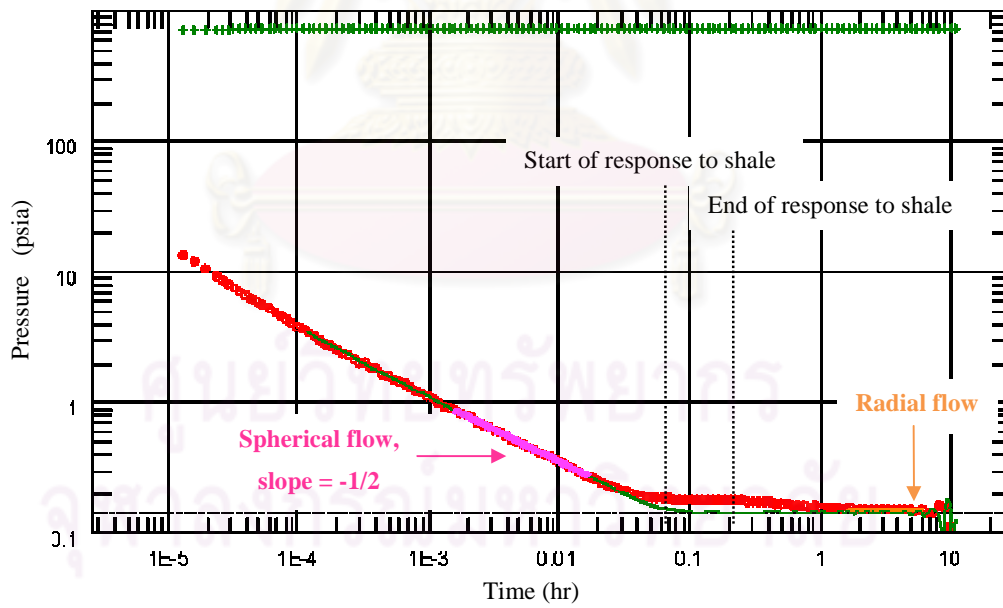
Figure 5.12-a: Single probe WFT derivative plot of case III

Dual Packer

Figure 5.12-b: Dual packer WFT derivative plot of case III

Well Test

Figure 5.12-c: Well test derivative plot of case III
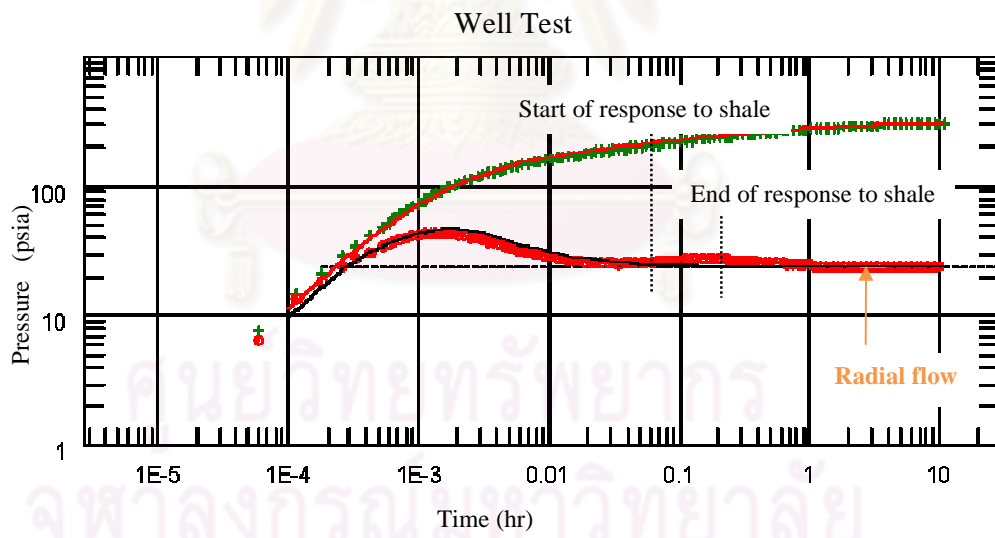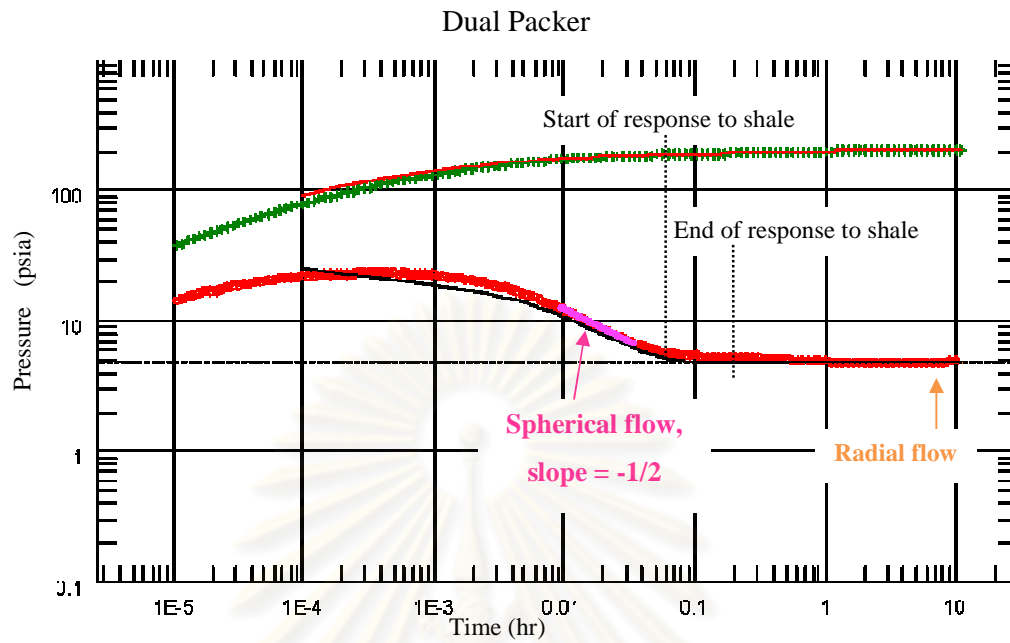
As can be seen in Figures 5.12-a, and 5.12-b, the spherical flow model can be matched to the curve at time before 0.1 hr. At late times, after 0.2 hr, the radial flow model can be matched to the curve for all plots (Figure 5.12-a, 5.12-b, and 5.12-c). The regression shows good match on log-log diagnostic plots between data and the model. From derivative plots of all tests, it is difficult to identify the hump. In other word, the effect of shale barrier is not distinguishable in this case. Table 5.6 shows a comparison of different shale volumes and the average permeabilities which depend on the radius of investigation of each test type.

Table 5.6: Shale volume and average permeability calculation for case III

	Single probe	Dual packer	Well test
Draw down period (min)	30	60	240
Build up period (min)	667	667	667
Radius of investigation (ft)	374	369	385
Volume of investigation (ft^3)	8,792,206	8,558,691	9,317,000
Volume of shale (ft^3)	12,205	12,205	12,205
Volume of sand (ft^3)	8,780,001	8,546,487	9,304,795
V_{sh} (%)	0.14	0.14	0.13
Average permeability, k_h (md)	7.89	7.89	7.90

The drawdown periods are different for the three test types but the buildup periods are equal for all three test types. So, the radiuses of investigation of these tests are about the same. This also results in almost similar volume of investigation, V_{sh} and average permeability.

Table 5.7: Interpreted horizontal and vertical permeabilities compared to clean sand and average permeability for case III

Test type	Compared with clean sand					
	k_h			k_v		
	Input (md)	Interpreted (md)	Error (%)	Input (md)	Interpreted (md)	Error (%)
Single probe	8.09	7.77	-3.99	0.809	1.10	35
Dual packer	8.09	7.35	-9.18	0.809	0.62	-23.8
Well test	8.09	7.99	-1.27	0.809	N/A	N/A

Table 5.7: Interpreted horizontal and vertical permeabilities compared to clean sand and average permeability for case III (continued)

| Test type | Compared with average permeability | | | | | |
| | k_h | | | k_v | | |
	Calculated (md)	Interpreted (md)	Error (%)	Calculated (md)	Interpreted (md)	Error (%)
Single probe	7.89	7.77	-1.57	0.79	1.10	38.8
Dual packer	7.89	7.35	-6.86	0.79	0.62	-21.9
Well test	7.76	7.99	-1.15	0.78	N/A	N/A

From results shown in Table 5.7, even the positions of hump in derivative plot are either partially or fully in the radial flow regime, the estimated horizontal permeabilities are still underestimated in all tests with less than 10% error. The reason is due to the fact that volume of shale is still small, compared to the volume of investigation needed to detect the shale barrier. The vertical permeability estimation for single probe WFT is overestimated with almost 40% error, similar to the base case, because the hump occurs after the spherical line which is taken for estimating the vertical permeability. This means that the effect of shale barrier is not taken into account for the estimation. For dual packer WFT, the estimated vertical permeability is underestimated with almost 30% error.

5.2.4 Case IV: Shale distance from wellbore = 101.6 ft

Figure 5.13 exhibits the shale configuration of case IV. The upper picture shows the top view and the cross-sectional view of the grid model. The lower picture depicts the side view of the reservoir model with a wellbore and a shale barrier located 101.6 ft away from the wellbore. The following is the dimension of the shale barrier.

Shale dimension: Δr = 25.9 ft, $\Delta \theta$ = 136.3 °, Δz = 5.8 ft
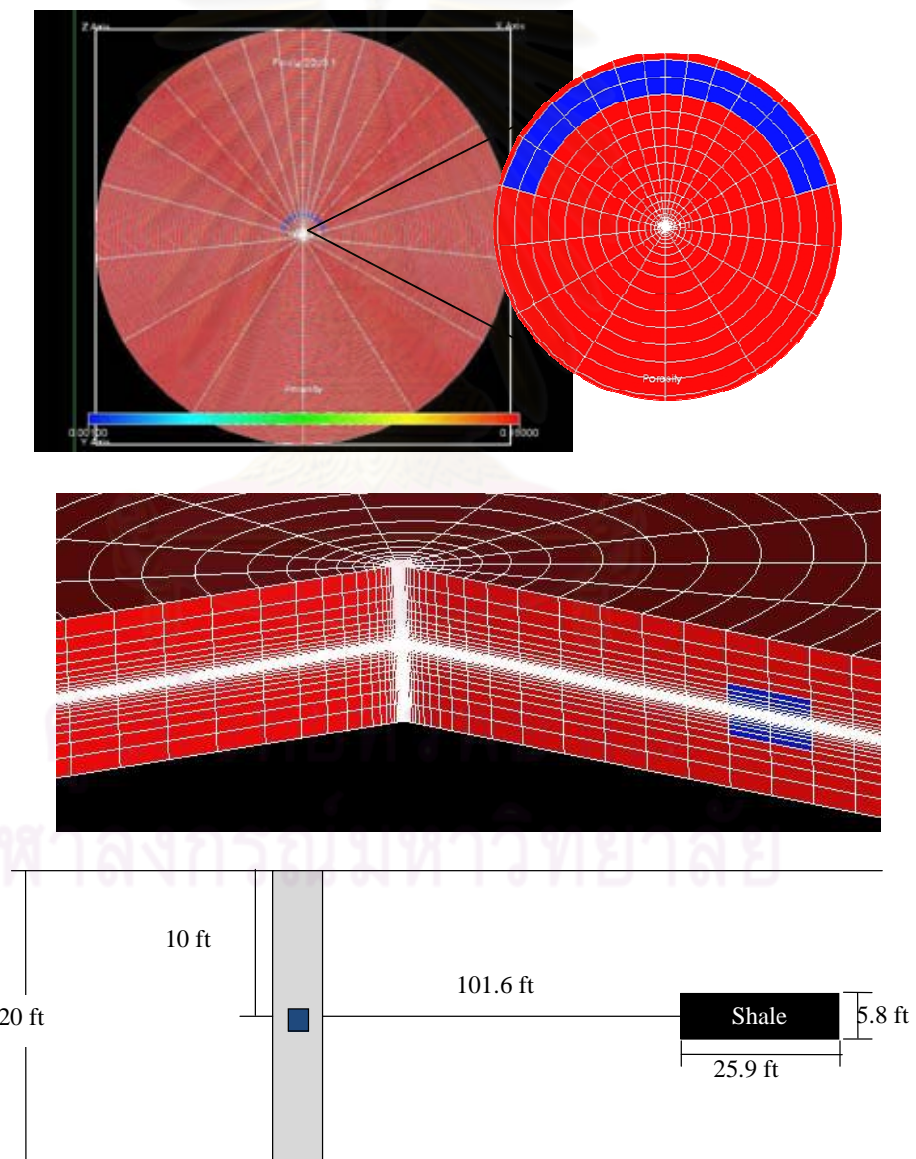
Figure 5.13: Shale configuration of case IV

Figure 5.14-a, 5.14-b and 5.14-c show pressure responses simulated from a reservoir simulator for single probe, dual packer and well test, respectively.
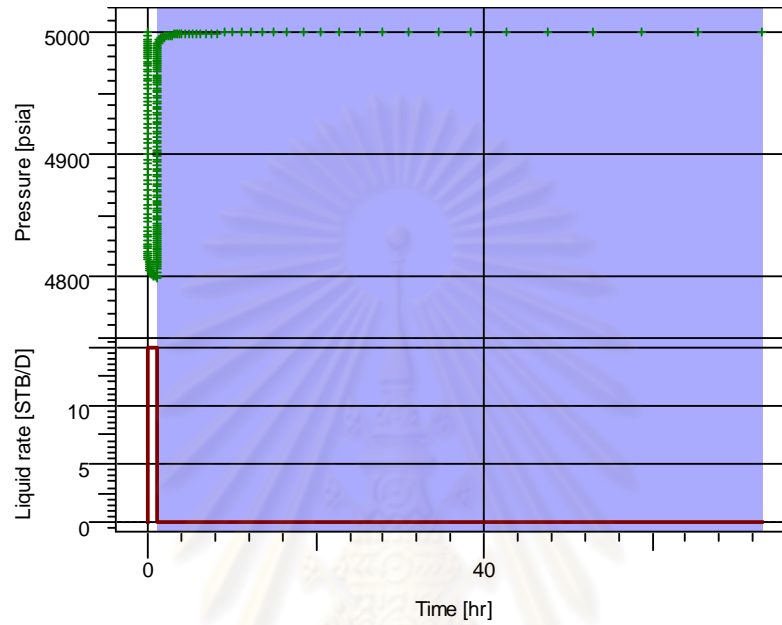
Figure 5.14-a: Pressure history of single probe for case IV
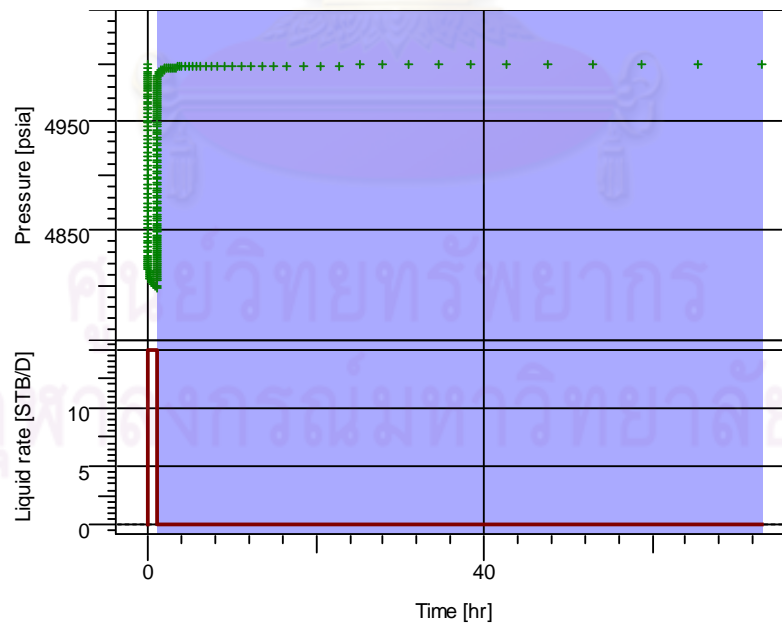
Figure 5.14-b: Pressure history of dual packer for case IV
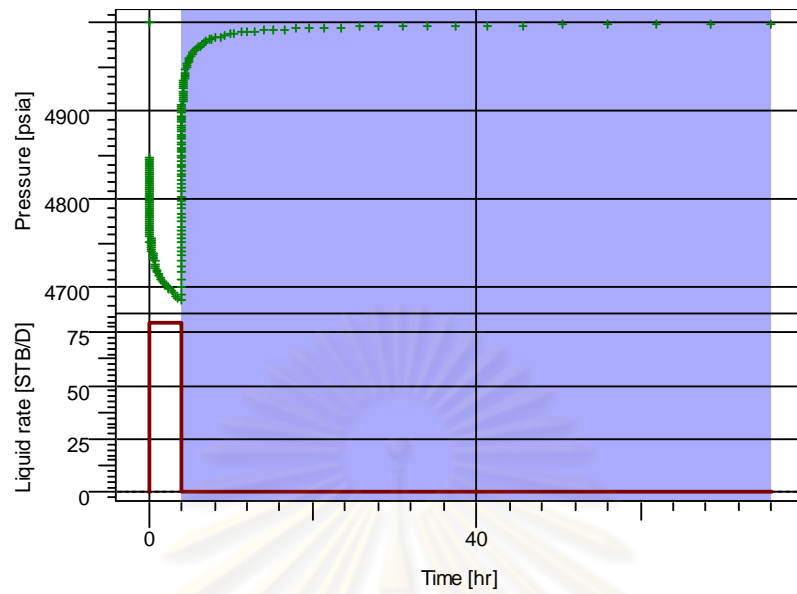
Figure 5.14-c: Pressure history of well test for case IV

Single Probe
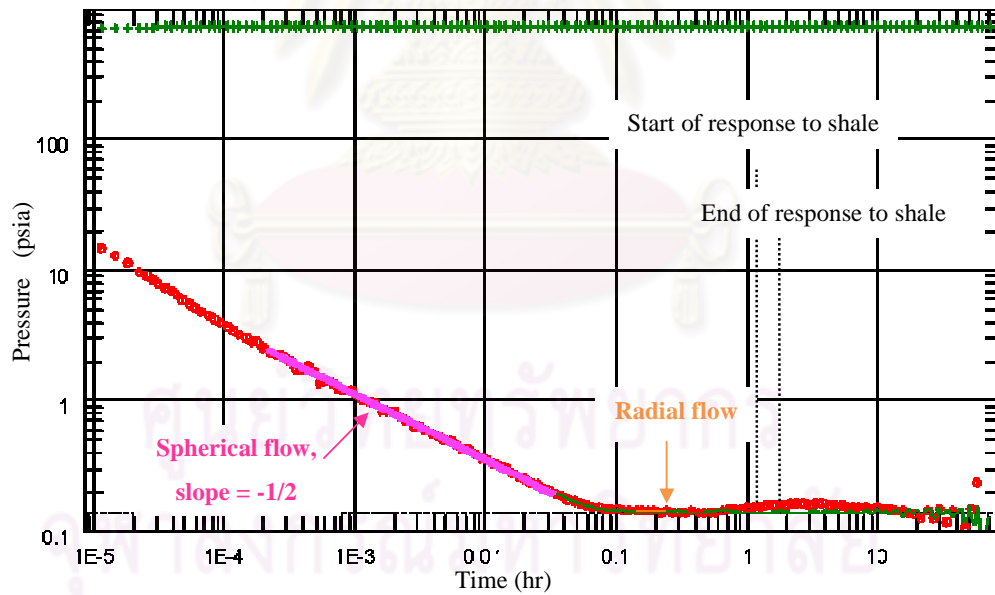
Figure 5.15-a: Single probe WFT derivative plot of case IV
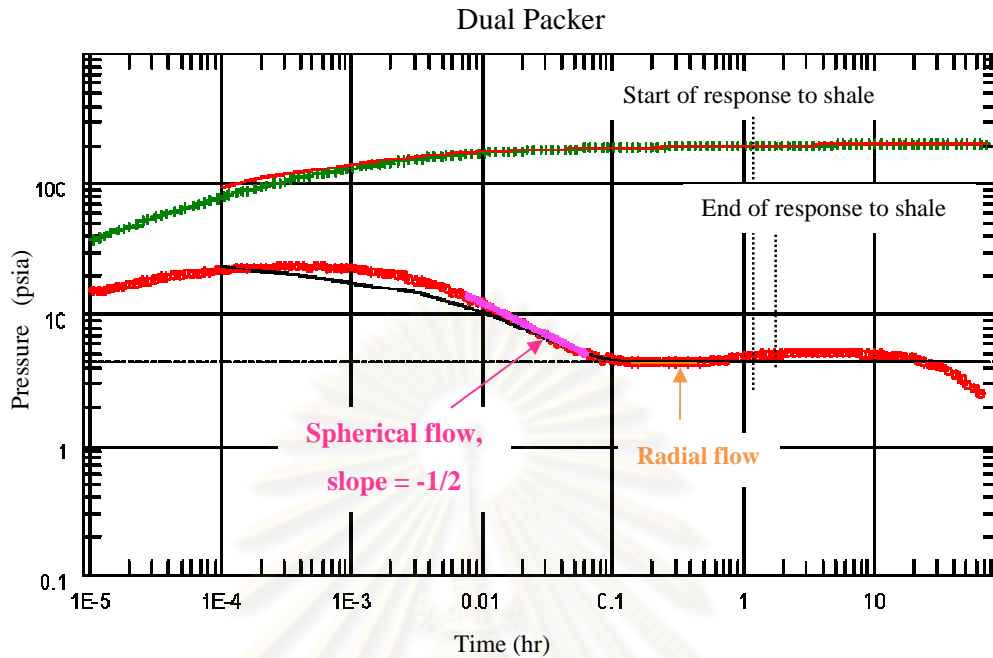
Dual Packer

Figure 5.15-b: Dual packer WFT derivative plot of case IV
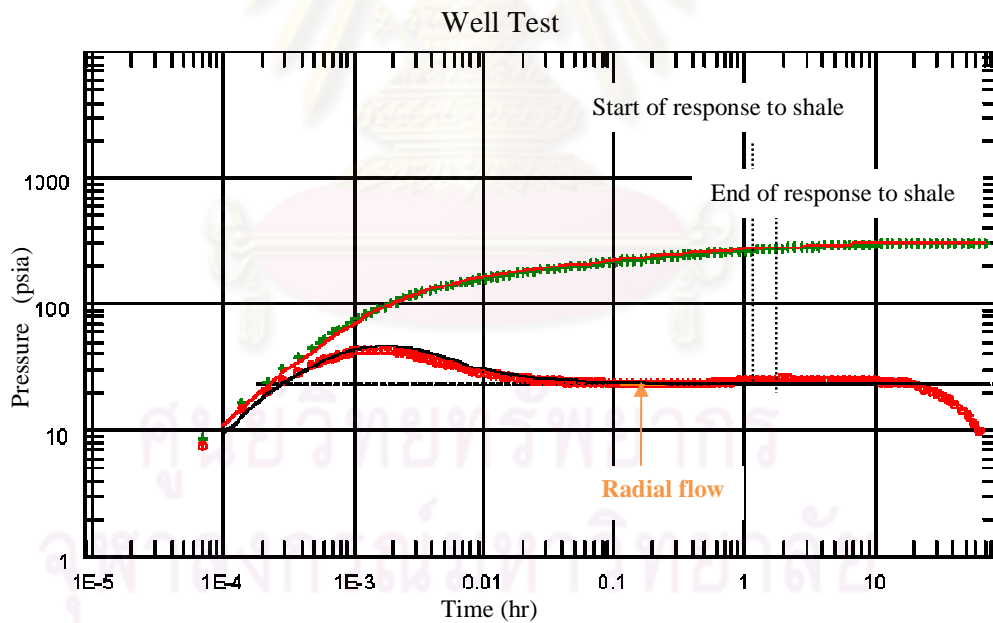
Well Test

Figure 5.15-c: Well test derivative plot of case IV

As can be seen in Figures 5.15-a, and 5.15-b, the spherical flow model can be matched to the curve at time before 0.1 hr. At late times, after 0.2 hr, the radial flow model can be matched to the curve for all plots (Figure 5.15-a, 5.15-b, and 5.15-c). The regression shows good match on log-log diagnostic plots between data and the

model. From derivative plots of all tests, it is difficult to identify the hump. In other word, the effect of shale barrier is not distinguishable in this case. Table 5.8 shows a comparison of different shale volumes and the average permeabilities which depend on the radius of investigation of each test type.

Table 5.8: Shale volume and average permeability calculation for case IV

	Single probe	Dual packer	Well test
Draw down period (min)	30	60	240
Build up period (min)	4320	4320	4320
Radius of investigation (ft)	966	991	991
Volume of investigation (ft^3)	58,655,520	61,730,806	61,730,806
Volume of shale (ft^3)	41,630	41,630	41,630
Volume of sand (ft^3)	58,613,890	61,689,175	61,689,175
V_{sh} (%)	0.07	0.07	0.07
Average permeability, k_h (md)	8.00	8.01	8.01

The drawdown periods are different for the three test types but the buildup periods are equal for all three test types. So, the radiuses of investigation of these tests are about the same. This also results in almost similar volume of investigation, V_{sh} and average permeability.

Table 5.9: Interpreted horizontal and vertical permeabilities compared to clean sand and average permeability for case IV

Test type	Compared with clean sand					
	k_h			k_v		
	Input (md)	Interpreted (md)	Error (%)	Input (md)	Interpreted (md)	Error (%)
Single probe	8.09	8.01	-0.13	0.809	1.03	27.0
Dual packer	8.09	8.17	0.95	0.809	0.81	-0.1
Well test	8.09	8.18	1.08	0.809	N/A	N/A
Test type	Compared with average permeability					
	k_h			k_v		
	Calculated (md)	Interpreted (md)	Error (%)	Calculated (md)	Interpreted (md)	Error (%)
Single probe	8.00	8.01	0.09	0.80	1.03	28.1
Dual packer	8.01	8.17	2.06	0.80	0.81	1.02
Well test	8.01	8.18	2.19	0.80	N/A	N/A

Table 5.9 shows that the estimated horizontal permeabilities from all tests are consistent with less than 5% error. The effect of shale barrier is negligible in this case. Even the volume of shale is increased more than 3 times of the shale volume in the previous case, it is still small compared to the volume of investigation which is greatly increased and almost reaches the reservoir boundary. This small volumetric fraction of shale results in the calculation of average permeability close to clean sand's effective permeability as shown in Table 5.9. The vertical permeability estimation for single probe WFT is overestimated with almost 30% error. For dual packer WFT, the estimated vertical permeability is consistent with less than 5% error.

Figures 5.16-a, 5.16-b, and 5.16-c compare derivative plots of base case, case I, case II, case III, and case IV, separated by test type, in order to allow us to see the effect of distance between shale barrier and well bore on derivative plots.
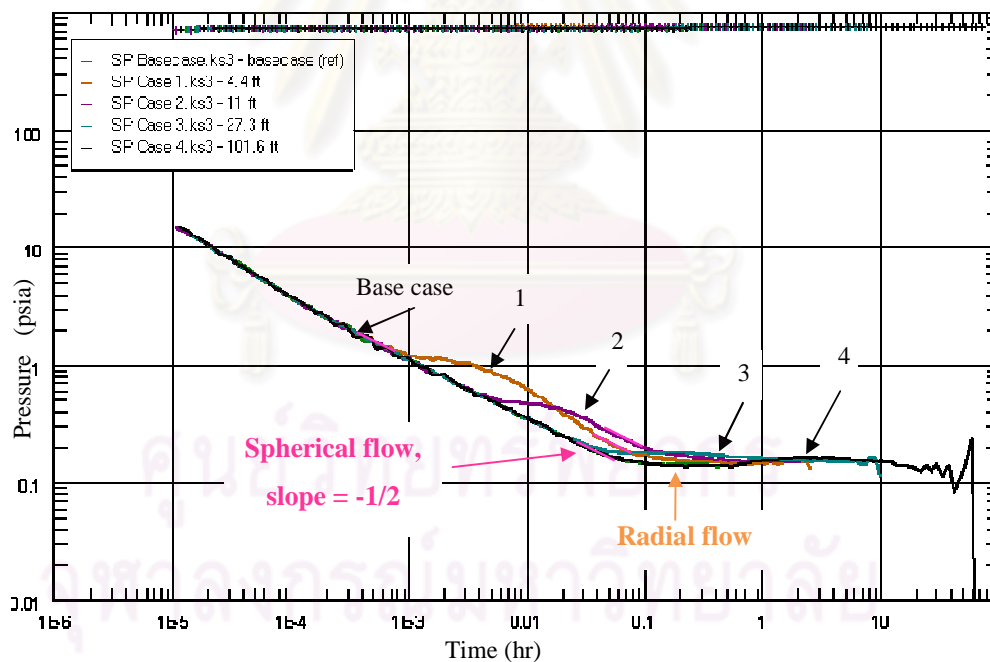
Figure 5.16-a: Single probe WFT derivative plot comparison of all distances of shale barrier from the wellbore
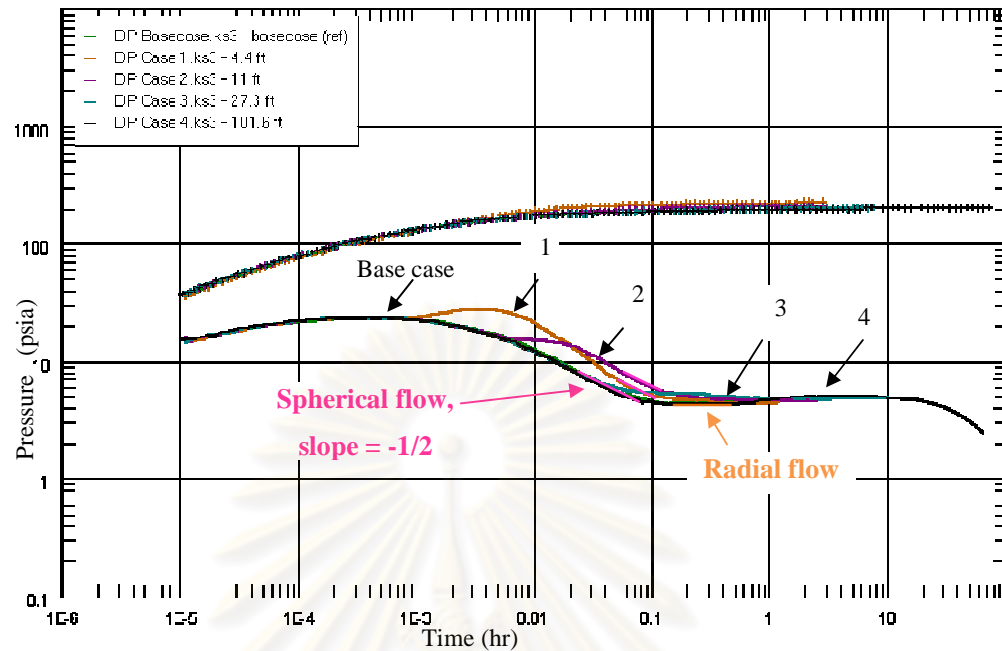
Figure 5.16-b: Dual packer WFT derivative plot comparison of all distances of shale barrier from the wellbore
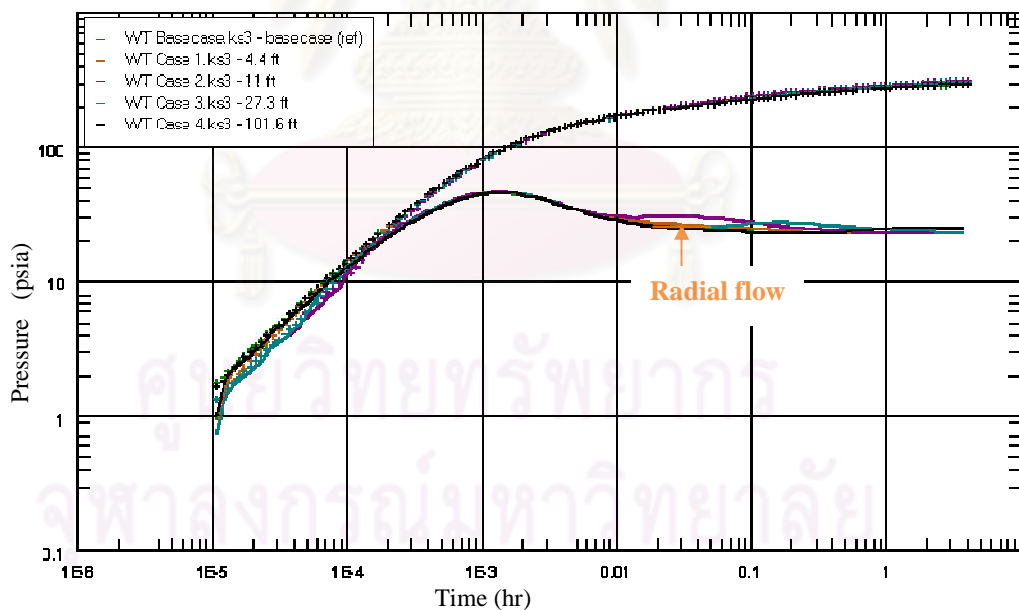
Figure 5.16-c: Well test derivative plot comparison of all distances of shale barrier from the wellbore

As can be seen from Figures 5.16-a, 5.16-b, and 5.16-c, the hump or deviation in derivative plots due to shale barrier is identifiable from single probe WFT, and dual

packer WFT. For well test, it is difficult or impossible to identify it. Since the scale of well test is so large that it makes the effect of shale barrier look small and not obviously distinguishable.

In summary, the derivatives of case I and case II exhibit a hump during the spherical flow for both single probe and dual packer tests. This hump corresponds to a shale barrier. The magnitude of the hump in case I is a larger than that of case II as the distance between well bore and shale in case I is shorter than that in case II. Also, the magnitude of the hump in case II is larger than that in case III. When the distance between shale barrier and the wellbore is further away from the well bore, the magnitude of the hump will be smaller. However, when the distance between shale barrier and the wellbore is far enough like in case IV, it is not possible to detect the effect from derivative plots since the magnitude of the hump is too small. In addition, the duration of the effect of shale barrier is increasing, oppositely, from case I to case III as it moves rightward in the log scale of time axis. Table 5.10 summarizes the pressure drop, the radius of investigation, and the estimated permeabilities of case I-IV and base case.

Table 5.10: Summary of estimated permeabilities for case I, II, III, IV, and the base case

Case #	Base case	I	II	III	IV
Distance to shale (ft)	-	4.4	11.0	27.3	101.6
Single probe					
Pressure drop (psia)	744	745	744	744	743
Int. R_{inv} (ft)	79	186	184	374	966
V_{sh} (%)	-	0.12	0.21	0.14	0.07
Int. k_h (md)	7.73	7.68	7.50	7.77	8.01
Int. k_v/k_h	0.142	0.089	0.063	0.141	0.128
Cal. k_v (md)	1.098	0.684	0.472	1.096	1.025
Dual packer					
Pressure drop (psia)	201	227	212	204	202
Int. R_{inv} (ft)	115	189	188	369	991
V_{sh} (%)	-	0.12	0.20	0.14	0.07
Int. k_h (md)	7.90	7.69	7.62	7.35	8.17
Int. k_v/k_h	0.103	0.078	0.056	0.084	0.099
Cal. k_v (md)	0.814	0.597	0.428	0.617	0.809

Table 5.10: Summary of estimated permeabilities for case I, II, III, IV, and the base case (continued)

Case #	Base case	I	II	III	IV
Distance to shale (ft)	-	4.4	11.0	27.3	101.6
Well test					
Pressure drop (psia)	299	303	313	320	314
Int. R_{inv} (ft)	234	233	233	385	991
V_{sh} (%)	-	0.08	0.13	0.13	0.07
Int. k_h (md)	8.19	8.15	8.15	7.99	8.18

*Int. = Interpreted value from derivative plots, **Cal. = Calculated value from interpreted values

Figures 5.17-5.20 show the comparison of interpretation error (%) in permeability estimation among 3 different test types (single probe WFT, dual packer WFT, and conventional well test) for different distances between shale barrier and well bore.

Figure 5.17: k_h estimation error (%) compared to clean sand's k_h for different distances of shale barrier from the well bore

From Figure 5.17, it can be seen that single probe WFT underestimates the horizontal permeabilities more than dual packer does in base case and case I-II in which the shale barriers are detected during the spherical flow regime. But, when the shale barrier is detected during the radial flow regime (case III), dual packer

underestimates the horizontal permeability more than single probe does. For well test, the estimated horizontal permeabilities are closed to clean sand's horizontal permeability. It means that it is difficult to identify the effect of shale barrier in pressure derivative plots of well test. For case IV, the estimation error from all three test types are small ($\sim 1\%$) which are corresponding to the conclusion that the shale barrier cannot be detected from pressure derivative plots when the shale barriers are far away from the wellbore.

Figure 5.18: k_h estimation error (%) compared to average k_h for different distances of shale barrier from the well bore

Figure 5.18 shows the same trend as in Figure 5.17 for single probe and dual packer for case I-III and base case, except that the magnitude of error estimated from single probe and dual packer is less than that in Figure 5.17 for case I-III. So, the estimated the horizontal permeabilities from single probe and dual packer in case I-III are closer to average horizontal permeabilities than clean sand's horizontal permeabilities. In addition, the estimated horizontal permeabilities from well test are overestimated with more error than that in Figure 5.17.
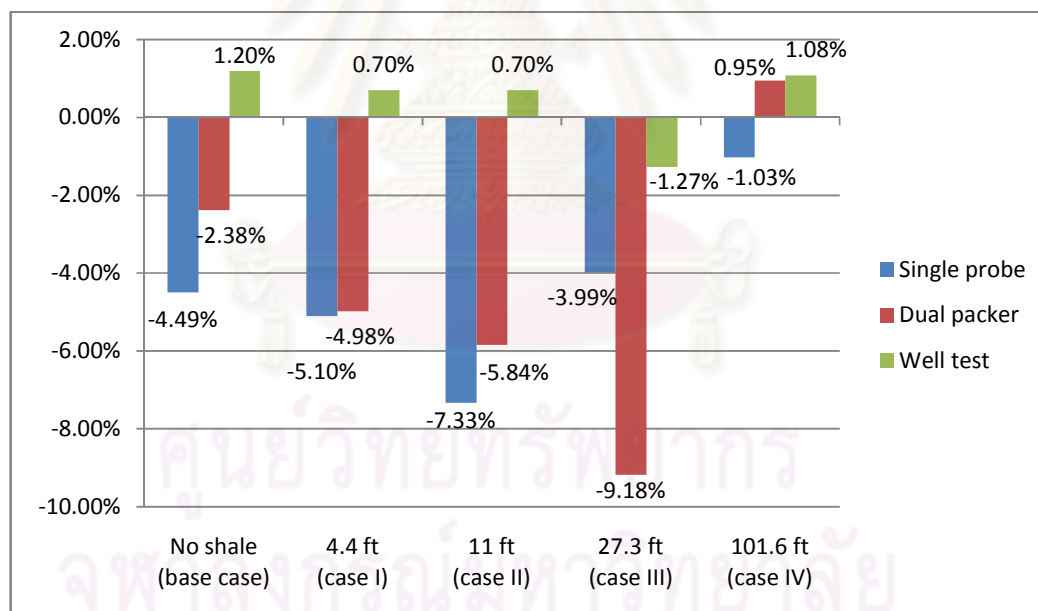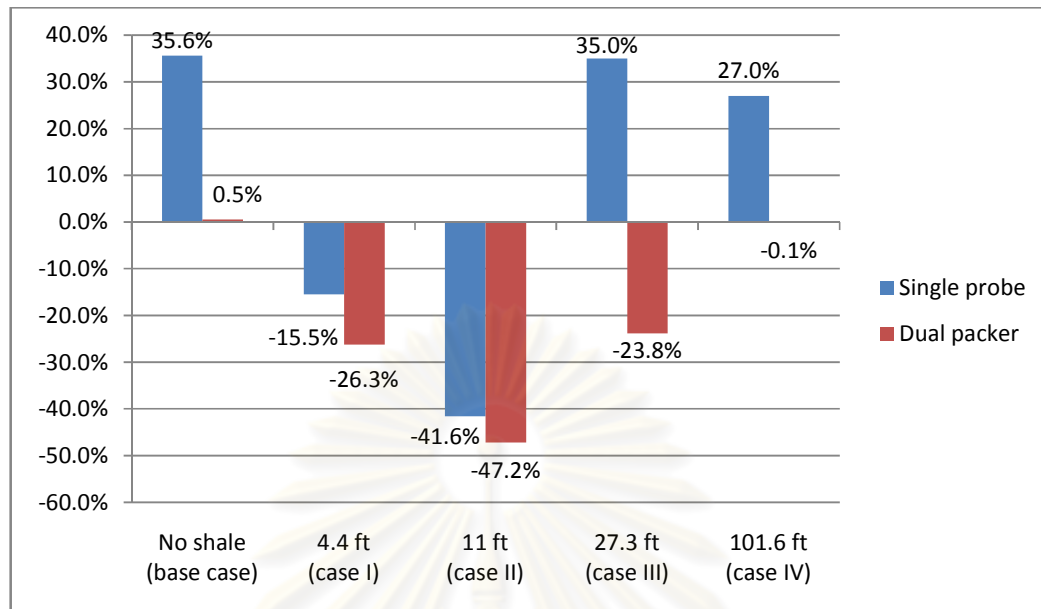
Figure 5.19: k_v estimation error (%) compared to clean sand's k_v for different

distances of shale barrier from the well bore

Figure 5.19 shows that when there is no shale barrier, single probe overestimates the vertical permeability with high error (35.6%) while dual packer estimates the vertical permeability more correctly with 0.5% error. From case I-II where the shale barriers are detected during the spherical flow regime, dual packer estimates the vertical permeabilities lower that single probe does. From case III, single probe overestimates the vertical permeability; while dual packer underestimates the vertical permeability. In case IV, the shale barrier does not highly affect the estimation of vertical permeability due to the effect occurs during the radial flow regime.
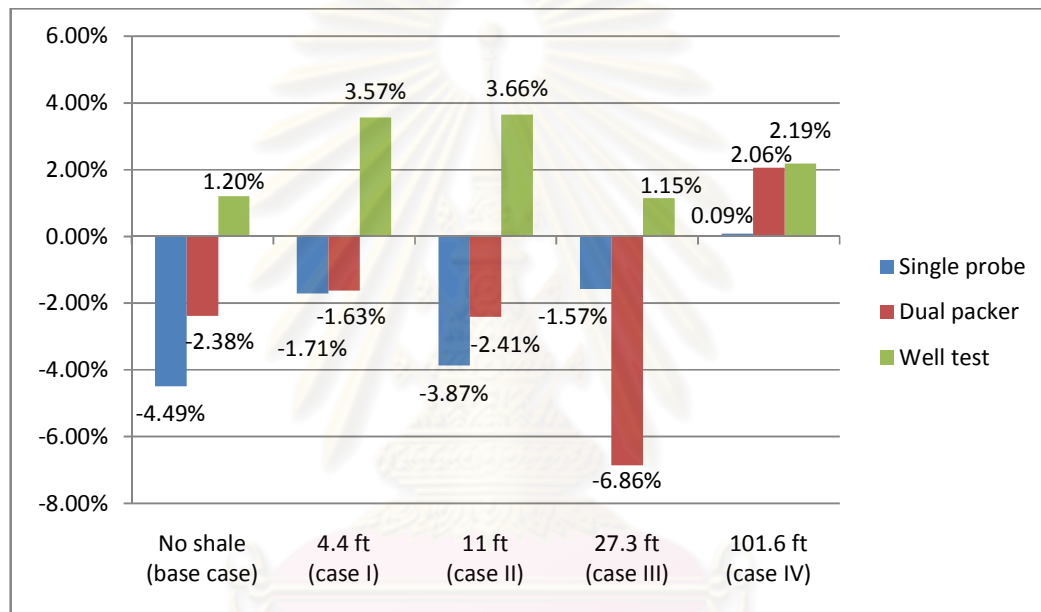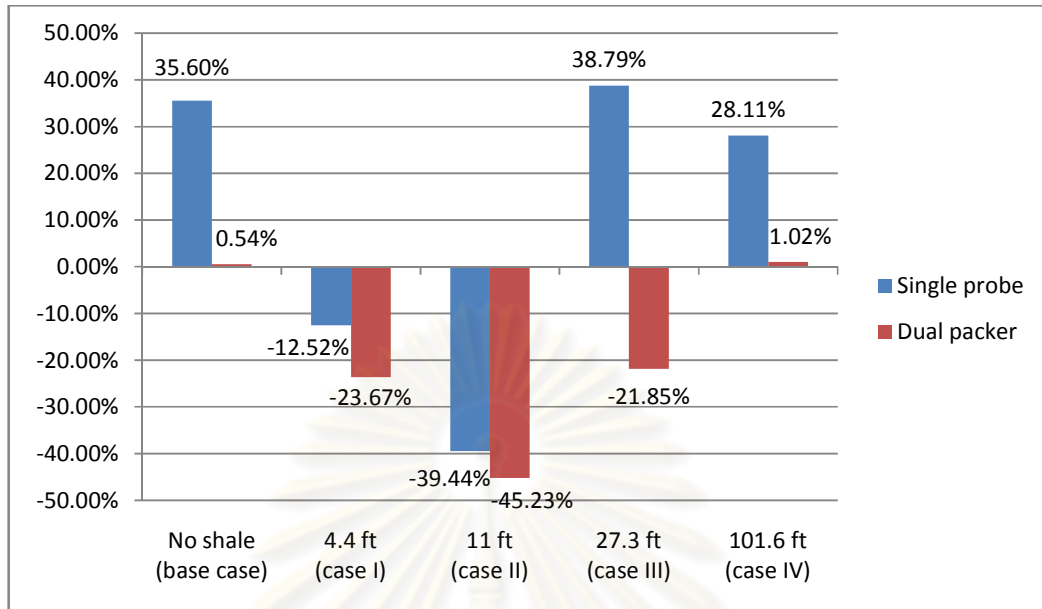
Figure 5.20: k_v estimation error (%) compared to average k_v for different distances of shale barrier from the well bore

Figure 5.20 shows the same trend as in Figure 5.19 and the estimation errors of the vertical permeabilities are slightly less than those in Figure 5.19.

5.3 Effect of amount of shale barrier

In this case study, the objective is to investigate the effects of amount of shale barrier on pressure derivatives and estimated permeabilities by varying the amount of shale barrier in the reservoir and fixing other parameters such as distance between wellbore and shale barrier, shape of shale barrier, and dimensions of shale barrier (Δr, $\Delta \theta$, and Δz). Due to the different grid size in θ - direction, the dimensions of shale barriers in each case are equal or slightly different in θ-direction.

5.3.1 Case V: 2 shale barriers

Figure 5.21 exhibits the shale configuration of case V. The upper picture shows the top view and the cross-sectional view of the grid model. The lower picture depicts the side view of the reservoir model with a wellbore and shale barriers located 4.4 ft away from the wellbore. The following is the dimension of the shale barrier.

<u>Shale dimension</u>: #1 $\Delta r = 15.8$ ft, $\Delta \theta = 62.3$ °, $\Delta z = 5.8$ ft

#2 $\Delta r = 15.8$ ft, $\Delta \theta = 62.3$ °, $\Delta z = 5.8$ ft
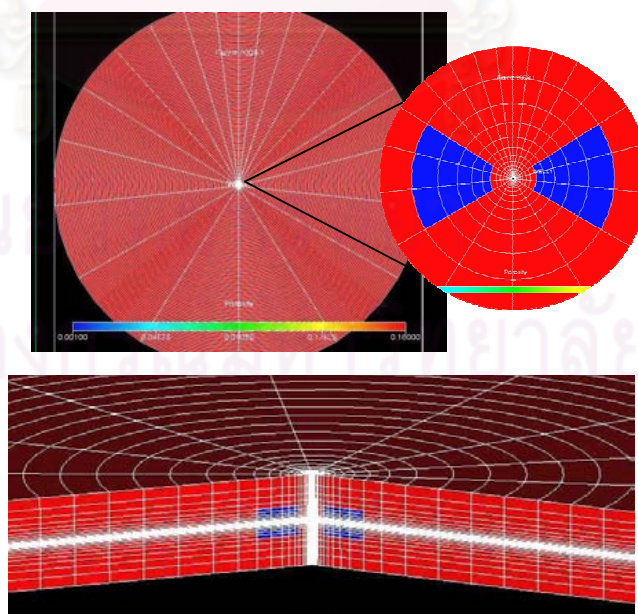
Figure 5.21: Shale configuration of case V
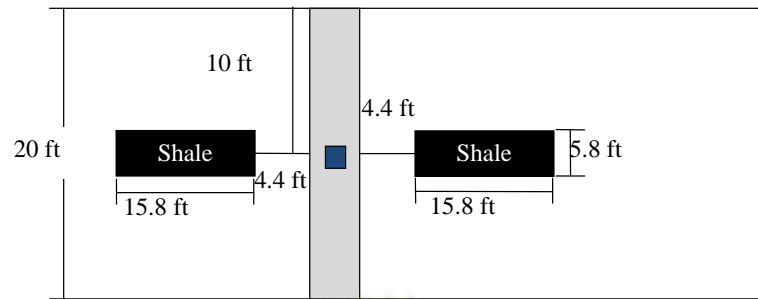
Figure 5.21: Shale configuration of case V (continue)

Figure 5.22-a, 5.22-b and 5.22-c show pressure responses simulated from a reservoir simulator for single probe, dual packer and well test, respectively.
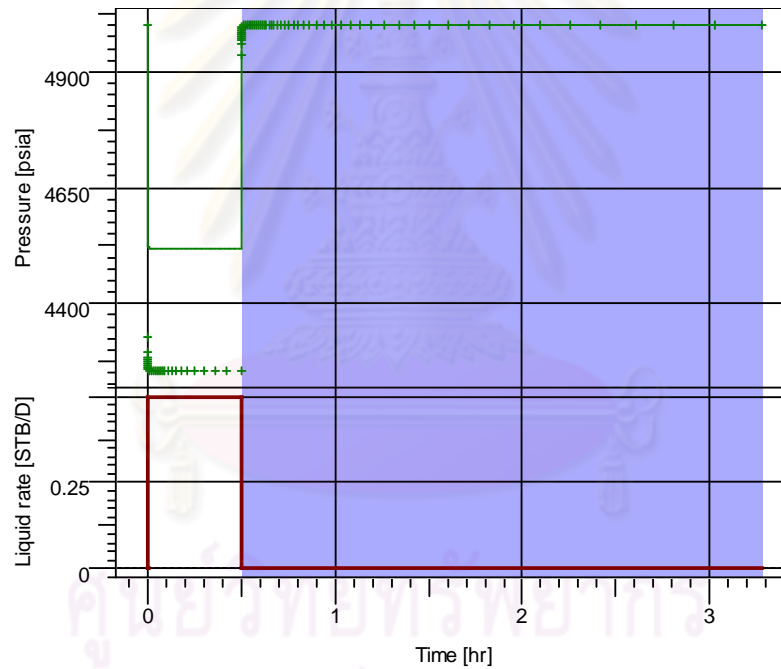
Figure 5.22-a: Pressure history of single probe WFT for case V
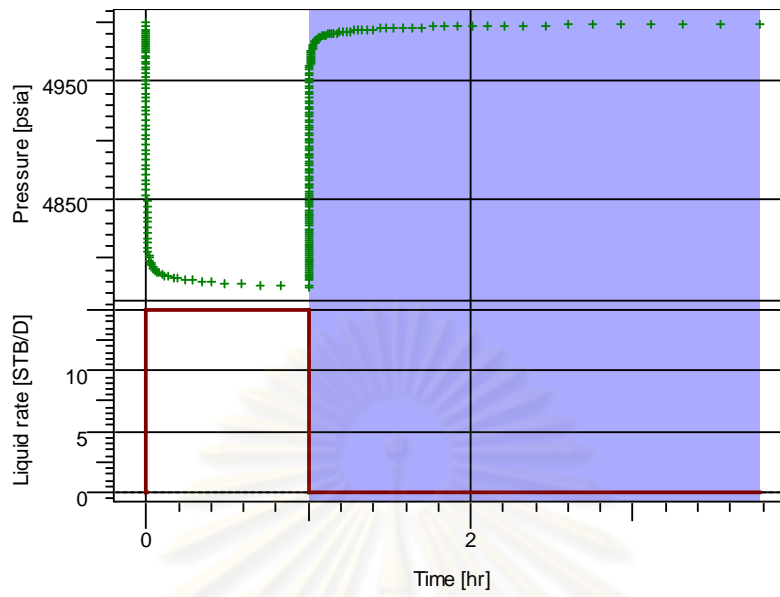
Figure 5.22-b: Pressure history of dual packer WFT for case V
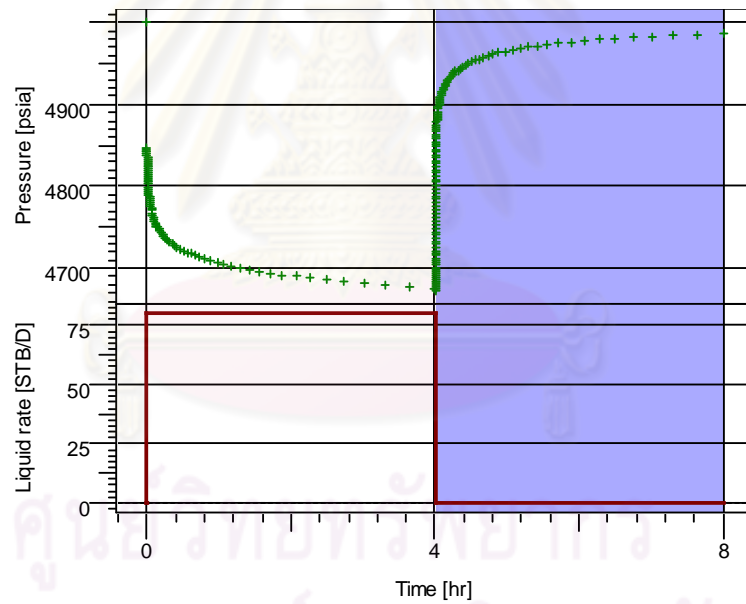
Figure 5.22-c: Pressure history of well test for case V

Single Probe
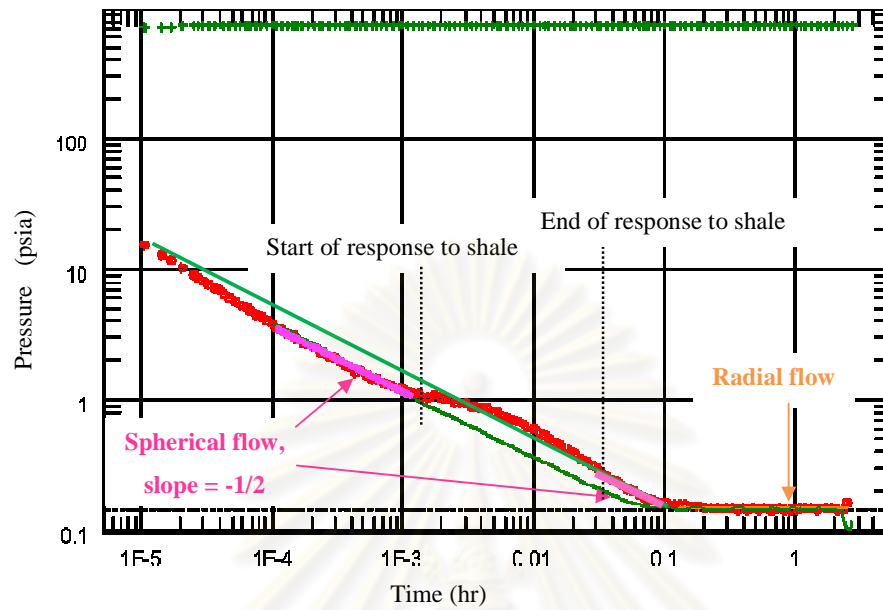
Figure 5.23-a: Single probe WFT derivative plot of case V

Dual Packer
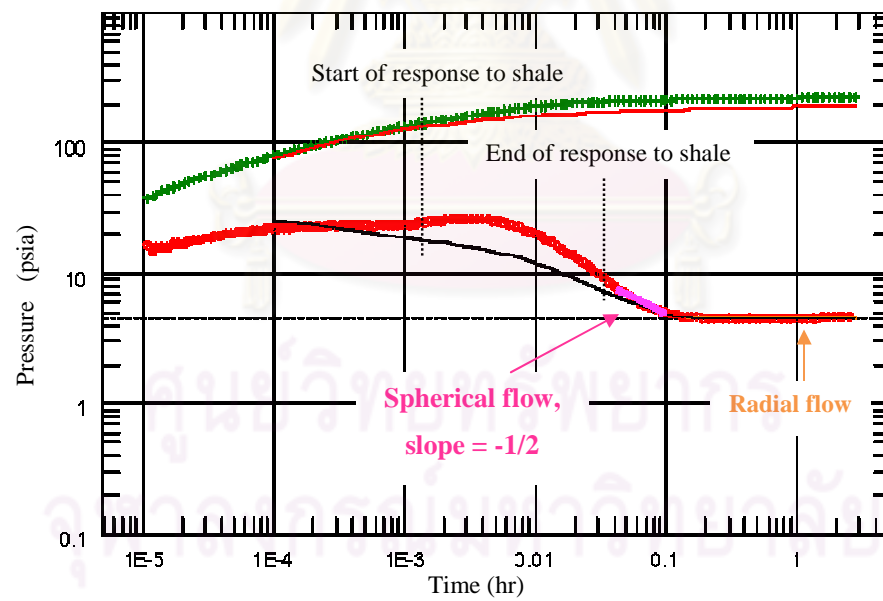
Figure 5.23-b: Dual packer WFT derivative plot of case V
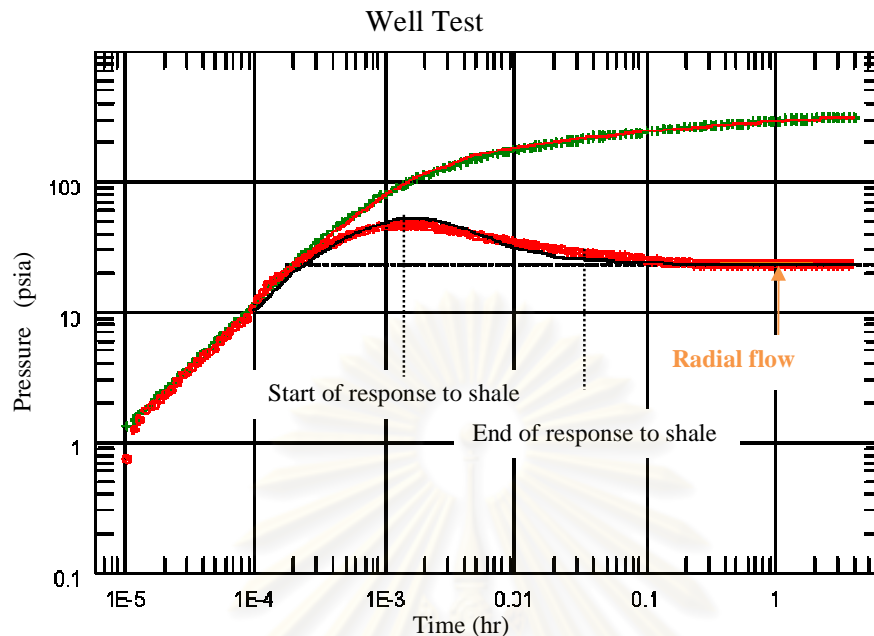
Figure 5.23-c: Well test derivative plot of case V

As can be seen in Figures 5.23-a, and 5.23-b, the spherical flow model can be matched to the curve at time before 0.1 hr. At late times, after 0.2 hr, the radial flow model can be matched to the curve for all plots (Figure 5.23-a, 5.23-b, and 5.23-c). The effect of the shale barrier can be seen as a hump in the derivative plots. From Figures 5.23-a and 5.23-b, the hump appears in the spherical flow. Actually, the distance between shale barrier and well bore would be a bit more than 4.4 ft since its direction is perpendicular to the probes position.

For single probe WFT, it is possible to calculate the vertical permeability from 2 positions, both before and after the occurrence of hump in the derivative, similar to cases I and II, but the latter one is selected for estimating the vertical permeability for the same reason.

Among 3 derivative plots, it is possible to identify the existence of shale barrier from the occurrence of hump in the derivative plots of single probe WFT and dual packer WFT. For well test derivative plots, it is difficult to identify the existence of shale barrier as the magnitude of the hump is small and unnoticeable. Table 5.11 shows a comparison of different shale volumes and the average permeabilities which depend on the radius of investigation of each test type.

Table 5.11: Shale volume and average permeability calculation for case V

	Single probe	Dual packer	Well test
Draw down period (min)	30	60	240
Build up period (min)	167	167	240
Radius of investigation (ft)	187	192	234
Volume of investigation (ft^3)	2,198,051	2,317,166	3,441,806
Volume of shale (ft^3)	4,475	4,475	4,475
Volume of sand (ft^3)	2,193,577	2,312,691	3,437,331
V_{sh} (%)	0.20	0.19	0.13
Average permeability, k_h (md)	7.83	7.84	7.88

The drawdown periods are different for the three test types but the buildup periods are equal for single probe and dual packer. So, the radiuses of investigation for single probe and dual packer are about the same. This also results in almost similar volume of investigation, V_{sh} and average permeability for single probe and dual packer. However, since the buildup period of well test is longer than those of the others, the radius of investigation, V_{sh} and the average permeability of well test are slightly different.

Table 5.12: Interpreted horizontal and vertical permeabilities compared to clean sand and average permeability for case V

Test type	Compared with clean sand					
	k_h			k_v		
	Input (md)	Interpreted (md)	Error (%)	Input (md)	Interpreted (md)	Error (%)
Single probe	8.09	7.81	-3.50	0.809	0.72	-10.5
Dual packer	8.09	7.92	-2.14	0.809	0.62	-23.1
Well test	8.09	8.22	1.57	0.809	N/A	N/A
Test type	Compared with average permeability					
	k_h			k_v		
	Calculated (md)	Interpreted (md)	Error (%)	Calculated (md)	Interpreted (md)	Error (%)
Single probe	7.83	7.81	-0.25	0.78	0.72	-7.48
Dual packer	7.84	7.92	1.07	0.78	0.62	-20.6
Well test	7.88	8.22	4.29	0.78	N/A	N/A

Table 5.12 shows the estimated horizontal and vertical permeabilities, compared with the clean sand's effective permeabilities and average permeabilities. When the amount of shale barrier is increased to 2 barriers with same shape and size, the estimated horizontal permeabilities are still consistent with the clean sand's and average permeability with less than 5% error similar to the result in case I. Also, the estimated vertical permeabilities from single probe and dual packer WFT are underestimated with up to 25% error similar to the estimates in the case of 1-shale barrier (case I).

5.3.2 Case VI: 3 shale barriers

Figure 5.24 exhibits the shale configuration of case VI. The upper picture shows the top view and the cross-sectional view of the grid model. The lower picture depicts the side view of the reservoir model with a wellbore and shale barriers located 4.4 ft away from the wellbore. The following is the dimension of the shale barrier.

Shale dimension: #1 $\Delta r = 15.8$ ft, $\Delta \theta = 59.2$ °, $\Delta z = 5.8$ ft

#2 $\Delta r = 15.8$ ft, $\Delta \theta = 58.5$ °, $\Delta z = 5.8$ ft

#3 $\Delta r = 15.8$ ft, $\Delta \theta = 62.3$ °, $\Delta z = 5.8$ ft
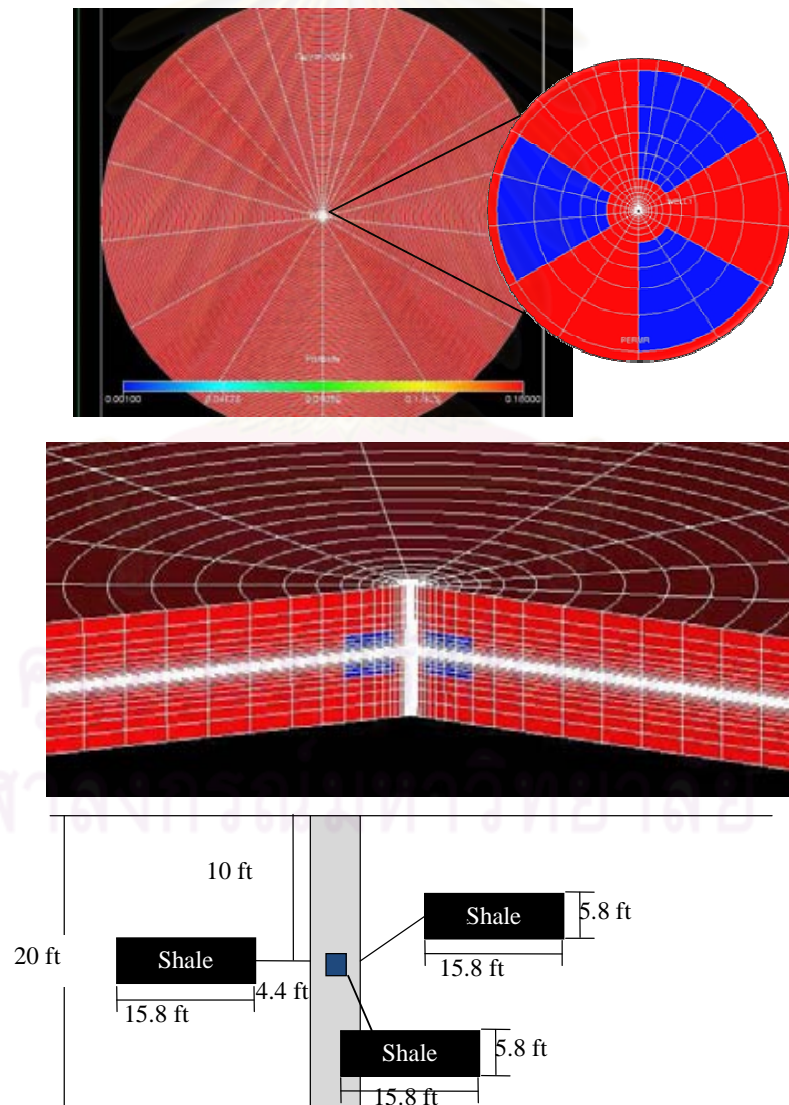
Figure 5.24: Shale configuration of case VI

Figure 5.25-a, 5.25-b and 5.25-c show pressure responses simulated from a reservoir simulator for single probe, dual packer and well test, respectively.
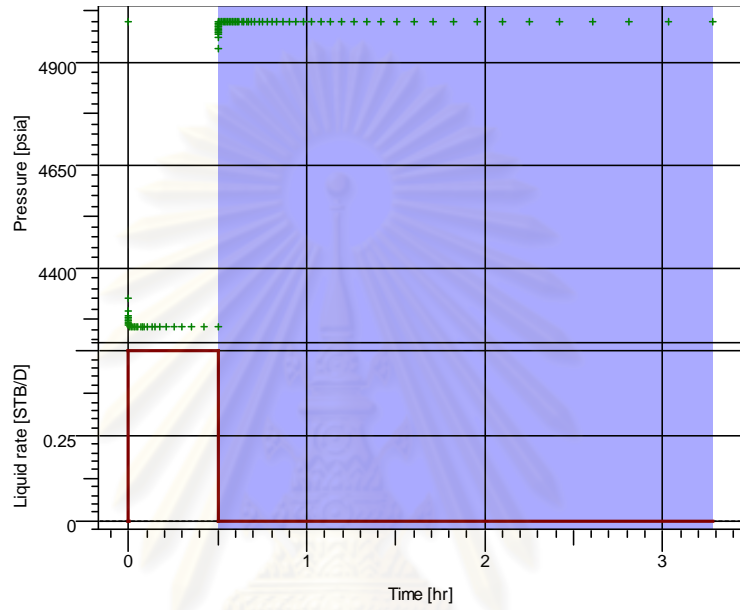
Figure 5.25-a: Pressure history of single probe WFT for case VI
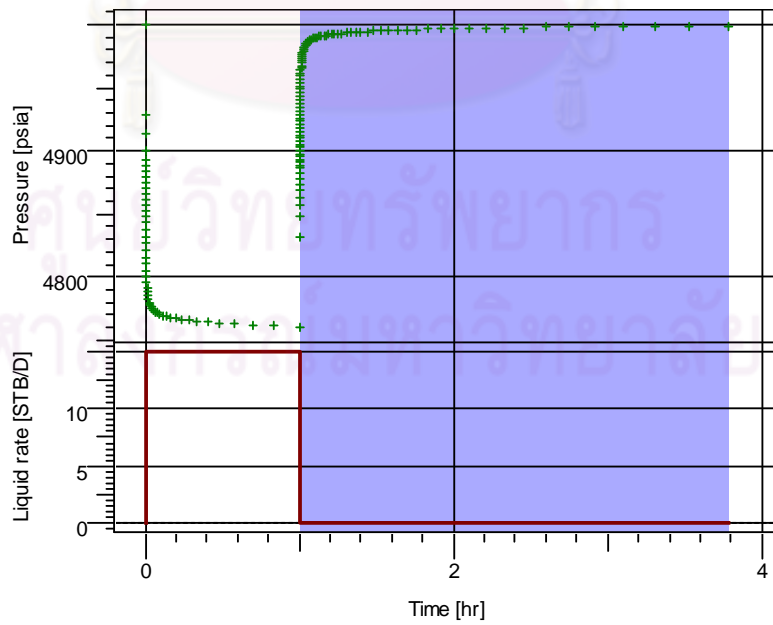
Figure 5.25-b: Pressure history of dual packer WFT for case VI
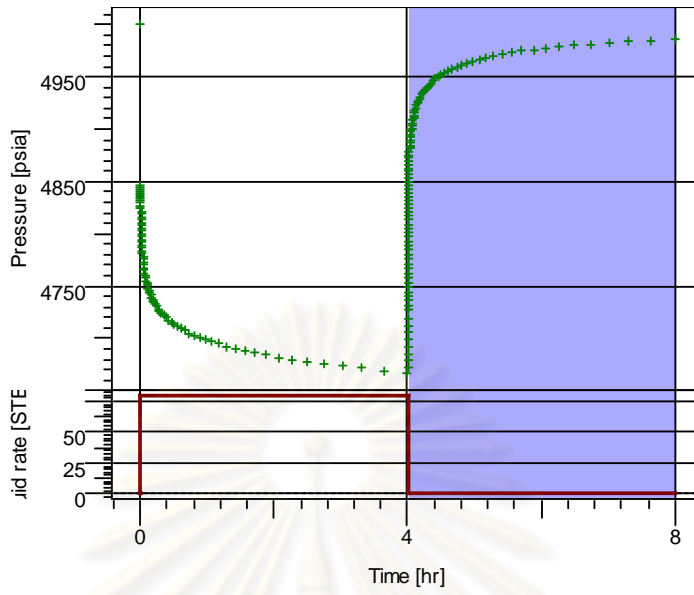
Figure 5.25-c: Pressure history of well test for case VI

Single Probe
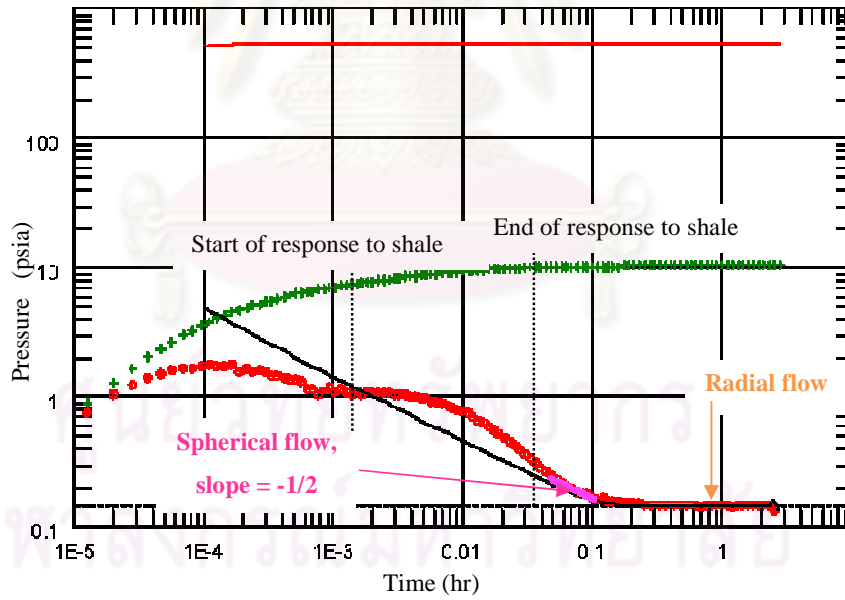
Figure 5.26-a: Single probe WFT derivative plot of case VI

Dual Packer

Figure 5.26-b: Dual packer WFT derivative plot of case VI

Well Test

Figure 5.26-c: Well test derivative plot of case VI
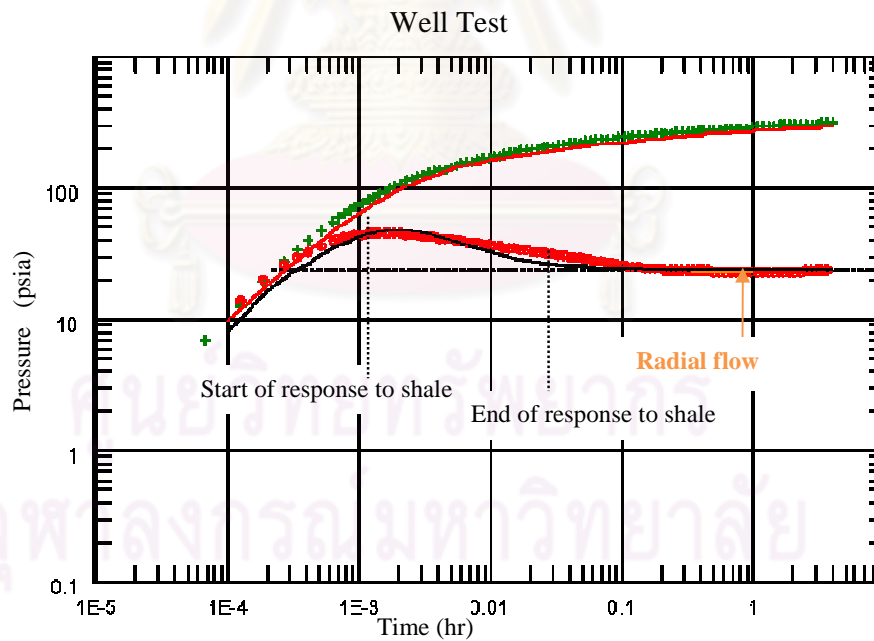
With 3 shale barriers, in Figure 5.26-a, the derivative plot of single probe WFT in case VI exhibits more than one hump during spherical flow. The first hump is resembled to the shape of well bore storage effect. For dual packer WFT, in Figure

5.26-b, the effect of shale barrier shows a larger hump than the well bore storage effect. There is also an increment in magnitude of hump in the derivative plot of well test, but it is so small and nearly unnoticeable. Table 5.13 shows a comparison of different shale volumes and the average permeabilities which depend on the radius of investigation of each test type.

Table 5.13: Shale volume and average permeability calculation for case VI

	Single probe	Dual packer	Well test
Draw down period (min)	30	60	240
Build up period (min)	167	167	240
Radius of investigation (ft)	186	195	234
Volume of investigation (ft^3)	2,174,606	2,390,143	3,441,806
Volume of shale (ft^3)	3,543	3,543	3,543
Volume of sand (ft^3)	2,171,062	2,386,600	3,438,262
V_{sh} (%)	0.16	0.15	0.10
Average permeability, k_h (md)	7.81	7.83	7.87

The drawdown periods are different for the three test types but the buildup periods are equal for single probe and dual packer. So, the radiuses of investigation for single probe and dual packer are about the same. This also results in almost similar volume of investigation, V_{sh} and average permeability for single probe and dual packer. However, since the buildup period of well test is longer than those of the others, the radius of investigation, V_{sh} and the average permeability of well test are slightly different.

Table 5.14: Interpreted horizontal and vertical permeabilities compared to clean sand and average permeability for case VI

Test type	Compared with clean sand					
	k_h			k_v		
	Input (md)	Interpreted (md)	Error (%)	Input (md)	Interpreted (md)	Error (%)
Single probe	8.09	7.02	-4.61	0.809	0.66	-18.3
Dual packer	8.09	8.23	1.69	0.809	0.56	-30.8
Well test	8.09	8.17	0.95	0.809	N/A	N/A

Table 5.14: Interpreted horizontal and vertical permeabilities compared to clean sand and average permeability for case VI (continued)

| Test type | Compared with average permeability | | | | | |
| | k_h | | | k_v | | |
	Calculated (md)	Interpreted (md)	Error (%)	Calculated (md)	Interpreted (md)	Error (%)
Single probe	7.81	7.02	-1.19	0.78	0.66	-15.8
Dual packer	7.83	8.23	5.16	0.78	0.56	-28.4
Well test	7.87	8.17	3.81	0.79	N/A	N/A

From Table 5.14, the estimated horizontal permeabilities are still consistent with the clean sand's and average permeabilities with less than 6% error. The estimated vertical permeabilities from single probe and dual packer WFT are resulted in more underestimation which is up to 30% error corresponding to the change in derivative plot.

5.3.3 Case VII: 4 shale barriers

Figure 5.27 exhibits the shale configuration of case VII. The upper picture shows the top view and the cross-sectional view of the grid model. The lower picture depicts the side view of the reservoir model with a wellbore and shale barriers located 4.4 ft away from the wellbore. The following is the dimension of the shale barrier.

Shale dimension: #1 Δr = 15.8 ft, $\Delta \theta$ = 33.6 °, Δz = 5.8 ft

#2 Δr = 15.8 ft, $\Delta \theta$ = 58.5 °, Δz = 5.8 ft

#3 Δr = 15.8 ft, $\Delta \theta$ = 44.3 °, Δz = 5.8 ft

#4 Δr = 15.8 ft, $\Delta \theta$ = 43.5 °, Δz = 5.8 ft
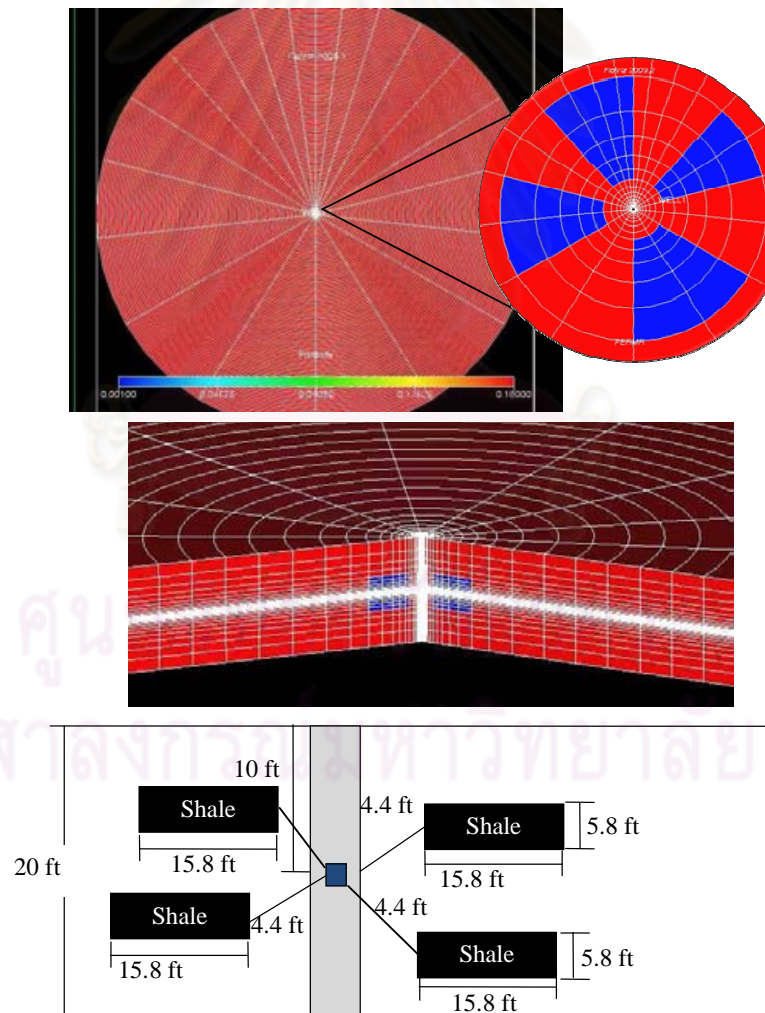
Figure 5.27: Shale configuration of case VII

Figure 5.28-a, 5.28-b and 5.28-c show pressure responses simulated from a reservoir simulator for single probe, dual packer and well test, respectively.
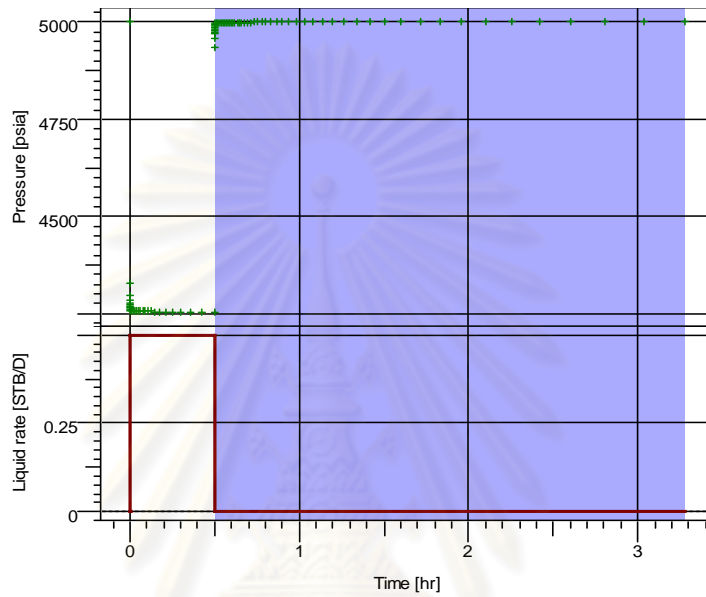
Figure 5.28-a: Pressure history of single probe WFT for case VII
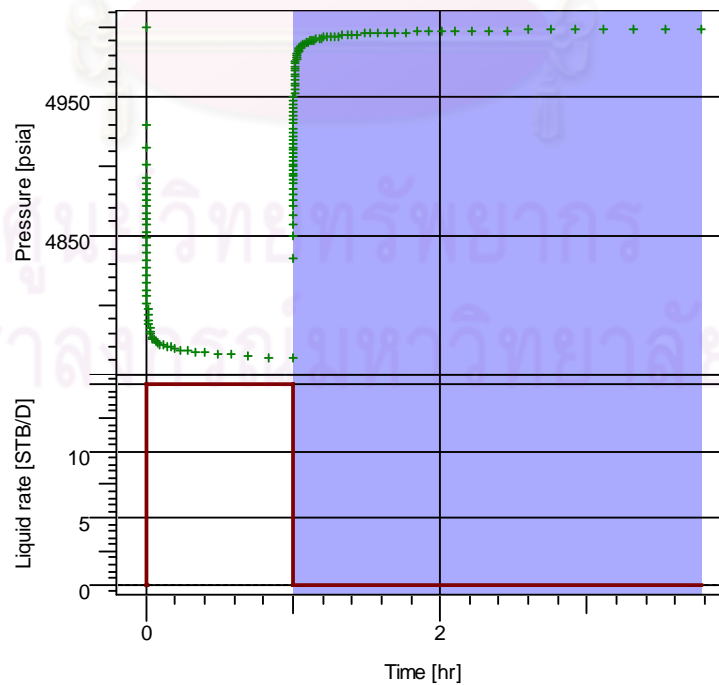
Figure 5.28-b: Pressure history of dual packer WFT for case VII
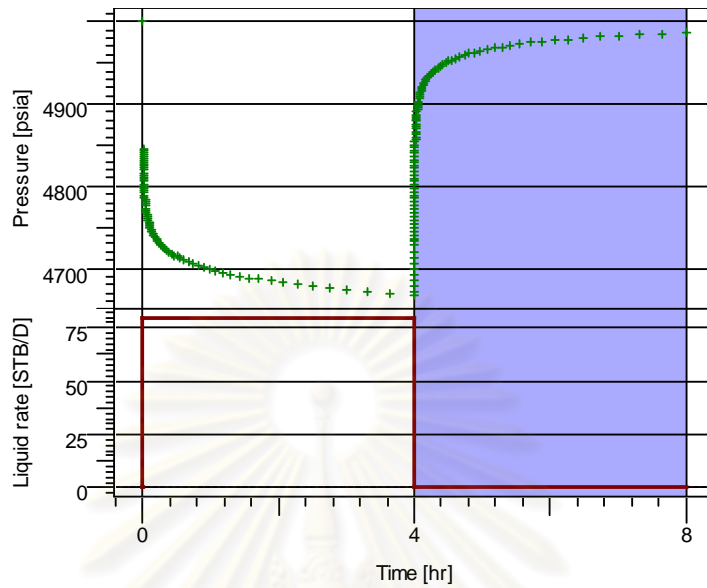
Figure 5.28-c: Pressure history of well test for case VII

Single Probe

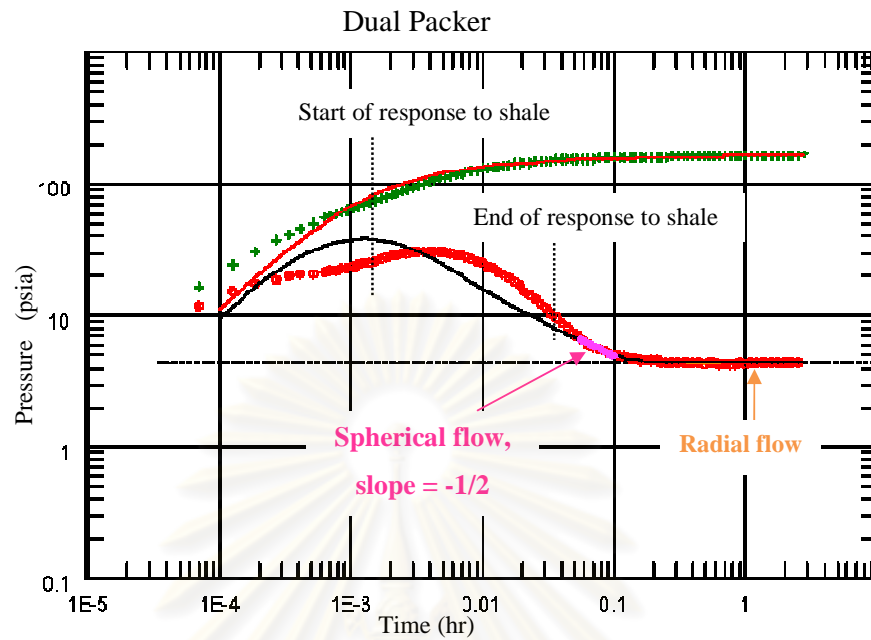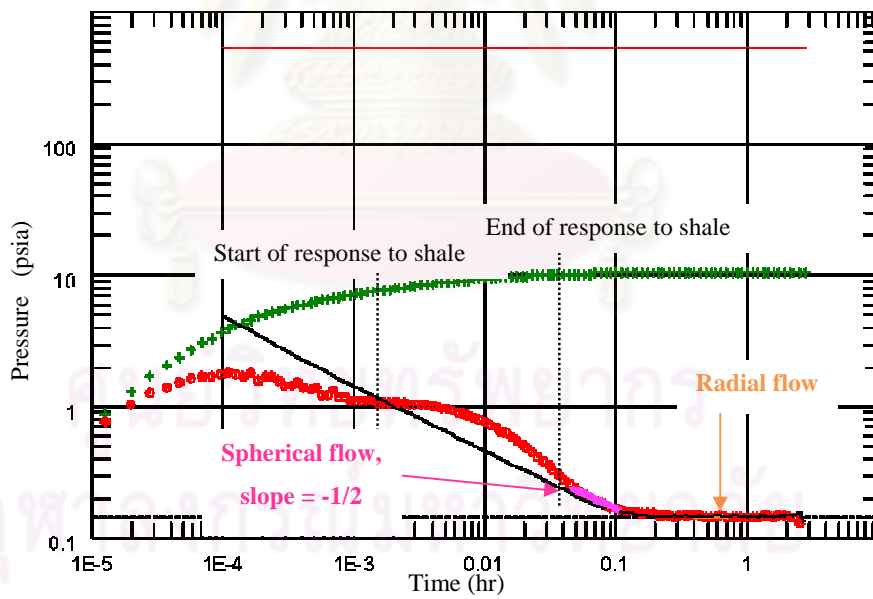Figure 5.29-a: Single probe WFT derivative plot of case VII
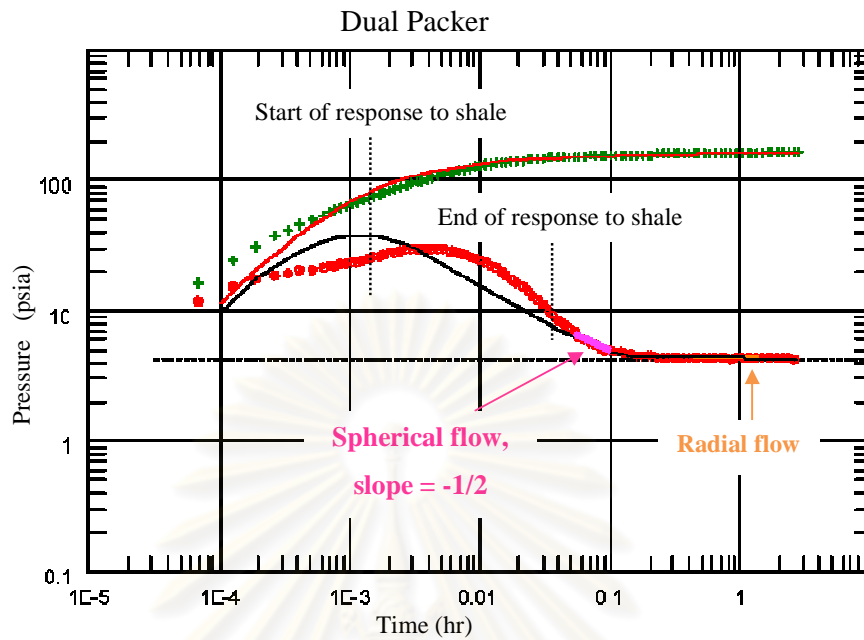
Dual Packer

Figure 5.29-b: Dual packer WFT derivative plot of case VII
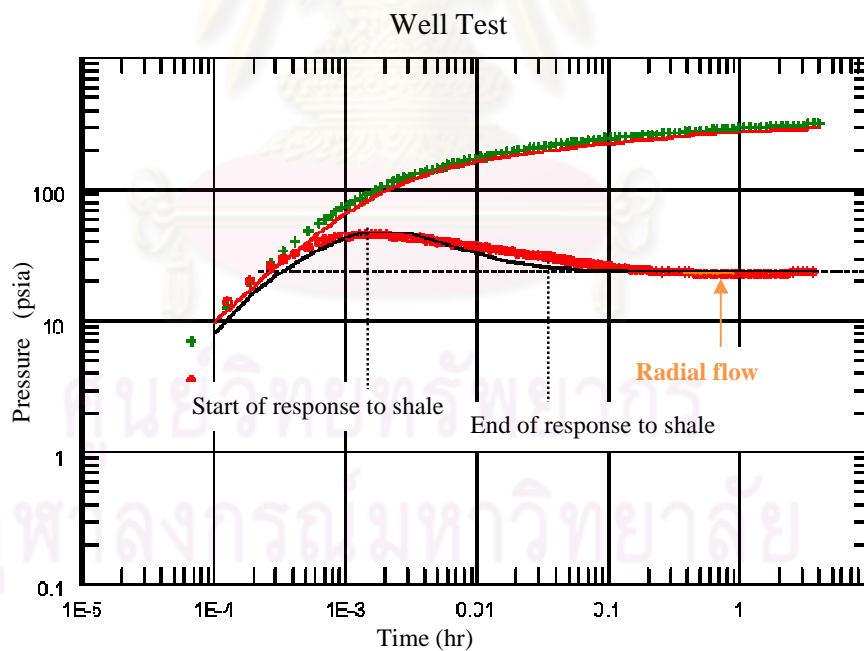
Well Test

Figure 5.29-c: Well test derivative plot of case VII

From Figure 5.29-a, the derivatives of single probe WFT in case VII exhibit more than one hump during spherical flow in the same fashion as in case VI. The first

hump is resembled to the shape of well bore storage effect. Also, for dual packer WFT's derivative plot, in Figure 5.29-b, the effect of shale barrier shows a larger hump than the well bore storage effect, in the same manner as that of case VI. The derivative plot of well test is not distinguishable from case VI. Table 5.15 shows a comparison of different shale volumes and the average permeabilities which depend on the radius of investigation of each test type.

Table 5.15: Shale volume and average permeabilities calculation for case VII

	Single probe	Dual packer	Well test
Draw down period (min)	30	60	240
Build up period (min)	167	167	240
Radius of investigation (ft)	187	196	234
Volume of investigation (ft^3)	2,198,051	2,414,720	3,441,806
Volume of shale (ft^3)	3,543	3,543	3,543
Volume of sand (ft^3)	2,194,508	2,411,177	3,438,262
V_{sh} (%)	0.16	0.15	0.10
Average permeability, k_h (md)	7.82	7.83	7.87

The drawdown periods are different for the three test types but the buildup periods are equal for single probe and dual packer. So, the radiuses of investigation for single probe and dual packer are about the same. This also results in almost similar volume of investigation, V_{sh} and average permeability for single probe and dual packer. However, since the buildup period of well test is longer than those of the others, the radius of investigation, V_{sh} and the average permeability of well test are slightly different.

Table 5.16: Interpreted horizontal and vertical permeabilities compared to clean sand and average permeability for case VII

| Test type | Compared with clean sand | | | | | |
| | k_h | | | k_v | | |
	Input (md)	Interpreted (md)	Error (%)	Input (md)	Interpreted (md)	Error (%)
Single probe	8.09	7.81	-3.50	0.809	0.61	-20.2
Dual packer	8.09	8.31	2.68	0.809	0.57	-29.1
Well test	8.09	8.17	0.95	0.809	N/A	N/A
Test type	Compared with average permeability					
	k_h			k_v		
	Calculated (md)	Interpreted (md)	Error (%)	Calculated (md)	Interpreted (md)	Error (%)
Single probe	7.82	7.81	0	0.78	0.61	-17.5
Dual packer	7.83	8.31	6.17	0.78	0.57	-26.6
Well test	7.87	8.17	3.81	0.79	N/A	N/A

Table 5.16 shows that the estimated horizontal permeabilities from dual packer WFT and well test are deviated with less than 7% error. Even the amount of shale barrier is increased (4 barriers), the effect of shale barrier, in this case, is not much different from that of the previous case. Also, the average permeability calculated in case V, VI, and VII are nearly the same as of case I. The same trend applies to the estimates of vertical permeabilities.

Figures 5.30-a, 5.30-b, and 5.30-c compare derivative plots of base case, case I, case V, case VI, and case VII, separated by test type, in order to allow us to see the effect of amount of shale barrier on derivative plots.
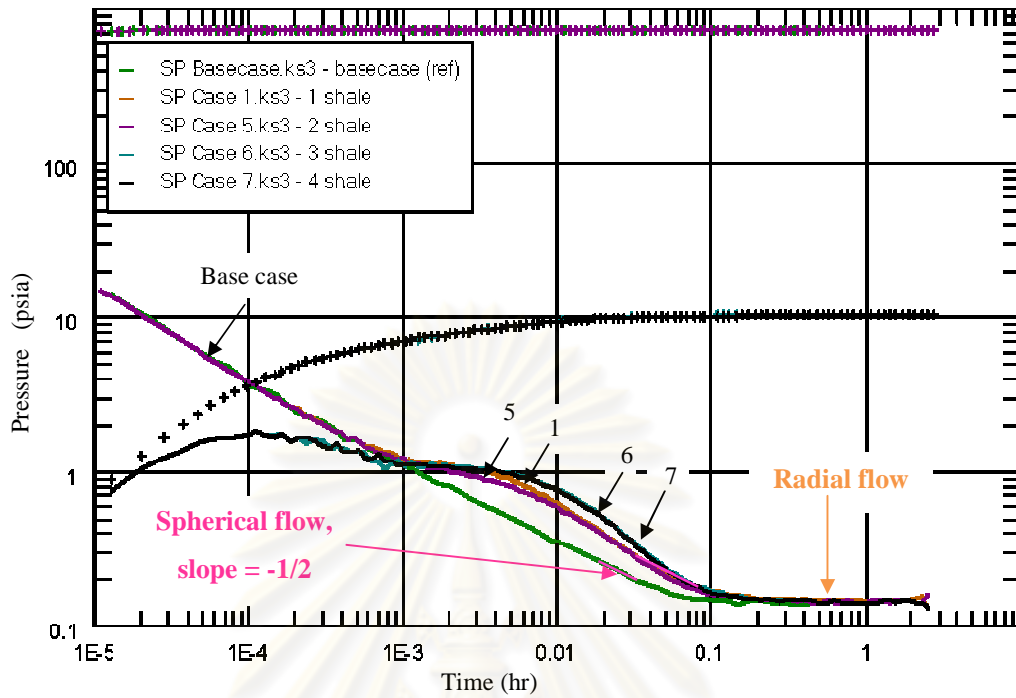
Figure 5.30-a: Single probe WFT derivative plot comparison for different amount of shale barrier
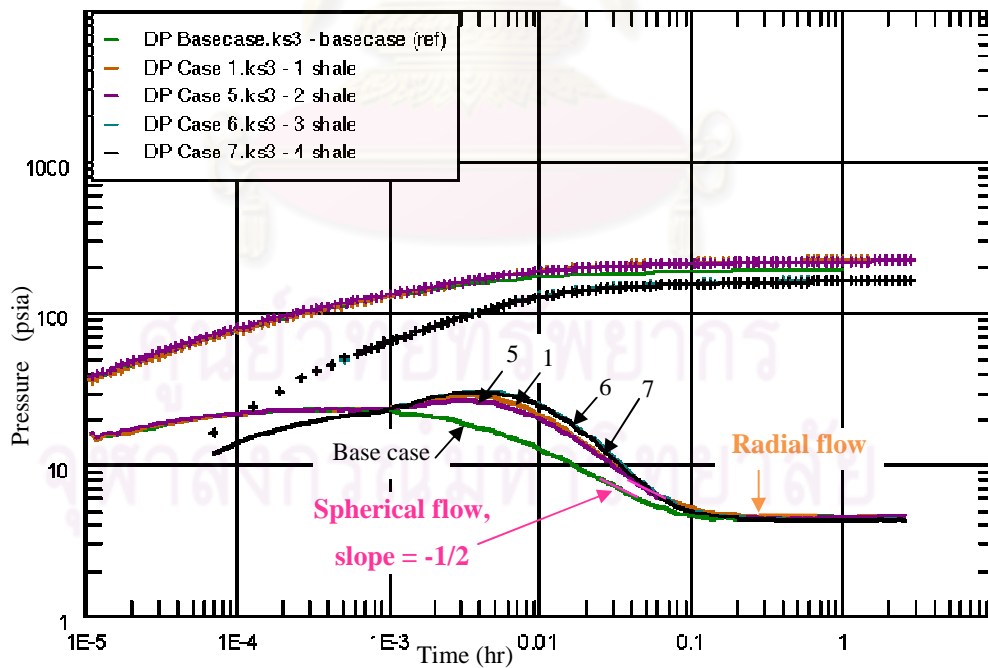
Figure 5.30-b: Dual packer WFT derivative plot comparison for different amount of shale barrier
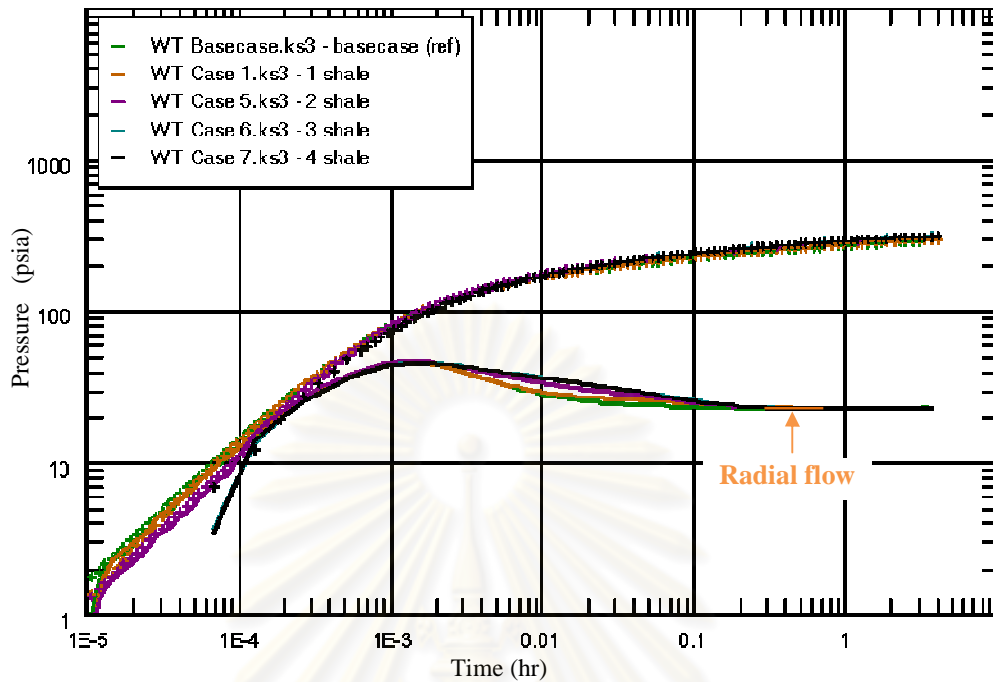
Figure 5.30-c: Well test derivative plot comparison for different amount of shale
barrier

As can be seen from Figures 5.30-a, 5.30-b, and 5.30-c, the hump or deviation
in derivative plots due to shale barrier is identifiable from single probe WFT and dual
packer WFT. For well test, it is difficult or impossible to identify it. Since the scale of
well test is so large that it makes the effect of shale barrier look small and not
obviously distinguishable.

In summary, when all shale barriers are the same in shape, size, and located at
the same distance from the well bore, only small difference in derivative plots can be
identified when the amount of shale is different. From Figure 5.30-a, the hump in
derivative plot of case V (2-shale) is a bit larger than of case I (1-shale). And, the
derivative plot of case VI (3-shale) and case VII (4-shale) are similar, even the
amount shale barrier is different. By the way, for single probe WFT, there would be
more than 1 hump exists in the derivative plot when the amount of shale is more than
2. Table 5.17 summarizes the pressure drop, the radius of investigation, and the
estimated permeabilities of case I, V-VII and base case.

Table 5.17: Summary of estimated permeabilities for case I, V, VI, VII and the base case

Case #	Base case	I	V	VI	VII
Amount of shale barriers	0	1	2	3	4
Single probe					
Pressure drop (psia)	744	745	745	745	745
Int. R_{inv} (ft)	79	186	187	186	187
Int. k_h (md)	7.73	7.68	7.81	7.72	7.81
Int. k_v/k_h	0.142	0.089	0.093	0.085	0.083
Cal. k_v (md)	1.098	0.684	0.724	0.658	0.646
Dual packer					
Pressure drop (psia)	201	227	225	240	238
Int. R_{inv} (ft)	115	189	192	195	196
Int. k_h (md)	7.90	7.69	7.92	8.23	8.31
Int. k_v/k_h	0.103	0.078	0.079	0.068	0.069
Cal. k_v (md)	0.814	0.597	0.623	0.560	0.574
Well test					
Pressure drop (psia)	299	303	313	321	321
Int. R_{inv} (ft)	234	233	234	234	234
Int. k_h (md)	8.19	8.15	8.22	8.17	8.17

*Int. = Interpreted value from derivative plots, **Cal. = Calculated value from interpreted values

Figures 5.31-5.34 show the comparison of interpretation error (%) in permeability estimation among 3 different test types (single probe WFT, dual packer WFT, and conventional well test) for different amounts of shale barrier existing in the reservoir.
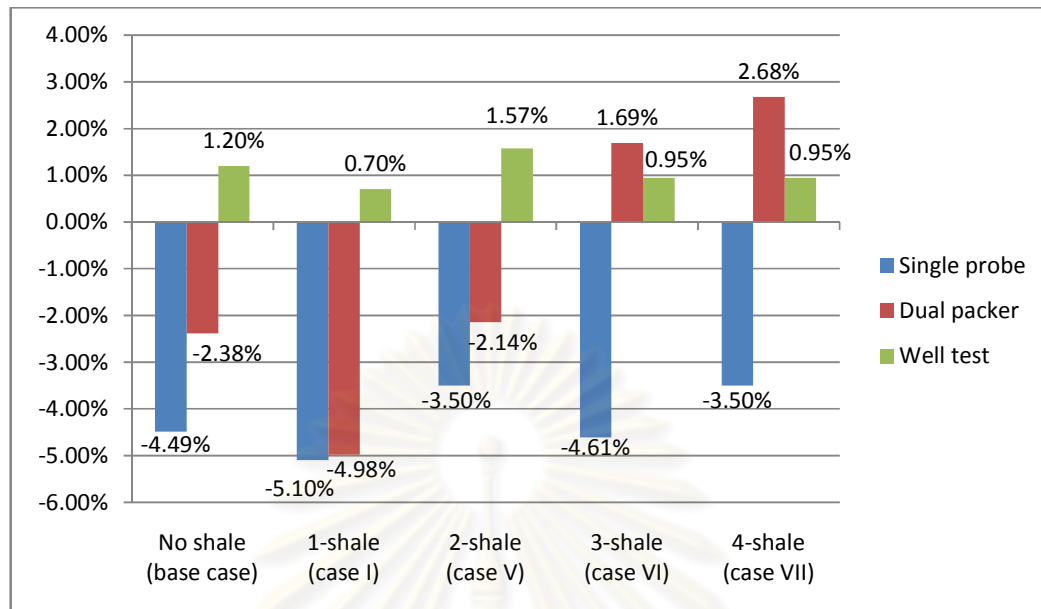
Figure 5.31: k_h estimation error (%) compared to clean sand's k_h for different amounts of shale

From Figure 5.31, it can be seen that single probe underestimates the horizontal permeabilities with error less than 6% for base case and case I, V-VII in which the shale barriers are detected during the spherical flow regime. Dual packer underestimates and overestimates the horizontal permeability with error less than 5%. For well test, the estimated horizontal permeabilities are overestimated compared to the clean sand's horizontal permeability with error less than 2%. This is corresponding to the conclusion that the shale barrier cannot be detected from pressure derivative plots when the shale barriers are far away from the wellbore.
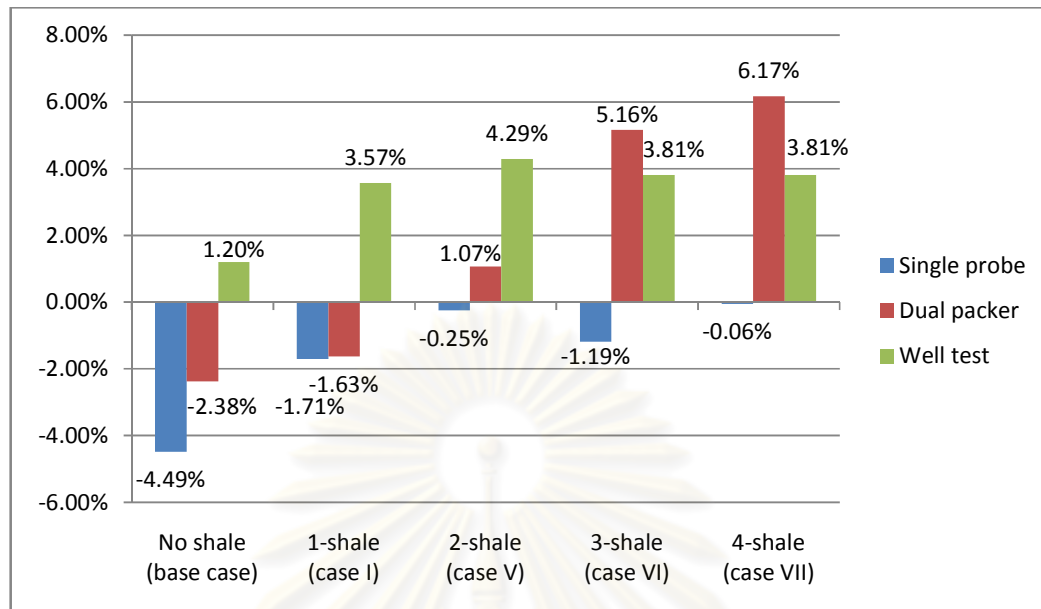
Figure 5.32: k_h estimation error (%) compared to average k_h for different amounts of shale

Figure 5.32 shows single probe underestimates the horizontal permeabilities in case I, V-VII with small error less than 2% compared to the average horizontal permeability. Dual packer underestimates the horizontal permeability in case I, and overestimates the horizontal permeabilities in case V-VII with error less than 7%. For well test, the horizontal permeabilities are overestimated with error less than 5%.
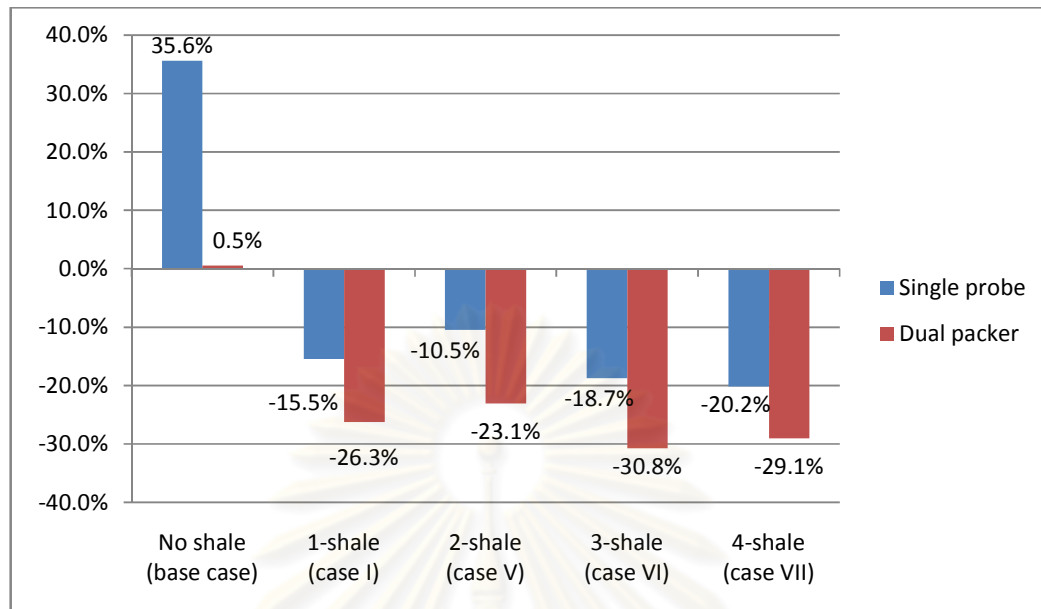
Figure 5.33: k_v estimation error (%) compared to clean sand's k_v for different amounts of shale

Figure 5.3 shows that single probe and dual packer underestimate the vertical permeabilities with error less than 21% and 21%, respectively.
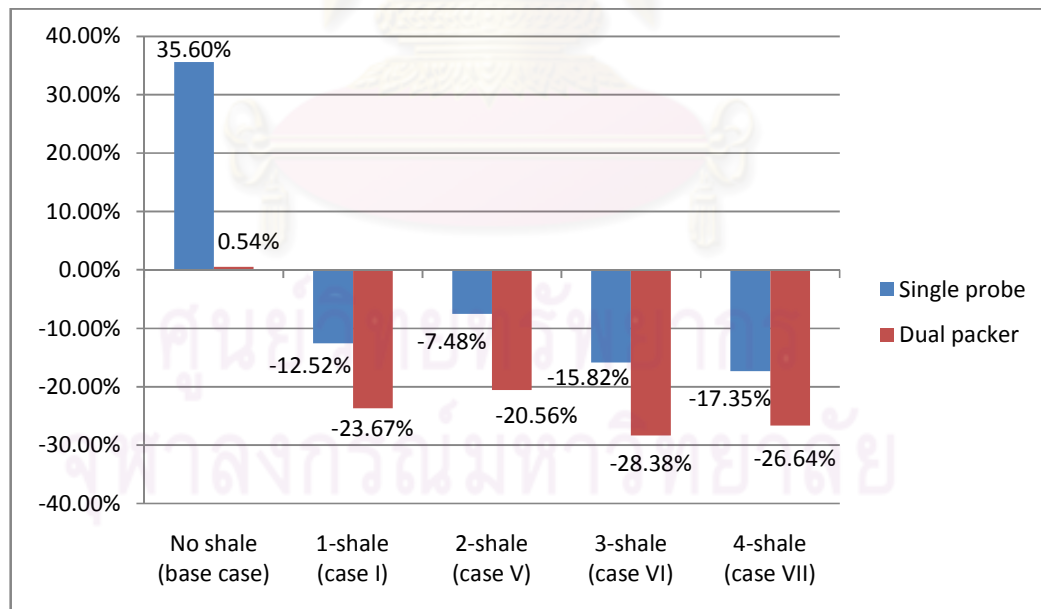
Figure 5.34: k_v estimation error (%) compared to average k_v for different amounts of shale

Figure 5.34 shows the same trend as in Figure 5.33, but with smaller estimation error than that in Figure 5.33.

5.4 Effect of shape of shale barrier

In this case study, the objective is to investigate the effects of shape of shale barrier on pressure derivatives and estimated permeabilities by varying the shape of shale barrier in the reservoir and fixing other parameters such as distance between wellbore and shale barrier, amount of shale barrier, and r,z-dimension of shale barrier.

Since the change of shape also affects shale size or volume of shale barrier, the effect of shape of shale barrier also means the effect of size of shale barrier as well.

5.4.1 Case VIII: Incomplete (1/3) circle shale barrier

Figure 5.35 exhibits the shale configuration of case VIII. The upper picture shows the top view and the cross-sectional view of the grid model. The lower picture depicts the side view of the reservoir model with a wellbore and a shale barrier located 4.4 ft away from the wellbore. The following is the dimension of the shale barrier.

Shale dimension: $\Delta r = 426.9$ ft, $\Delta \theta = 136.3\,°$, $\Delta z = 5.8$ ft
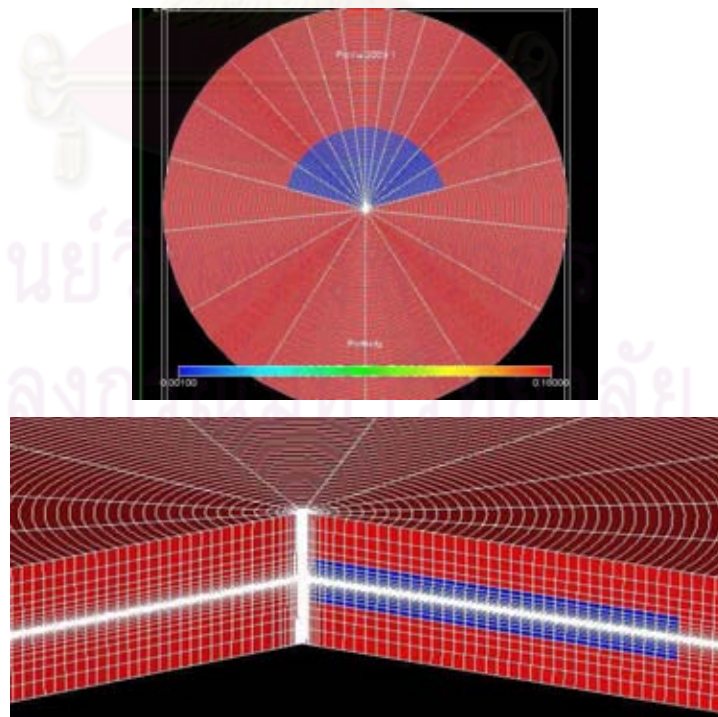
Figure 5.35: Shale configuration of case VIII
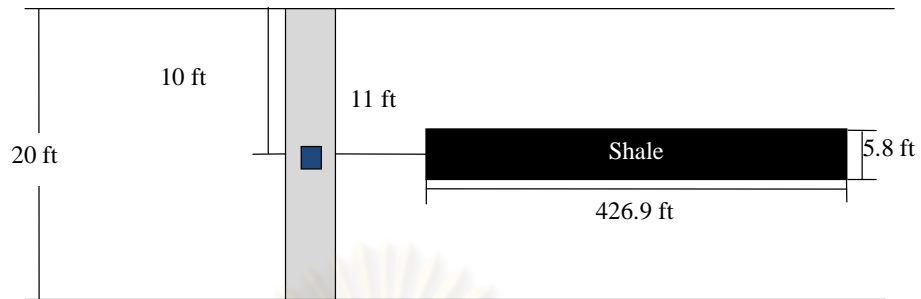
Figure 5.35: Shale configuration of case VIII (continued)

Figure 5.36-a, 5.36-b and 5.36-c show pressure responses simulated from a reservoir simulator for single probe, dual packer and well test, respectively.
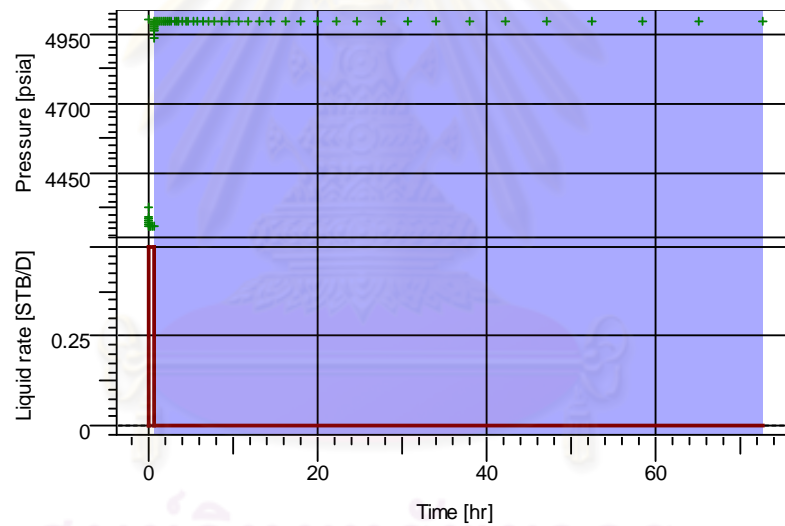
Figure 5.36-a: Pressure history of single probe WFT for case VIII
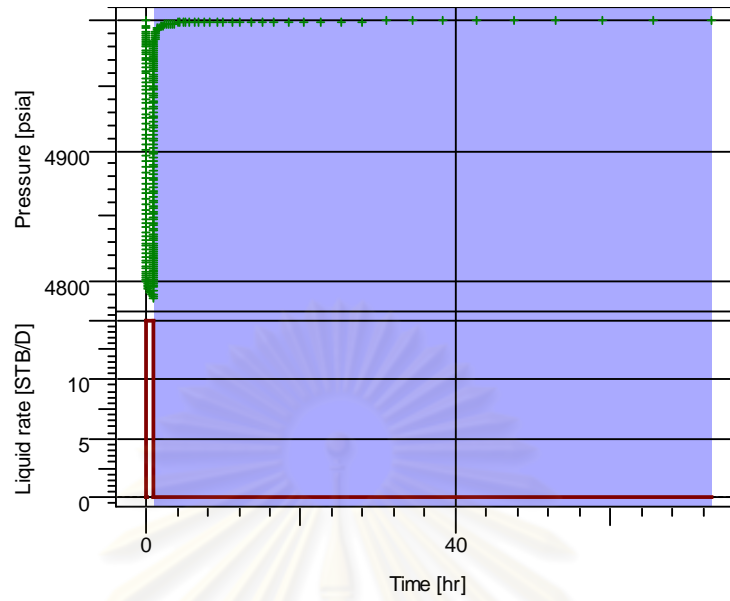
Figure 5.36-b: Pressure history of dual packer WFT for case VIII
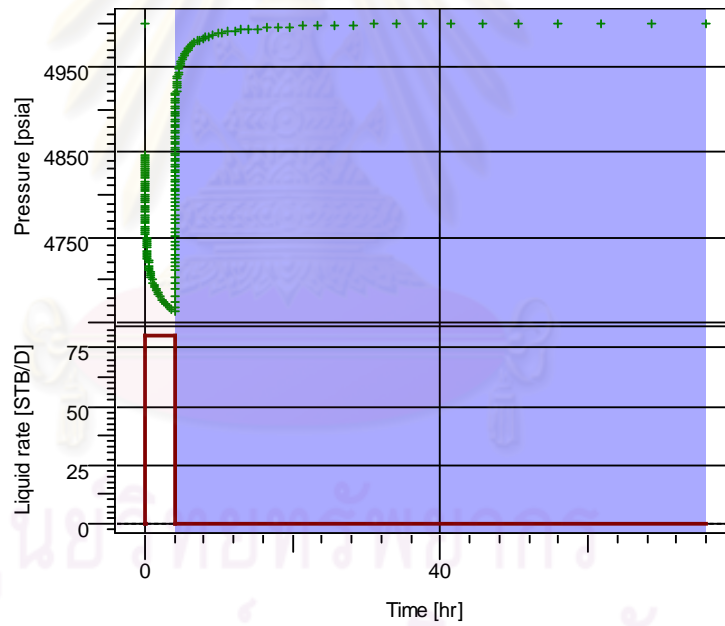
Figure 5.36-c: Pressure history of well test for case VIII

Single Probe
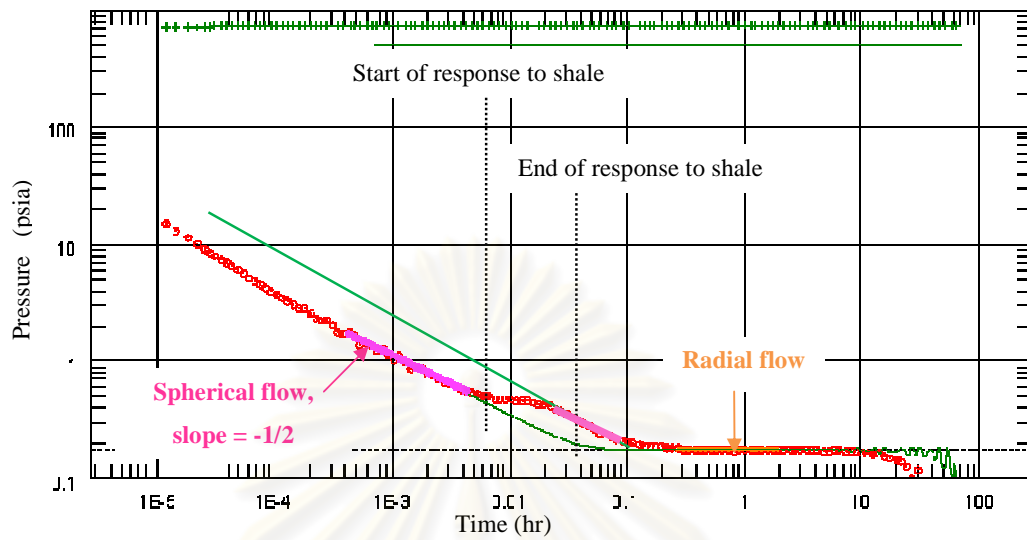
Figure 5.37-a: Single probe WFT derivative plot of case VIII

Dual Packer
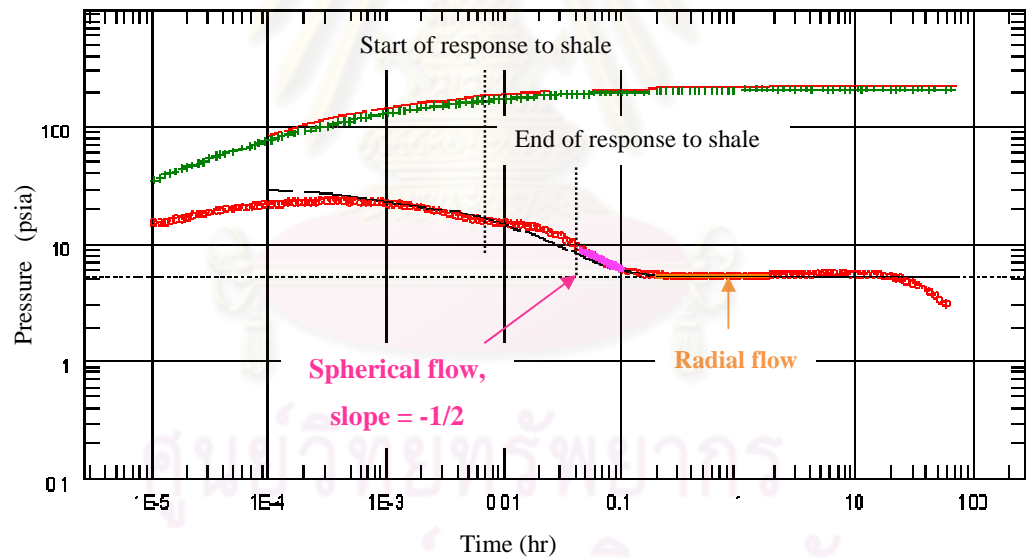
Figure 5.37-b: Dual packer WFT derivative plot of case VIII
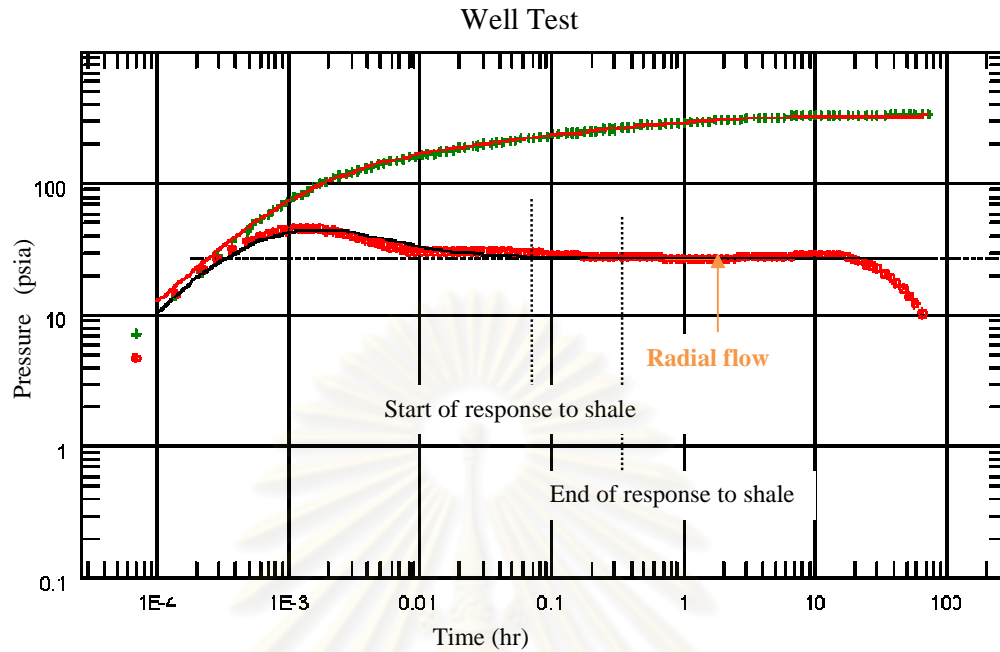
Figure 5.37-c: Well test derivative plot of case VIII

As can be seen in Figures 5.37-a and 5.37-b, the spherical flow model can be matched to the curve at time before 0.1 hr. At late times, after 0.2 hr, the radial flow model can be matched to the curve for all plots (Figures 5.37-a, 5.37-b, and 5.37-c). The effect of the shale barrier can be seen as a hump in the derivative plots. From Figures 5.37-a and 5.37-b, the hump appears in the spherical flow. Though, it is difficult to identify. From Figure 5.37-c, the hump seems to be rather between the well bore storage effect and radial flow regime.

For single probe WFT, it is possible to calculate the vertical permeability from 2 positions, both before and after the occurrence of hump in the derivative as same as in case I, II, and V. In this study, the spherical line that is taken for estimating the vertical permeability from single probe WFT's derivative plot is always the latter one, when possible, in order to take the effect of shale barrier into account.

Table 5.18 shows a comparison of different shale volumes and the average permeabilities which depend on the radius of investigation of each test type.

Table 5.18: Shale volume and average permeability calculation for case VIII

	Single probe	Dual packer	Well test
Draw down period (min)	30	60	240
Build up period (min)	4320	4320	4320
Radius of investigation (ft)	821	849	922
Volume of investigation (ft^3)	42,368,291	45,307,491	53,433,851
Volume of shale (ft^3)	1,346,528	1,346,528	1,346,528
Volume of sand (ft^3)	41,021,764	43,960,964	52,087,324
V_{sh} (%)	3.18	2.97	2.52
Average permeability, k_h (md)	6.40	6.46	6.59

The drawdown periods are different for the three test types but the buildup periods are equal for all three test types. So, the radiuses of investigation of these tests are about the same. This also results in almost similar volume of investigation, V_{sh} and average permeability.

Table 5.19: Interpreted horizontal and vertical permeabilities compared to clean sand and average permeability for case VIII

Test type	Compared with clean sand					
	k_h			k_v		
	Input (md)	Interpreted (md)	Error (%)	Input (md)	Interpreted (md)	Error (%)
Single probe	8.09	6.46	-20.2	0.809	0.61	-25.0
Dual packer	8.09	6.70	-17.2	0.809	0.54	-33.0
Well test	8.09	7.08	-12.5	0.809	N/A	N/A
Test type	Compared with average permeability					
	k_h			k_v		
	Calculated (md)	Interpreted (md)	Error (%)	Calculated (md)	Interpreted (md)	Error (%)
Single probe	6.40	6.46	0.89	0.64	0.61	-5.3
Dual packer	6.46	6.70	3.74	0.65	0.54	-16.1
Well test	6.59	7.08	4.47	0.66	N/A	N/A

From Table 5.19, since the volume of shale is increased up to 3% of volume of investigation, the effect of shale barrier on permeability estimation is more obvious than those in the other previous cases. Definitely, the increased volume of shale results in reduction of total permeability. When comparing the estimated

permeabilities with clean sand's permeability, the interpretation error (%) will be high and may be up to 20% error (underestimated) for horizontal permeability. However, when comparing the estimates to the average permeability, the interpretation error (%) is reduced to less than 5% (overestimated).

5.4.2 Case IX: Incomplete (1/2) circle shale barrier

Figure 5.38 exhibits the shale configuration of case IX. The upper picture shows the top view and the cross-sectional view of the grid model. The lower picture depicts the side view of the reservoir model with a wellbore and a shale barrier located 4.4 ft away from the wellbore. The following is the dimension of the shale barrier.

Shale dimension: $\Delta r = 426.9$ ft, $\Delta\theta = 180\,°$, $\Delta z = 5.8$ ft
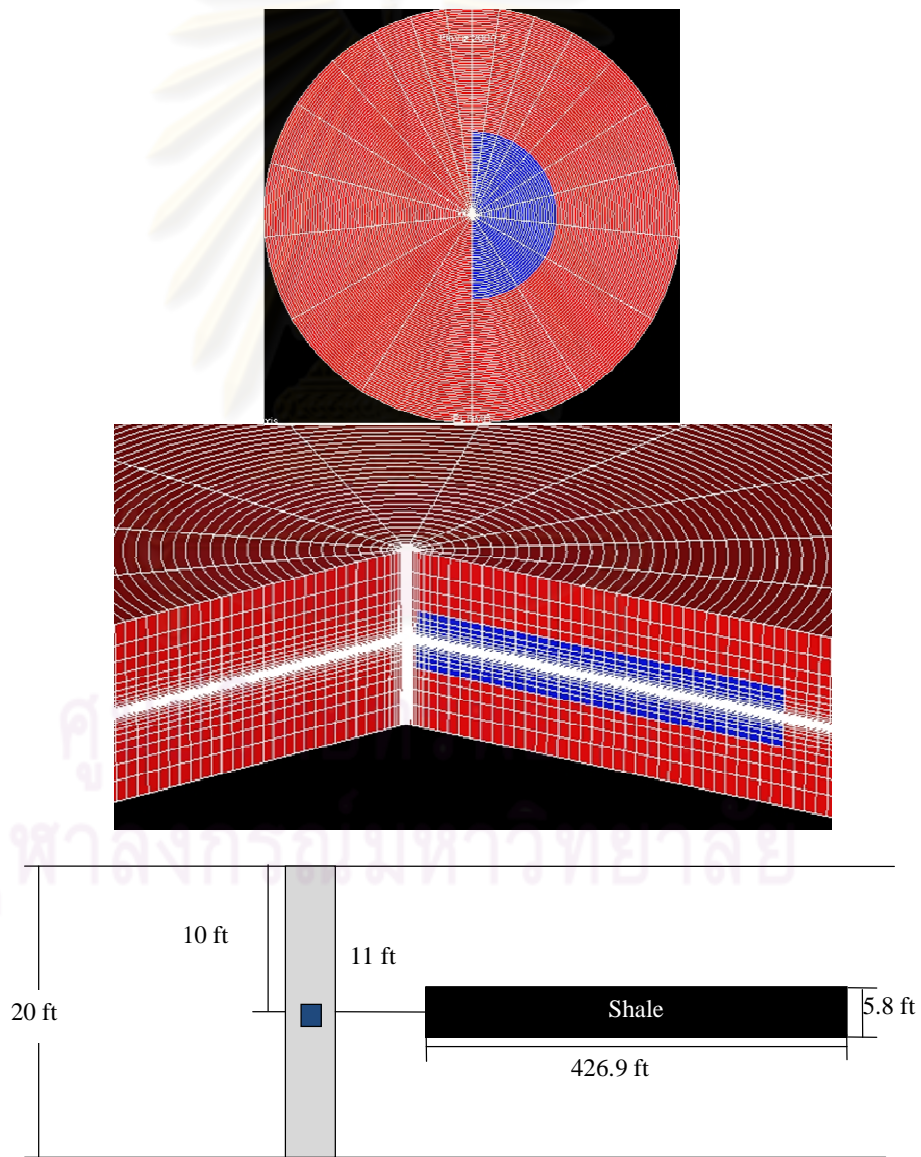
Figure 5.38: Shale configuration of case IX

Figure 5.39-a, 5.39-b and 5.39-c show pressure responses simulated from a reservoir simulator for single probe, dual packer and well test, respectively.

Figure 5.39-a: Pressure history of single probe WFT for case IX

Figure 5.39-b: Pressure history of dual packer WFT for case IX

Figure 5.39-c: Pressure history of well test for case IX
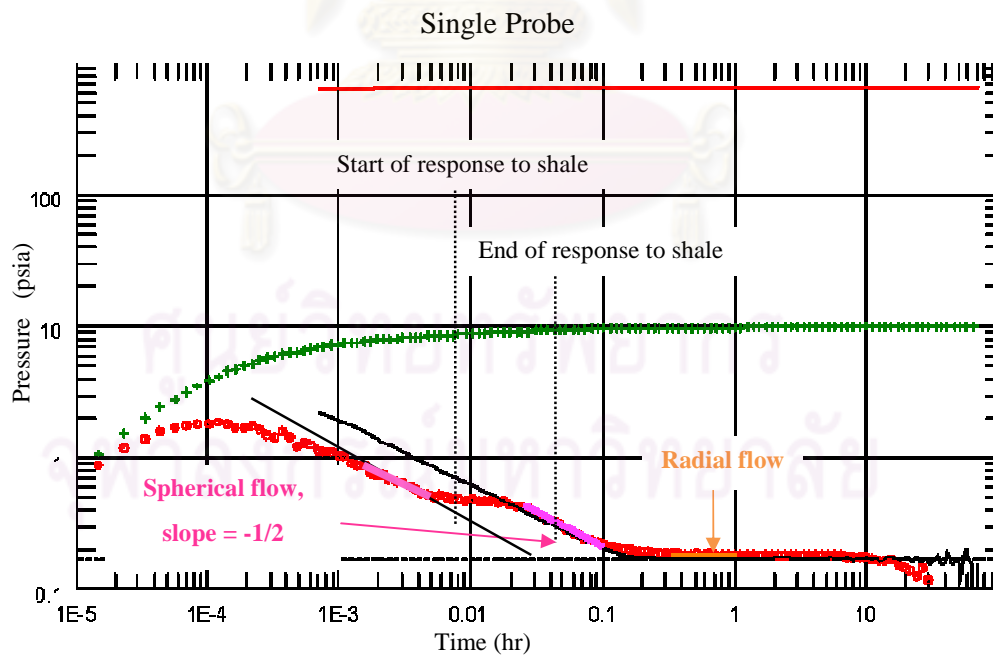
Single Probe

Figure 5.40-a: Single probe WFT derivative plot of case IX

Dual Packer

Figure 5.40-b: Dual packer WFT derivative plot of case IX

Well Test

Figure 5.40-c: Well test derivative plot of case IX

As can be seen in Figure 5.40-a, the derivative plot of single probe WFT in case IX exhibits more than one hump during spherical flow. The first hump is resembled to the shape of well bore storage effect. The second hump looks similar to

that in case VIII. Table 5.20 shows a comparison of different shale volumes and the average permeabilities which depend on the radius of investigation of each test type.

Table 5.20: Shale volume and average permeability calculation for case IX

	Single probe	Dual packer	Well test
Draw down period (min)	30	60	240
Build up period (min)	4320	4320	4320
Radius of investigation (ft)	832	929	908
Volume of investigation (ft^3)	43,511,233	54,248,291	51,823,451
Volume of shale (ft^3)	1,748,177	1,748,177	1,748,177
Volume of sand (ft^3)	41,763,046	52,500,114	50,075,274
V_{sh} (%)	4.02	3.22	3.37
Average permeability, k_h (md)	6.43	6.60	6.56

The drawdown periods are different for the three test types but the buildup periods are equal for all three test types. So, the radiuses of investigation of these tests are about the same. This also results in almost similar volume of investigation, V_{sh} and average permeability.

Table 5.21: Interpreted horizontal and vertical permeabilities compared to clean sand and average permeability for case IX

Test type	Compared with clean sand					
	k_h			k_v		
	Input (md)	Interpreted (md)	Error (%)	Input (md)	Interpreted (md)	Error (%)
Single probe	8.09	6.64	-18.0	0.809	0.499	-38.4
Dual packer	8.09	7.18	-11.3	0.809	0.440	-46.0
Well test	8.09	6.85	-15.4	0.809	N/A	N/A
Test type	Compared with average permeability					
	k_h			k_v		
	Calculated (md)	Interpreted (md)	Error (%)	Calculated (md)	Interpreted (md)	Error (%)
Single probe	6.43	6.64	3.35	0.64	0.499	-22.4
Dual packer	6.60	7.18	8.81	0.66	0.440	-33.3
Well test	6.56	6.85	4.35	0.66	N/A	N/A

From Table 5.21, the interpretation error (%) of estimated horizontal permeability compared to clean sand's permeability are high due to the increased volume of shale, similar to the results in case IX. When comparing the same result to the average permeability, the interpretation error (%) is less than 9% (overestimated). The estimated vertical permeability error from both tests are up to 50% (underestimated).

5.4.3 Case X: Incomplete (3/4) circle shale barrier

Figure 5.41 exhibits the shale configuration of case X. The upper picture shows the top view and the cross-sectional view of the grid model. The lower picture depicts the side view of the reservoir model with a wellbore and a shale barrier located 4.4 ft away from the wellbore. The following is the dimension of the shale barrier.

Shale dimension: $\Delta r = 426.9$ ft, $\Delta\theta = 278$ °, $\Delta z = 5.8$ ft
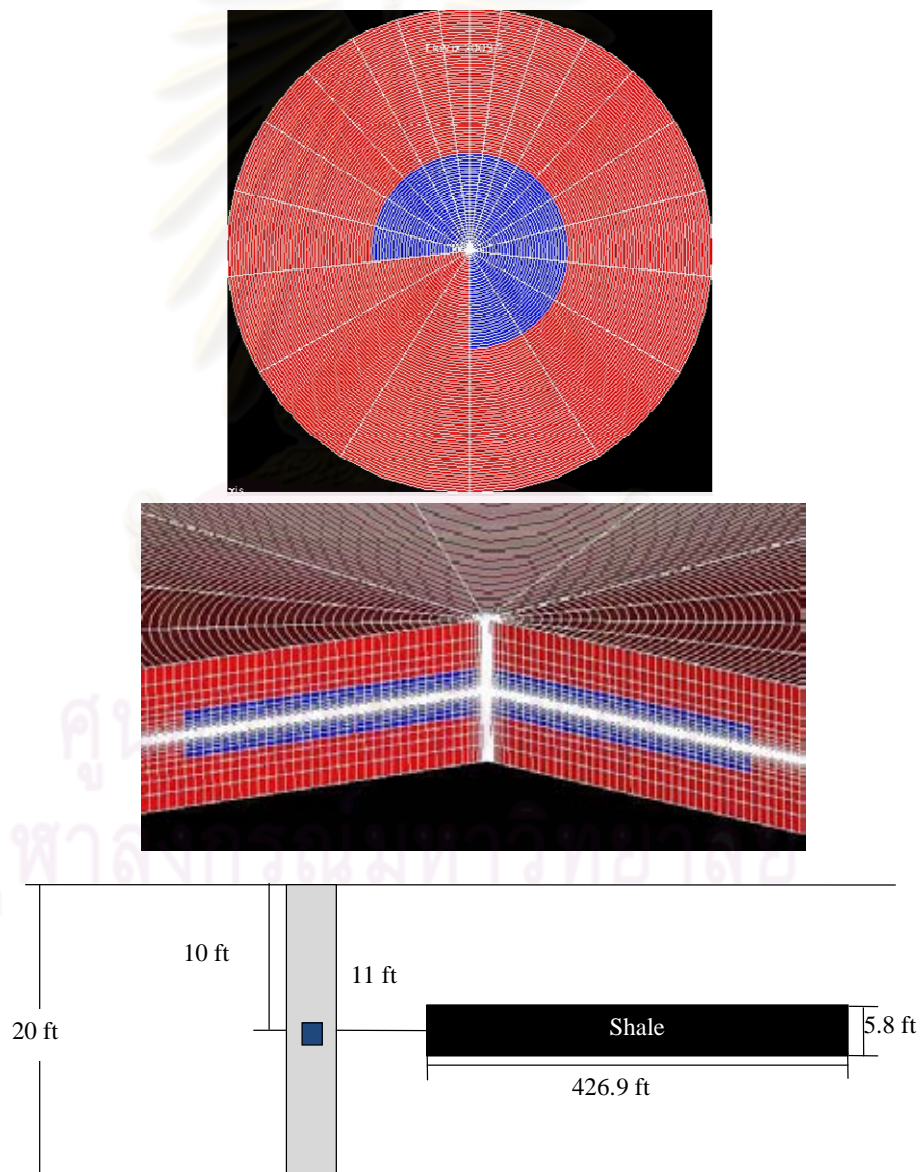
Figure 5.41: Shale configuration of case X

Figure 5.42-a, 5.42-b and 5.42-c show pressure responses simulated from a reservoir simulator for single probe, dual packer and well test, respectively.
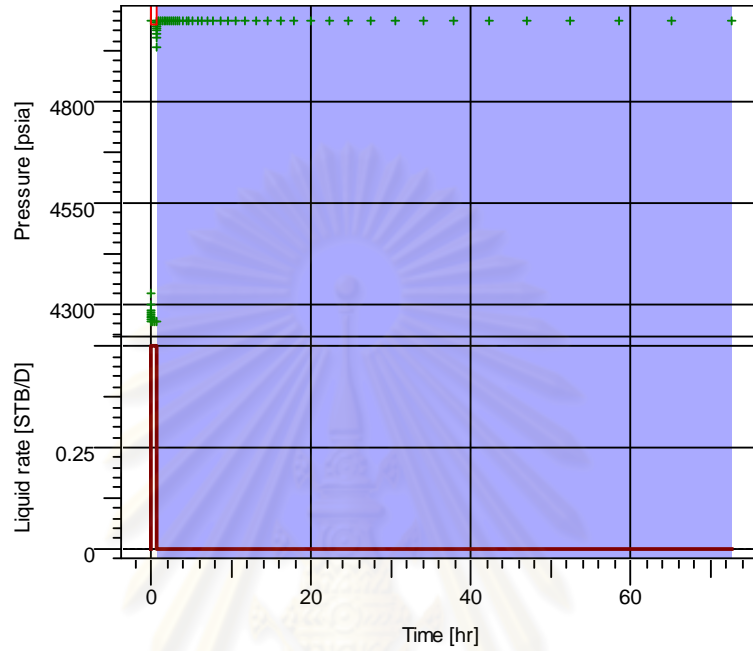

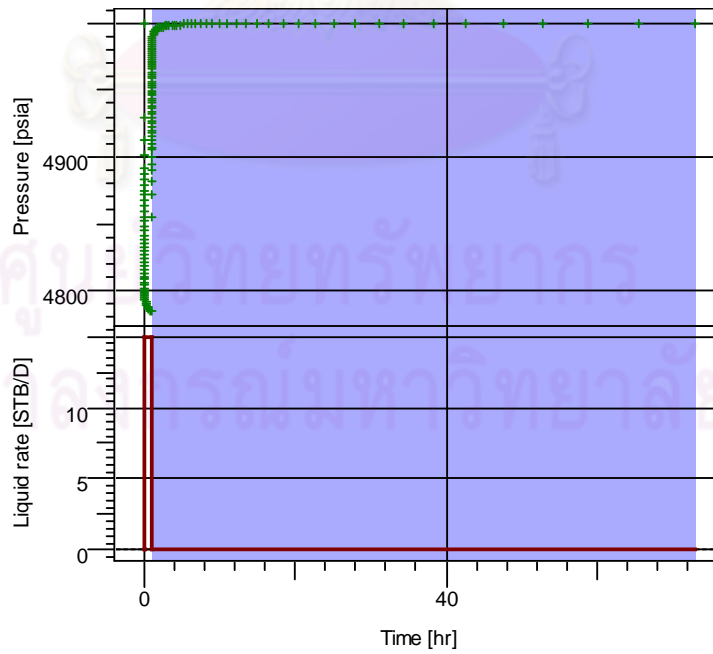Figure 5.42-a: Pressure history of single probe WFT for case X

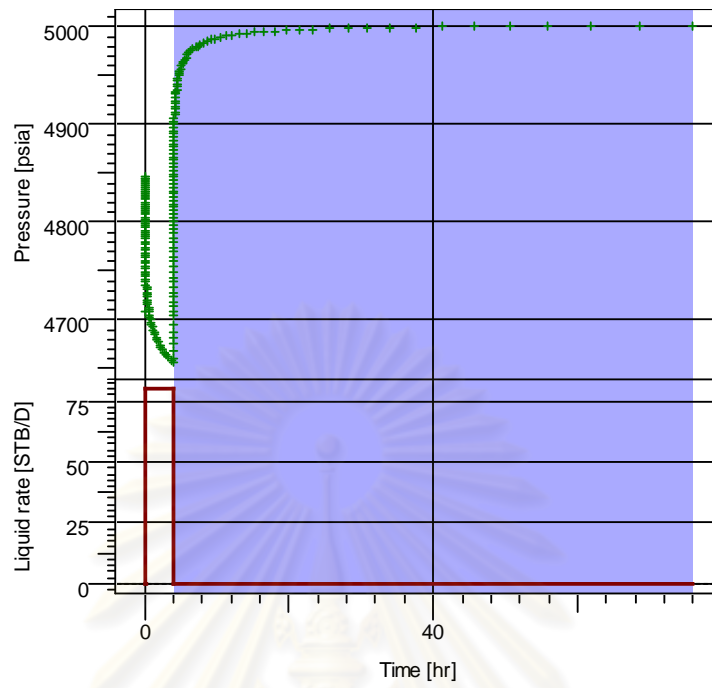Figure 5.42-b: Pressure history of dual packer WFT for case X

Figure 5.42-c: Pressure history of well test for case X

Single Probe
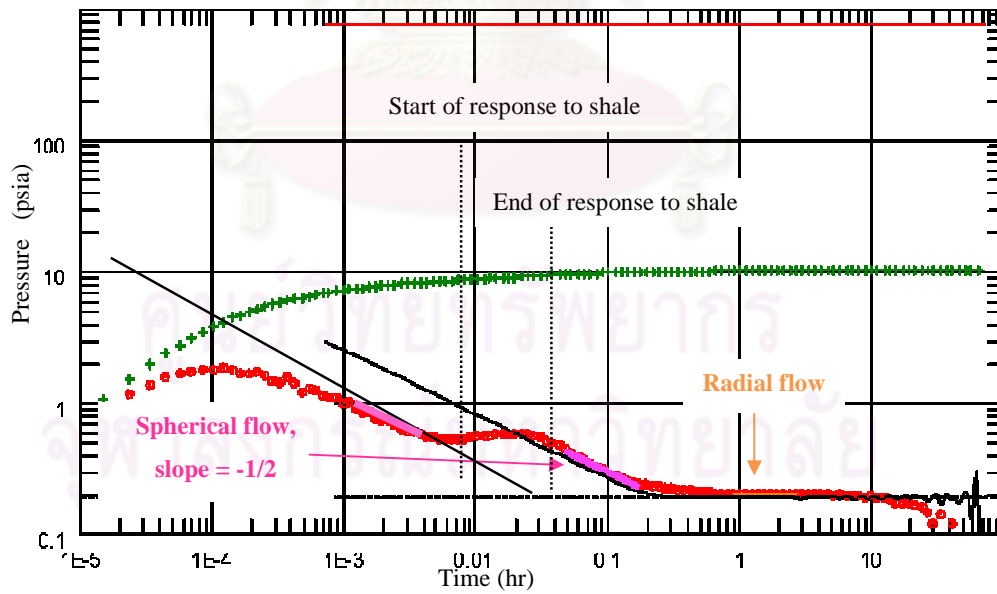
Figure 5.43-a: Single probe WFT derivative plot of case X

Dual Packer

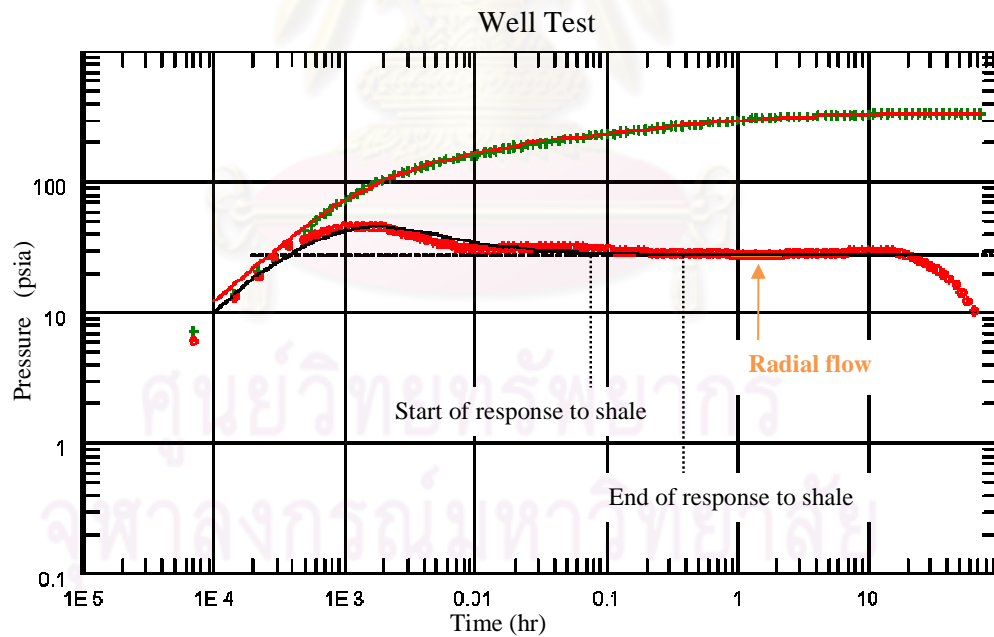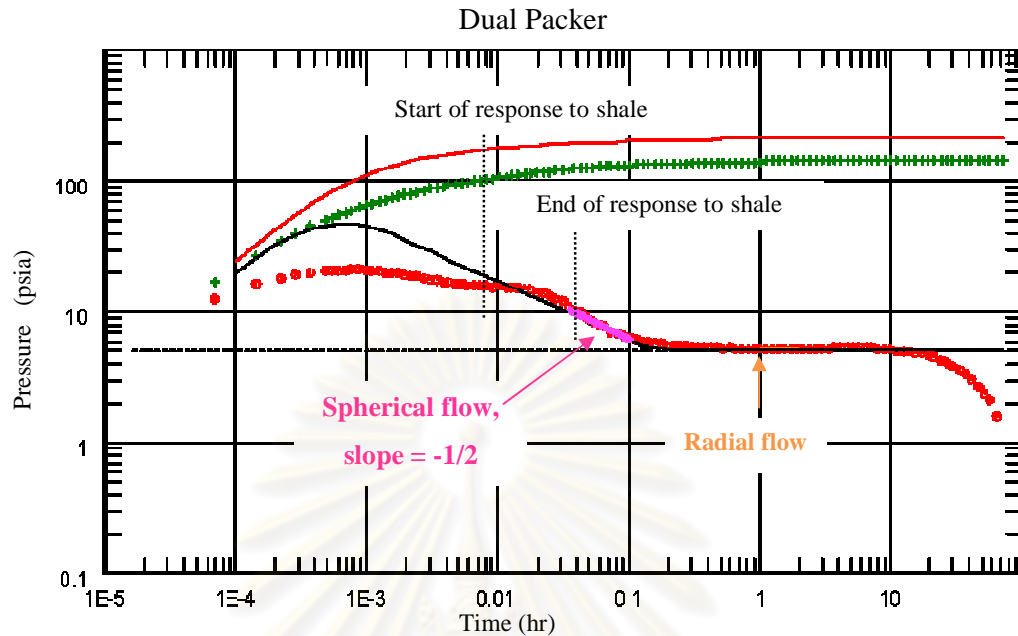Figure 5.43-b: Dual packer WFT derivative plot of case X

Well Test

Figure 5.43-c: Well test derivative plot of case X
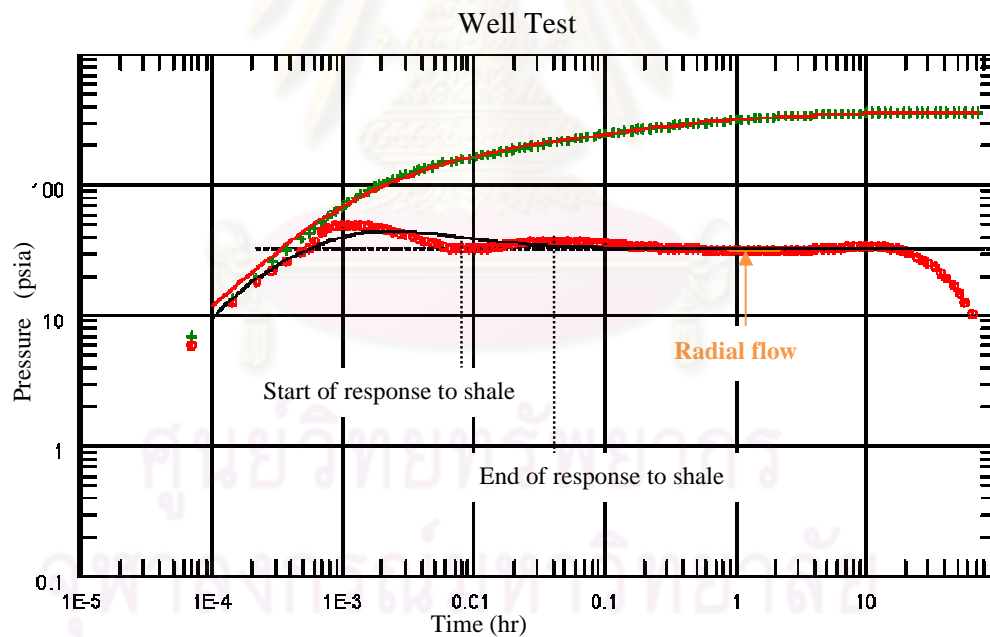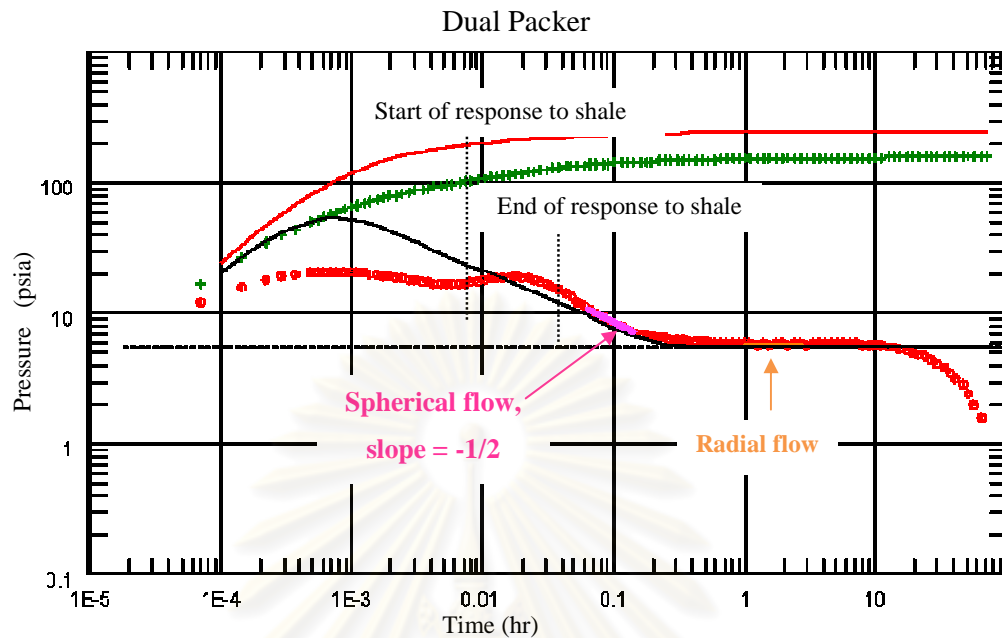
As can be seen in Figure 5.43-a, the derivative plot of single probe WFT in case IX exhibits more than one hump during spherical flow. The first hump is resembled to the shape of well bore storage effect similar to the earlier cases. The second hump looks similar to that in case VIII and IX. Table 5.22 shows a

comparison of different shale volumes and the average permeabilities which depend on the radius of investigation of each test type.

Table 5.22: Shale volume and average permeability calculation for case X

	Single probe	Dual packer	Well test
Draw down period (min)	30	60	240
Build up period (min)	4320	4320	4320
Radius of investigation (ft)	785	878	842
Volume of investigation (ft^3)	38,734,143	48,455,566	44,563,451
Volume of shale (ft^3)	2,690,250	2,690,250	2,690,250
Volume of sand (ft^3)	36,043,893	45,765,316	41,873,201
V_{sh} (%)	6.95	5.55	6.04
Average permeability, k_h (md)	6.33	6.51	6.45

The drawdown periods are different for the three test types but the buildup periods are equal for all three test types. So, the radiuses of investigation of these tests are about the same. This also results in almost similar volume of investigation, V_{sh} and average permeability.

Table 5.23: Interpreted horizontal and vertical permeabilities compared to clean sand and average permeability for case X

Test type	Compared with clean sand					
	k_h			k_v		
	Input (md)	Interpreted (md)	Error (%)	Input (md)	Interpreted (md)	Error (%)
Single probe	8.09	5.91	-27.0	0.809	0.352	-56.5
Dual packer	8.09	6.42	-20.7	0.809	0.322	-60.0
Well test	8.09	5.90	-27.1	0.809	N/A	N/A
Test type	Compared with average permeability					
	k_h			k_v		
	Calculated (md)	Interpreted (md)	Error (%)	Calculated (md)	Interpreted (md)	Error (%)
Single probe	6.33	5.91	-6.57	0.63	0.352	-44.3
Dual packer	6.51	6.42	-1.42	0.65	0.322	-50.5
Well test	6.45	5.90	-8.45	0.65	N/A	N/A

From Table 5.23, the interpretation errors (%) of estimated horizontal

permeabilities compared to clean sand's permeability are high due to the increased volume of shale. When comparing the same result to the average permeability, the interpretation error (%) is less than 9% (underestimated). The estimated vertical permeability error from both tests is increased to 60% error (underestimated) due to the increase of shale volume.

5.4.4 Case XI: Complete circle shale barrier

Figure 5.54 exhibits the shale configuration of case XI. The upper picture shows the top view and the cross-sectional view of the grid model. The lower picture depicts the side view of the reservoir model with a wellbore and a shale barrier located 4.4 ft away from the wellbore. The following is the dimension of the shale barrier.

Shale dimension: $\Delta r = 426.9$ ft, $\Delta \theta = 360$ °, $\Delta z = 5.8$ ft
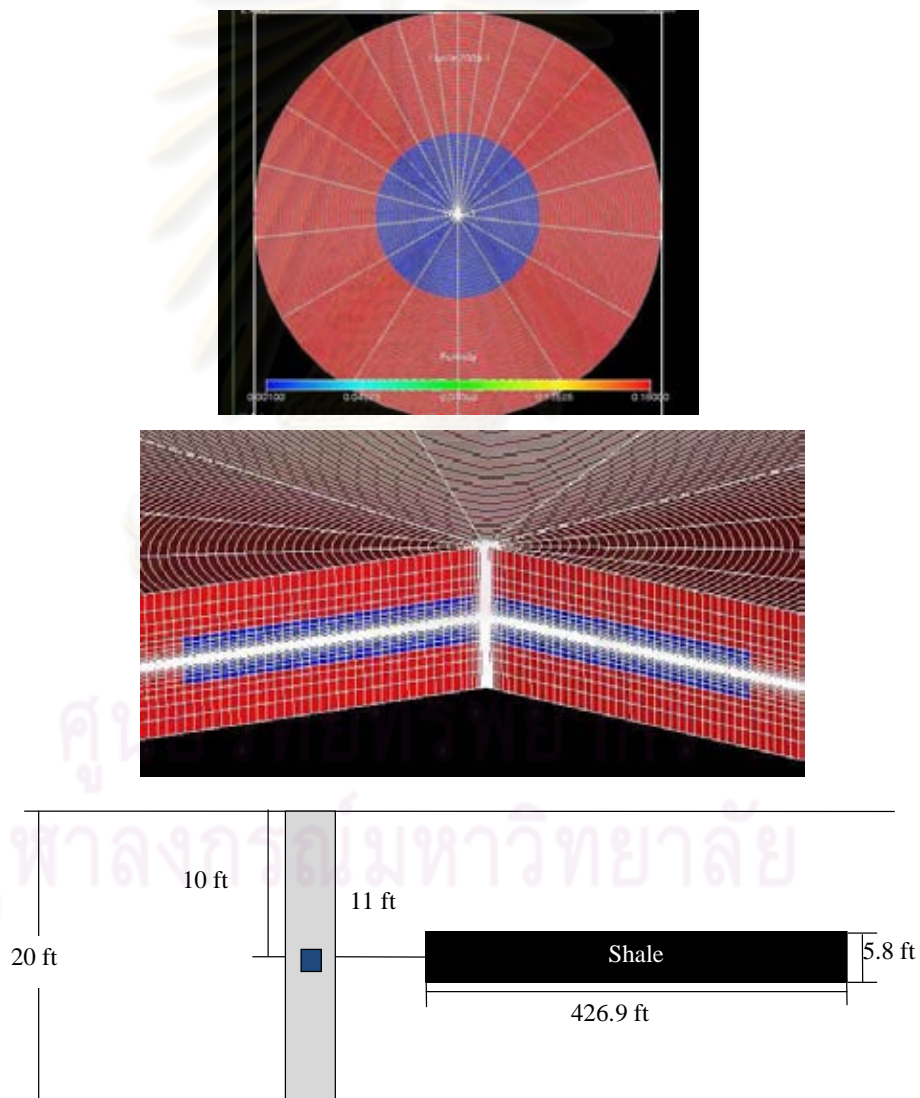
Figure 5.44: Shale configuration of case XI

Figure 5.45-a, 5.45-b and 5.45-c show pressure responses simulated from a reservoir simulator for single probe, dual packer and well test, respectively.
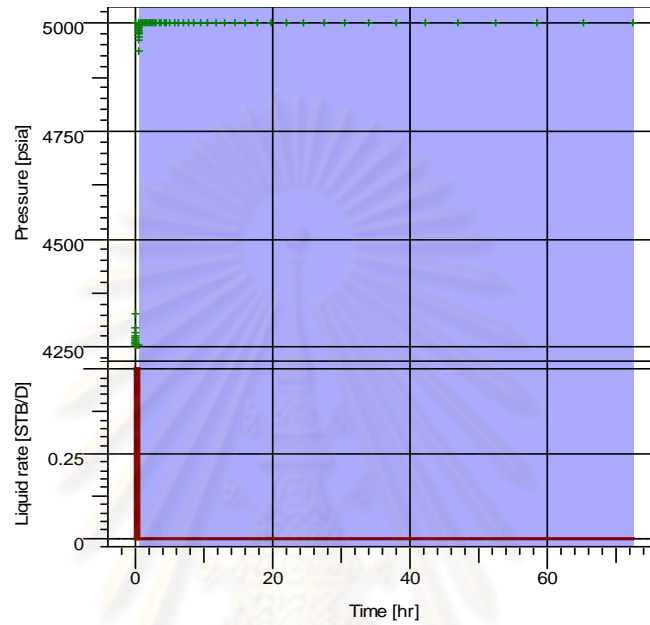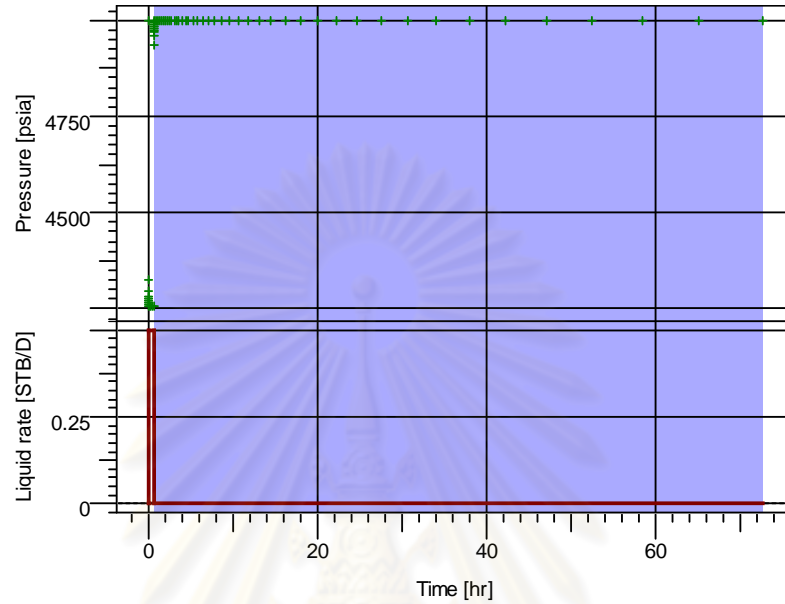

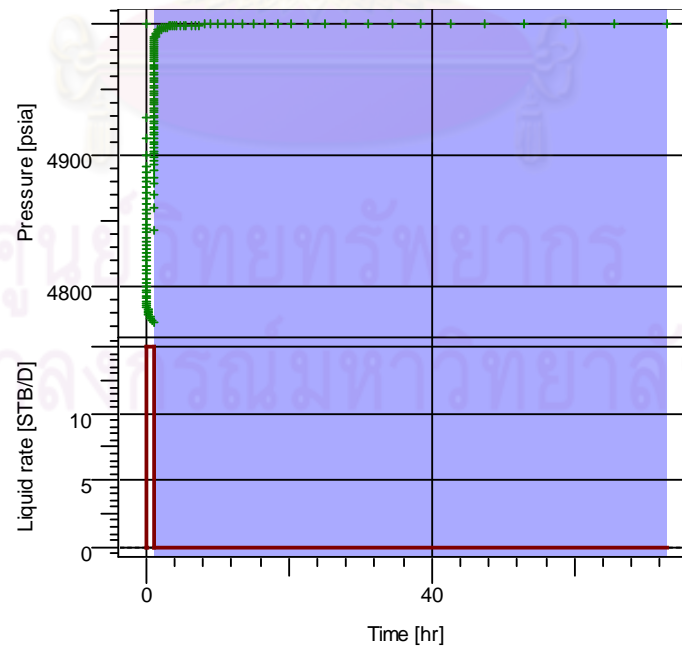Figure 5.45-a: Pressure history of single probe WFT for case XI
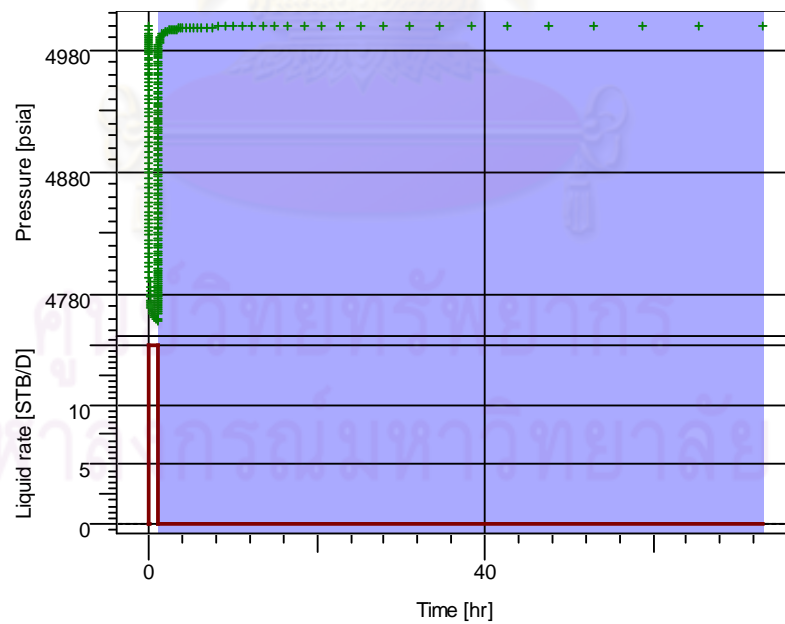
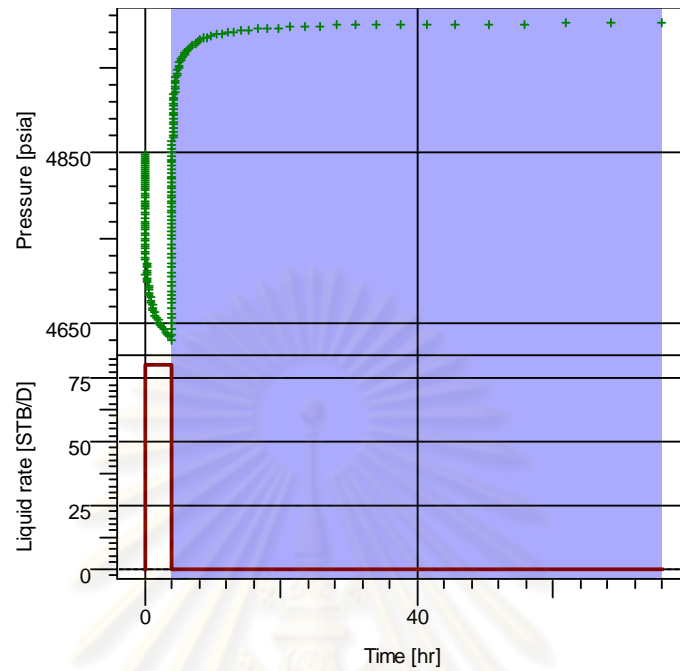Figure 5.45-b: Pressure history of dual packer WFT for case XI
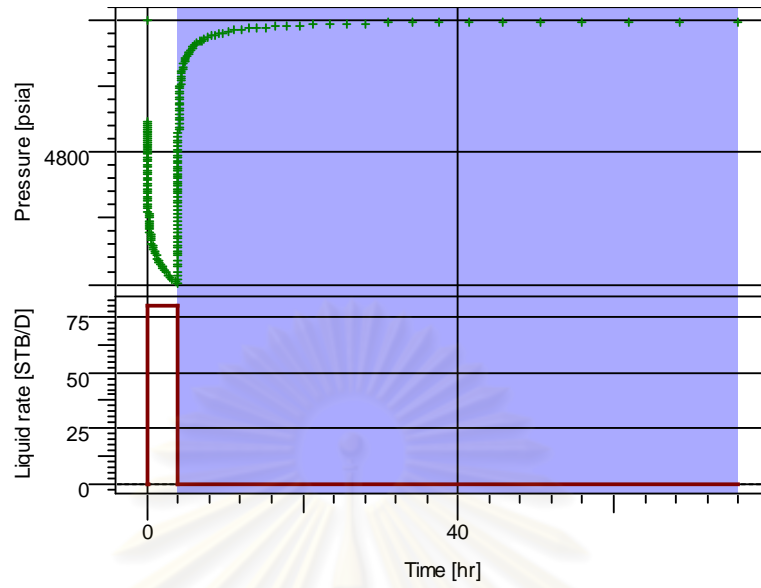
Figure 5.45-c: Pressure history of well test for case XI

Single Probe
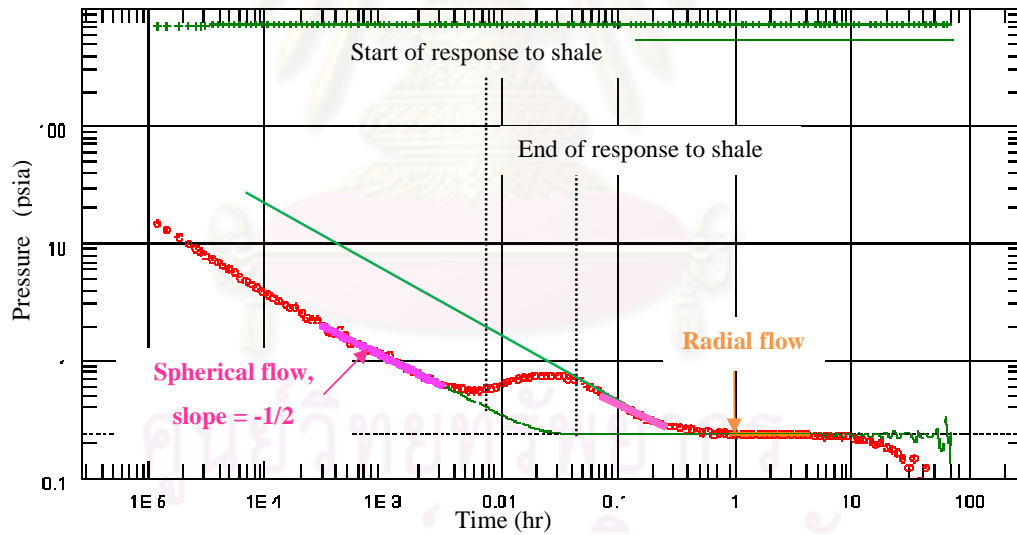
Figure 5.46-a: Single probe WFT derivative plot of case XI

Dual Packer

Figure 5.46-b: Dual packer WFT derivative plot of case XI

Well Test

Figure 5.46-c: Well test derivative plot of case XI
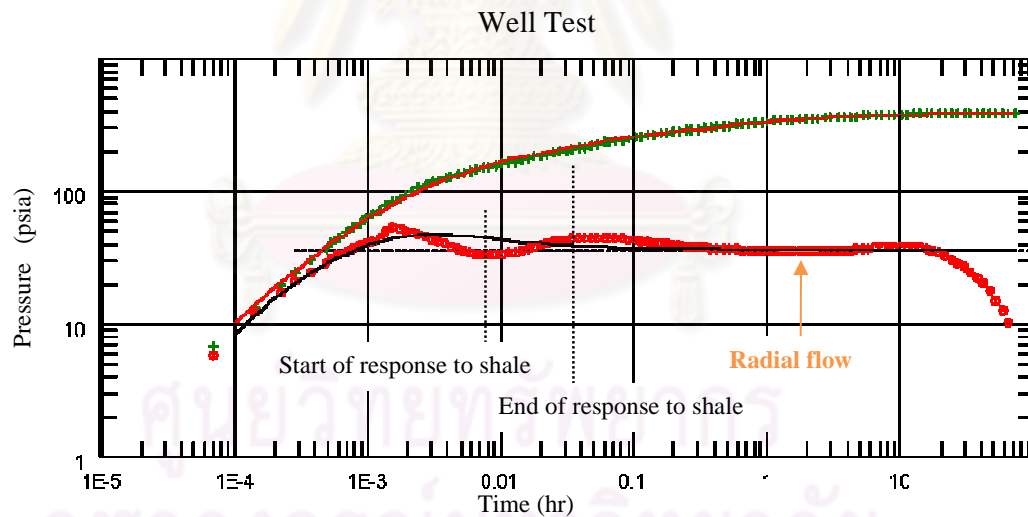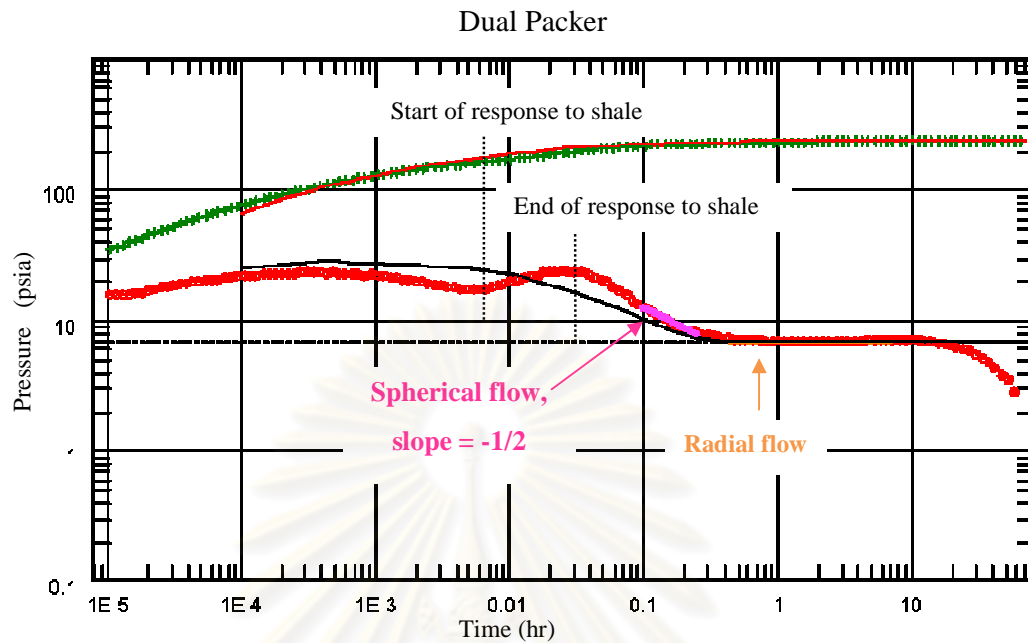
As can be seen from Figure 5.46, when the shape of shale barrier is changed from incomplete circular to circular, the deviation in derivative plots is changed as well. For single probe WFT and dual packer WFT, only one hump or deviation exists. For well test derivative plot, the effect of shale barrier is more obvious and is identifiable. A spike can be observer during well bore storage in the derivative plot.

Table 5.24 shows a comparison of different shale volumes and the average permeabilities which depend on the radius of investigation of each test type.

Table 5.24: Shale volume and average permeability calculation for case XI

	Single probe	Dual packer	Well test
Draw down period (min)	30	60	240
Build up period (min)	4320	4320	4320
Radius of investigation (ft)	710	740	795
Volume of investigation (ft^3)	31,686,286	34,420,571	39,727,286
Volume of shale (ft^3)	3,496,354	3,496,354	3,496,354
Volume of sand (ft^3)	28,189,932	30,924,217	36,230,932
V_{sh} (%)	11.03	10.16	8.80
Average permeability, k_h (md)	6.14	6.22	6.35

The drawdown periods are different for the three test types but the buildup periods are equal for all three test types. So, the radiuses of investigation of these tests are about the same. This also results in almost similar volume of investigation, V_{sh} and average permeability.

Table 5.25: Interpreted horizontal and vertical permeabilities compared to clean sand and average permeability for case XI

Test type	Compared with clean sand					
	k_h			k_v		
	Input (md)	Interpreted (md)	Error (%)	Input (md)	Interpreted (md)	Error (%)
Single probe	8.09	4.82	-40.4	0.809	0.31	-62.0
Dual packer	8.09	5.10	-37.3	0.809	0.27	-67.0
Well test	8.09	5.26	-35.0	0.809	N/A	N/A
Test type	Compared with average permeability					
	k_h			k_v		
	Calculated (md)	Interpreted (md)	Error (%)	Calculated (md)	Interpreted (md)	Error (%)
Single probe	6.14	4.82	-21.5	0.61	0.31	-49.1
Dual packer	6.22	5.10	-18.3	0.62	0.27	-56.6
Well test	6.35	5.26	-17.1	0.64	N/A	N/A

From Table 5.25, the interpretation error (%) of estimated horizontal permeabilities compared to clean sand's permeability is increased to 40% error (underestimated) due to the increased volume of shale. When comparing the same result to the average permeability, the interpretation error (%) is up to 18% (underestimated). The estimated vertical permeability error from both tests is increased to 70% (underestimated) also due to the increase of shale volume.
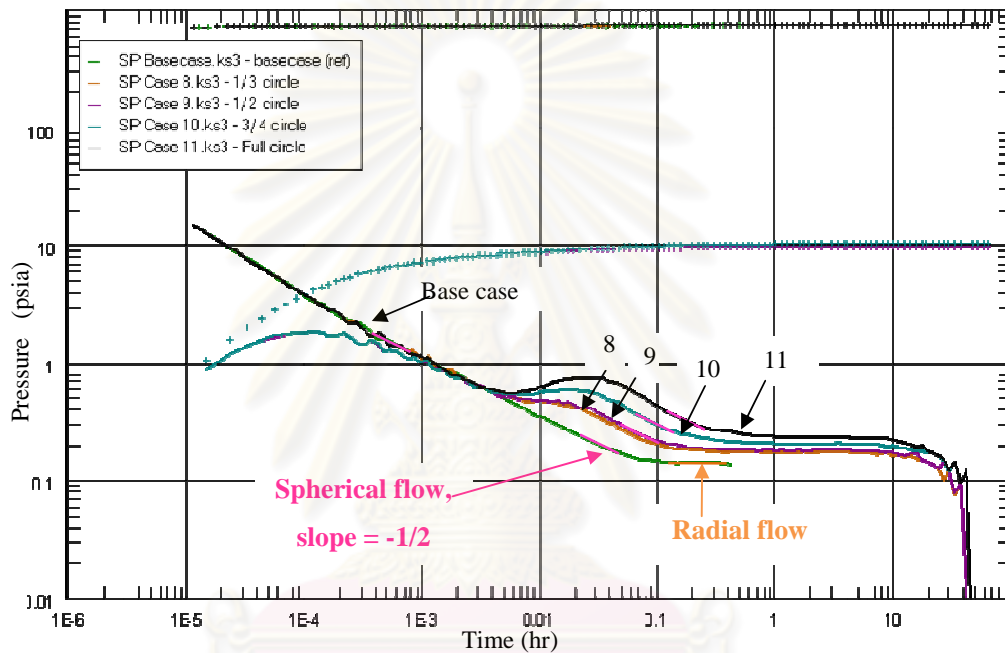
Figure 5.47-a: Single probe WFT derivative plot comparison for different shapes of shale barrier
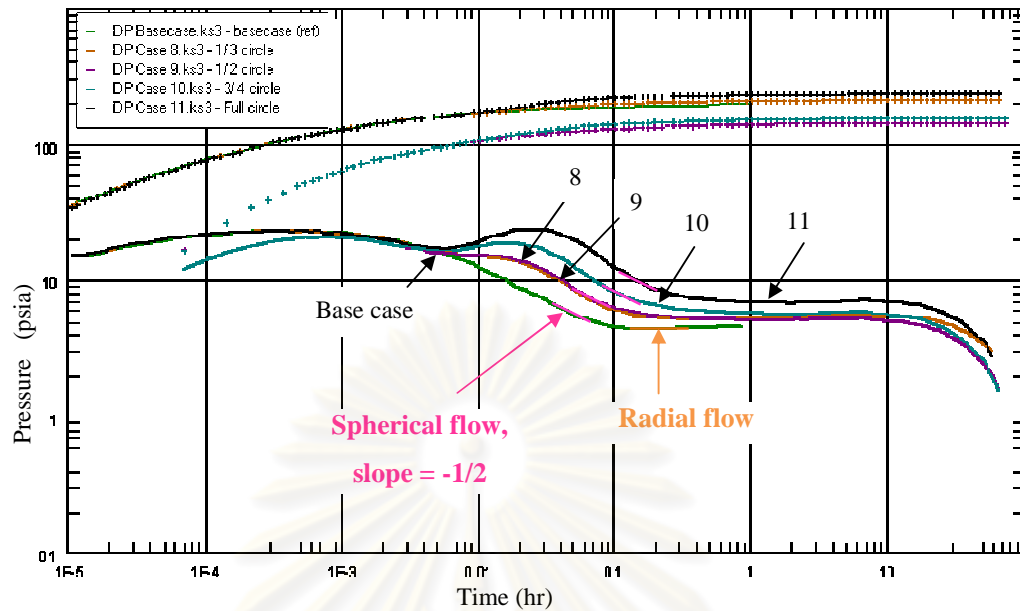
Figure 5.47-b: Dual packer WFT derivative plot comparison for different shapes of shale barrier
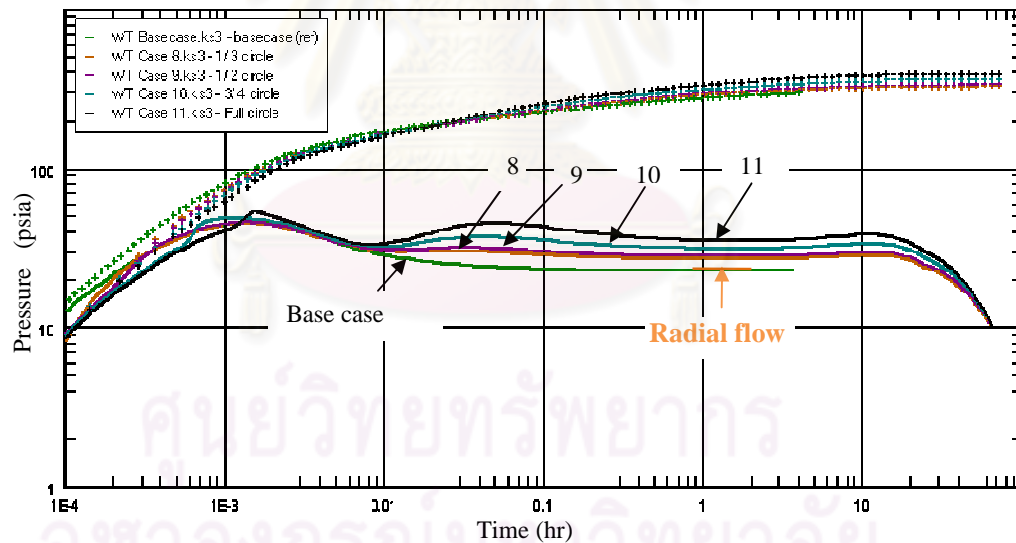
Figure 5.47-c: Well test derivative plot comparison for different shapes of shale barrier

As can be seen from Figures 5.47-a, 5.47-b, and 5.47-c, the humps or deviations in derivative plots from single probe WFT, dual packer WFT are identifiable and distinguishable between each case. However, it is not possible to identify the effect of shale barrier from one derivative plot of well test, except that

there are more than 1 derivative plot available for comparison.

In summary, the shape of shale barrier affects the shape of hump on the derivative plots. The larger shape or more complete shape of shale barrier exhibits a larger hump in the derivative plot. Table 5.26 summarizes the pressure drop, the radius of investigation and the estimated permeabilities of case VIII-XI and base case.

Table 5.26: Summary of estimated permeabilities for case VIII, IX, X, XI and base case

Case #	Base case	VIII	IX	X	XI
Completeness of circle	-	1/3	1/2	3/4	Full
Single probe					
Pressure drop (psia)	744	744	744	745	745
Int. R_{inv} (ft)	79	821	832	785	710
Int. k_h (md)	7.73	6.46	6.64	5.91	4.82
Int. k_v/k_h	0.142	0.094	0.075	0.060	0.064
Cal. k_v (md)	1.098	0.607	0.499	0.352	0.308
Dual packer					
Pressure drop (psia)	201	213	216	227	242
Int. R_{inv} (ft)	115	849	929	878	740
Int. k_h (md)	7.90	6.70	7.18	6.42	5.08
Int. k_v/k_h	0.103	0.081	0.061	0.050	0.053
Cal. k_v (md)	0.814	0.542	0.440	0.322	0.270
Well test					
Pressure drop (psia)	299	340	347	371	400
Int. R_{inv} (ft)	234	922	908	842	795
Int. k_h (md)	8.19	7.08	6.85	5.90	5.26

*Int. = Interpreted value from derivative plots, **Cal. = Calculated value from interpreted values

Figures 5.48-5.51 show the comparison of interpretation error (%) in permeability estimation among 3 different test types (single probe WFT, dual packer WFT, and conventional well test) for different shapes of shale barrier in the reservoir.
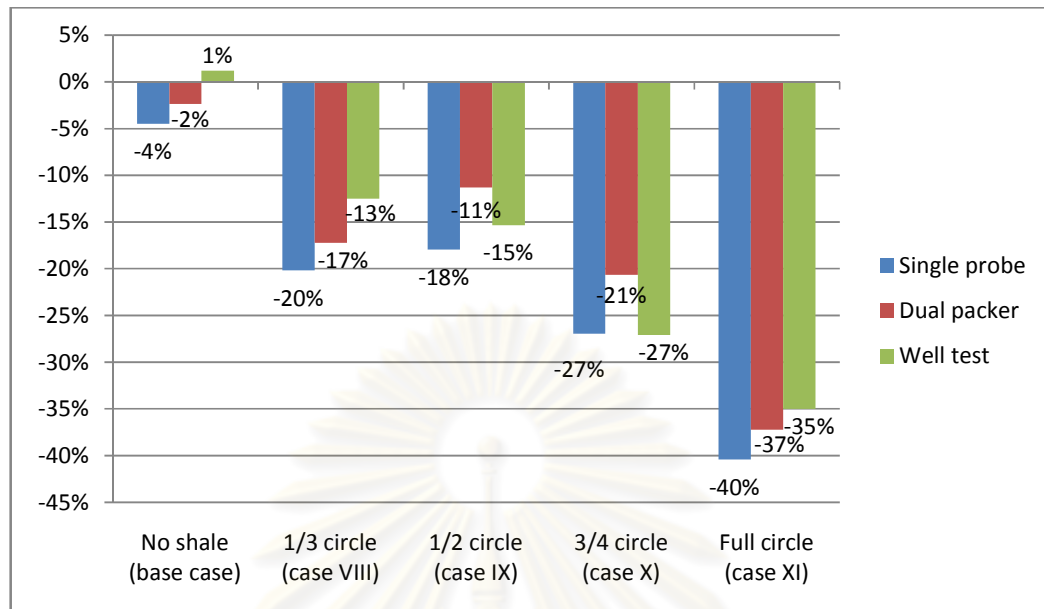
Figure 5.48: k_h estimation error (%) compared to clean sand's k_h for different shapes of shale barrier

Figure 5.48 shows that when the volume of shale barrier is large enough (more than 2% of volume of investigation), the estimation of the horizontal permeabilities from the three test types are obviously underestimated up to 40% error compared to clean sand' horizontal permeability.
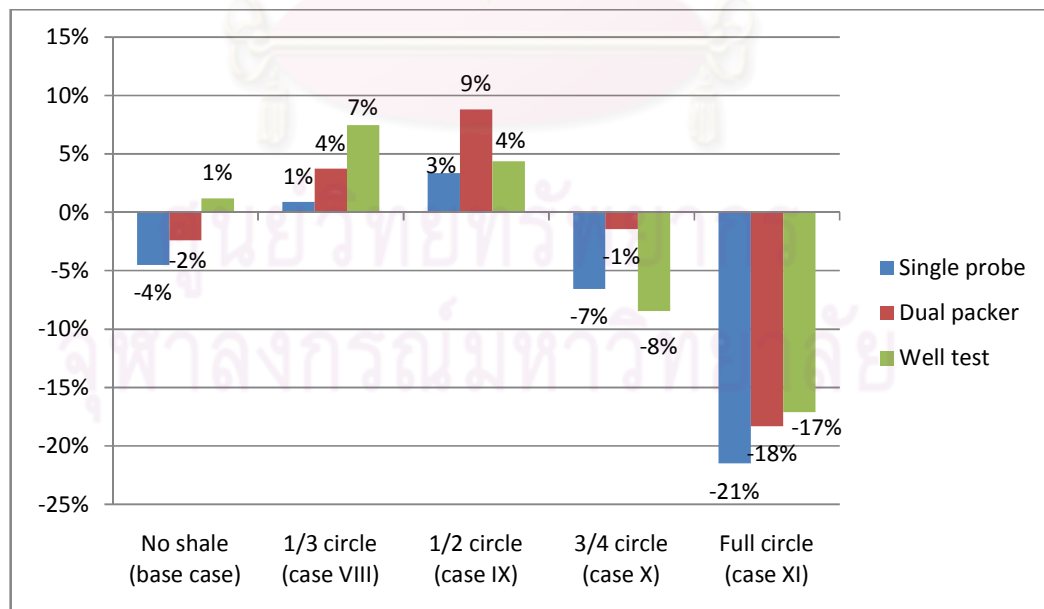
Figure 5.49: k_h estimation error (%) compared to average k_h for different shapes of shale barrier

Figure 5.49 shows that when comparing the estimated horizontal

permeabilities to the average horizontal permeability, the estimation errors are less than that in Figure 5.48. In case VIII-IX, the three test types overestimate the horizontal permeabilities with error less than 10%. In case X, the three test types underestimate the horizontal permeabilities with error less than 9%. In case XI, the estimation errors are up to 21%.
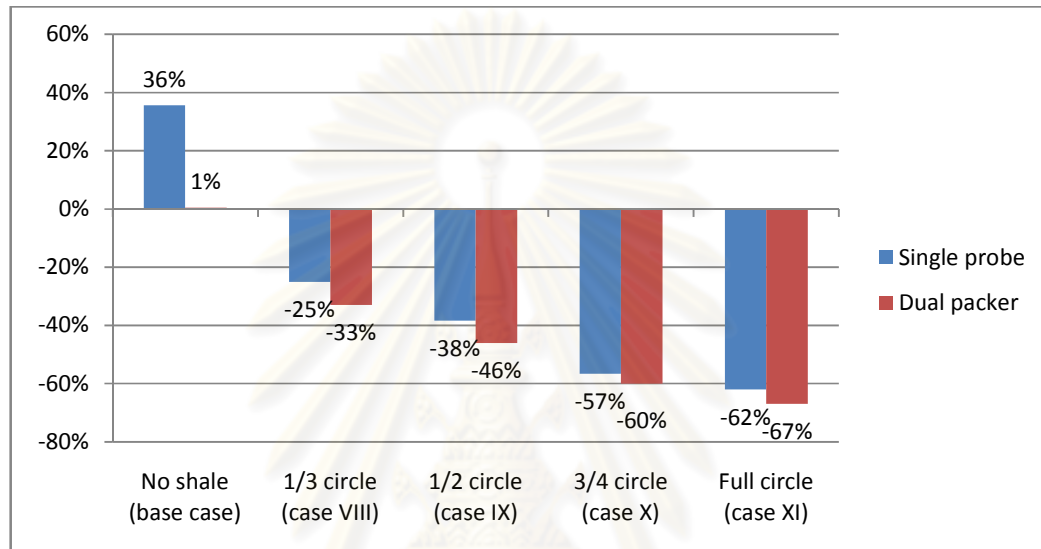
Figure 5.50: k_v estimation error (%) compared to clean sand's k_v for different shapes of shale barrier

Figure 5.50 shows the estimation errors in vertical permeabilities are increasing when the volume of shale barrier is larger. And when the shape of shale barrier is a complete circular shape, single probe and dual packer underestimate the vertical permeabilities with the highest error up to 67%.
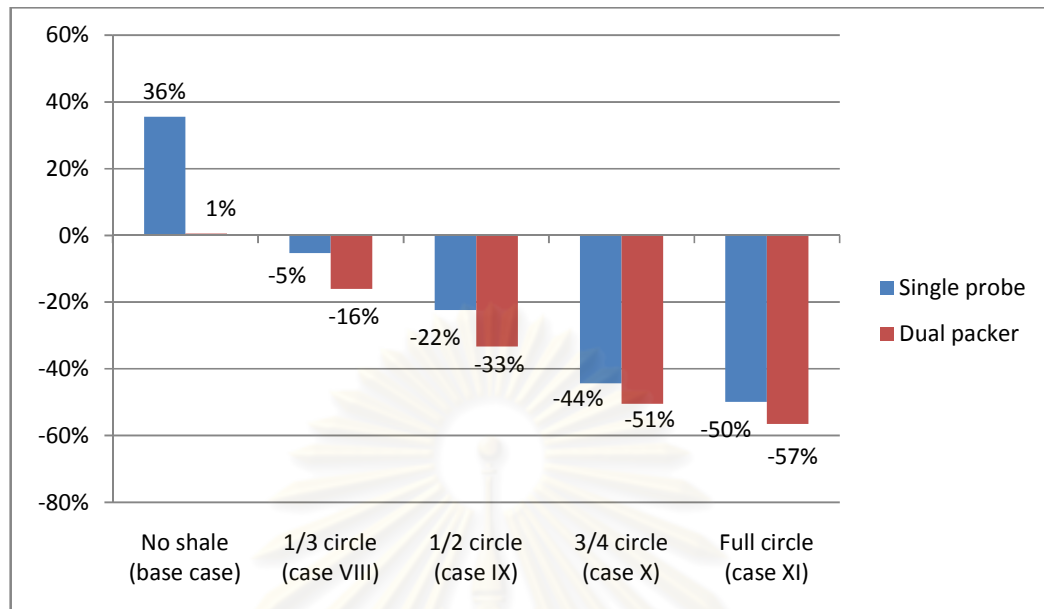
Figure 5.51: k_v estimation error (%) compared to average k_v for different shapes of shale barrier

Figure 5.51 shows the same trend as in Figure 5.50, and the estimation errors are smaller than that in Figure 5.50.

CHAPTER VI
CONCLUSIONS AND RECOMMENDATIONS

This chapter concludes the effect of various parameters of shale barrier on pressure transient obtained from single probe WFT, dual packer WFT, and well test and discusses about limitation from the study and the recommendations for future works.

6.1 Conclusions

In this study, a reservoir simulator is used as a tool to predict the pressure response when testing in a well with two different wireline formation tests (single probe, and dual packer) and conventional well test under different reservoir conditions. After that, Pressure Transient Analysis (PTA) can be performed by using a pressure transient interpretation software. The work described in this report focuses on a single layered reservoir with different configurations of laminated shale layer varied by distance from the wellbore, amount and shape.

First, a single layered reservoir with different distances between shale barrier and the well bore is simulated. The effects of distance on derivative plots and estimated permeabilities are considered and compared among 3 test types.

Secondly, a single layered reservoir with different amounts of shale barrier is simulated. The effects of number of shale barrier on derivative plots and estimated permeabilities are considered and compared among 3 test types.

Finally, a single layered reservoir with different shapes of shale barrier is simulated. The effects of shape of shale barrier on derivative plots and estimated permeabilities are considered and compared among 3 test types.

From the simulation and interpretation results shown and discussed in chapter 5, the conclusions are described as follows:

Single probe and dual packer wireline formation test can be alternative methods to evaluate the reservoir parameters such as horizontal permeability, vertical

permeability, while well test can be used to evaluate the reservoir parameters such as horizontal permeability, reservoir boundary but not vertical permeability due to the fact that full perforation is normally operated.

Especially, in thinly laminated shale condition, pressure derivative plots from single probe and dual packer can be used to indicate the existence of impermeable shale barriers which have major impact to well productivity or water/gas coning effects. When the shale barrier is detected, a hump is seen on the derivative plot, and it is more obvious when the detection is occurred during the spherical flow regime. Also, the permeability reduction can be found on the estimation of both horizontal and vertical permeabilities either much or less depending on during which flow regimes the shale barriers are detected.

In addition, to see fully developed radial flow regime including the effect of shale barrier on derivative plot in thinly laminated reservoir and to estimate the horizontal permeability correctly, both types of wireline formation test (single probe and dual packer) needs to be conducted for a long period of time. Length of time depends on location of shale.

The distance between shale layer and the well bore affects the deviation in the derivative plots. The duration of hump in the derivative plot lasts longer when the distance from the wellbore to shale barrier is longer. In the other words, the effect of shale barrier lasts longer when it occurs during the radial flow regime than when it occurs during the spherical flow regime. Oppositely, the magnitude of the effect is smaller when the shale is detected far away from the well bore or during the radial flow regime. When the shale barrier is detected during the spherical flow, the effect of shale barrier can be seen more clearly in the derivative plots.

The different amount of shale barrier does not have significant effect on permeability estimation, when all shale barriers are of the same shape, size, and distance from the well bore. However, different amounts of shale results differently on the pressure derivative plots. When there are more than two separated shale barriers, the derivative plot exhibits two humps, and the first hump is resembled to well bore storage effect.

The shape/size of shale barrier does have effect on derivative plot and permeability estimation. When the shape of the shale barrier is circular and its area is symmetrically surrounding the well bore, the reduction in permeability estimation is

higher than the case when the shape of shale is incomplete circular. And, the magnitude of the hump on derivative plot is larger when the shape of shale is circular, compared to the case when the shape of shale is incomplete circular, or the larger shale barriers show larger magnitude of deviation.

However, from single probe wireline formation tester, when shale barrier is detected during spherical flow, it is possible to estimate spherical permeability before and after the effect of shale barrier is felt on the derivative plot in most cases. When the hump on derivative plot is detected during the radial flow regime, single probe wireline formation test tends to overestimate vertical permeability while dual packer wireline formation test does not.

Well test derivative plots do not show much detail of shale barrier effect and, in most of the cases, it is difficult to identify whether the effect of shale barriers exists or not. Also, the shale barrier does not have much effect on horizontal permeability estimation from well test due to its small scale compared to well test's scale of measurement.

So, dual packer wireline formation tester can be the best alternative among the three available methods in this study to evaluate the reservoir parameters in thinly laminated reservoir condition.

6.2 Recommendations

The following points are recommendations for future study:

1. In this study, a single well model with radial grid is used. The shape of shale barrier is limited to the shape of radial grid. A Cartesian grid with local grid refinement can be used to simulate more various shapes of shale.

2. In this study, the shale position is always in the middle of reservoir layer in the vertical direction. Various vertical positions can be tested to observe other possible different effects on the derivative plot and permeability estimation.

3. In this study, only oil is used in the simulation, future study should focus on variety of fluids such as gas or gas condensate.

REFERENCES

[1] Bixel, H.C., Larkin, B.K., and Van Poollen, H.K.. Effect of Linear Discontinuities on Pressure Build-Up and Drawdown Behavior. Journal of Petroleum Technology August 1963 : 885-895.

[2] Bixel, H.C., and Van Poollen, H.K.. Pressure Drawdown and Buildup in the Presence of Radial Discontinuities. Society of Petroleum Engineers Journal September 1967 : 301-309.

[3] Tippie, D.B., and Van Poollen, H.K.. Effect of Reservoir Discontinuities upon Buildup Behavior Following Short Flow Time. paper SPE 6756 presented at 52nd Annual Fall Technical Conference and Exhibition of the Society of Petroleum Engineers of AIME, held in Denver, Colorado, USA. : October 9-12, 1997.

[4] Richardson, J.G., Harris, D.G., Rossen, R.H., and Van Hee, G.. The Effect of Small, Discontinous Shales on Oil Recovery. paper SPE 6700 presented at the SPE-AIME 52nd Annual Fall Technical Conference and Exhibition held in Denver, USA. : October 9-12, 1977.

[5] Grey, K.E.. Aproximating Well-to-Fault Distance from Pressure Build-Up Tests. paper SPE 6700 presented at the SPE-AIME 52nd Annual Fall Technical Conference and Exhibition held in Denver, USA. : October 9-12, 1977.

[6] Azari, M., and Ershaghi, I.. Estimation of Distance to a Slanted Flow Barrier From Pressure Transient Test Data. paper SPE 11830 presented at the Rocky Moutain Regional Meeting held in Salt Lake City, UT. : May 23-25, 1983.

[7] Martinez-Romero, N., and Cinco-Ley, H.. Detection of Linear Impermeable Barriers by Transient Pressure Analysis. paper SPE 11833 presented at the Rocky Moutain Regional Meeting held in Salt Lake City, UT. : May 23-25,

1983.

[8] Sageev, A., and Horne, R.N.. Pressure Transient Analysis in a Reservoir With a Compressible or Impermeable Circular Subregion: Gas Cap or EOR-Induced. paper SPE 12076 presented at the 58th Annual Technical Conferenceand Exhibition held in San Francisco, CA, USA. : October 5-8, 1983.

[9] Britto, P.R., and Grader, A.S.. The Effects of Size, Shape, and Orientation of an impermeable Region on Transient Pressure Testing. paper SPE 16376 presented at the 1987 SPE Californnia Regional Meeting held in Ventura, USA. : April 8-10, 1987.

[10] Kamal, M.M., and Pan, Y.. Use of Transient Data To Calculate Absolute Permeability and Average Fluid Saturations. paper SPE 113903 presented at the SPE Western Regional and Pacific Section AAPG Joint Meeting, Bakersfield, California, USA. : march 29 - April 2, 2008.

[11] Al-Harbi, B.M., BinAkresh, S.A., Al-Ajaji, A.A., and Pinilla Forero, E.J.. Pressure Transient Analysis: Characterizing the Reservoir and Much More. paper SPE 136932 presented at the 2010 SPE/DGS Annual Technical Symposium and Exhibition held in Al-Khobar, Saudi Arabia. : Apirl 4-7, 2010.

[12] Stewart, G., and Wittmann, M.. Interpretation of the Pressure Response of the Repeat Formation Tester. paper SPE 8362 presented at the 54th Annual Fall Technical Conference and Exhibition of the Society of Petroleum Engineers of AIME, held in Las vegas, Nevada, USA. : September 23-26, 1979.

[13] Yildiz, T., and Langlinais, J.. A Reservoir Model for Wireline Formation Testing. paper SPE 18952 presented at the 1989 SPE Rocky Mountain Regional/Low Permeability Reservoirs Symposium and Exhibition held in Denver, USA. : March 6-8, 1989.

[14] Da Prat, G., Colo, C., Martinez, R., Cardinali, G., and Conforto, G.. A New Approach To Evaluate Layer Productivity Before Well Completion. paper SPE 54672 presented at the 1996 SPE Annual Technical Conference and Exhibition, Denver, Colorado, USA. : October 6-9, 1999.

[15] Siswantoro, M.P., Indra, T.B., and Prasetyo, I.A.. The Application of Modular Formation Dynamics Tester -MDT with a Dual Packer Module in Difficult Conditions in Indonesia. paper SPE 54273 presented at the 1999 SPE Asia Pacific Oil and Gas Conference and Exhibition held in Jakarta, Indonesia. : April 20-22, 1999.

[16] Whittle, T.M., Lee, J., and Gringarten, A.C.. Will Wireline Formation Tests Replace Well Tests ?. paper SPE 84086 presented at the SPE Annual Technical Conference and Exhibition held in Denver, Colorado, USA. : October 5-8, 2003.

[17] Daungkaew, S., Prosser, D.J., Manescu, A., and Morales, M.. An Illustration of the Information that can be Obtained from Pressure Transient Analysis of Wireline Formation Test Data. paper SPE 88560 presented at the SPE Asia Pacific Oil and Gas Conference and Exhibition held in Perth, Australia. : October 18-20, 2004.

[18] Gok, I.M., Onur, M., and Kuchuk, F.J.. Estimating Formation Properties in Heterogeneous Reservoirs Using 3D Interval Pressure Transient Test and Geostatistical Data. paper SPE 93672 presented at the 14th SPE Middle East Oil & Gas Show and Conference held in Bahrain International Exhibition Center, Bahrain. : March 12-15, 2005.

[19] Daungkaew, S., Harfoushian, J.H., Cheong, B., Akinsanmi, O., Toulekima, S., and Yeo, J.. Mini-DST Applications for Shell Deepwater Malaysia. paper SPE 109279 presented at the 2007 SPE Asia Pacific Oil & Gas Conference and

Exhibition held in Jakarta, Indonesia. : 30 October - 1 November, 2007.

[20] Jackson, R.R., De Santo, I., Weinheber, P., and Guadagnini, E.. Specialized Techniques for Formation Testing and Fluid Sampling in Unconsolidated Formation in Deepwater Reservoirs. paper SPE 120443 presented at the 2009 SPE Middle East Oil & Gas Show and Conference held in the Bahrain International Exhibition Center, Kingdom of Bahrain. : March 15-18, 2009.

[21] Bertolini, C., Tripaldi, G., Manassero, E., Beretta, E., Viberti, D., and Verga, F.. A Cost Effective and User Friendly Approach for mini-DSTs Design. paper SPE 122886 presented at the 2009 SPE EUROPEC/EAGE Annual Conference and Exhibition held in Amsterdam, The Netherlands. : June 8-11, 2009.

[22] Ayan, C., Hafez, H., Hurst, S., Kuchuk, F., O'Callaghan, A., Peffer, J., Pop, J., and Zeybek, M.. Characterizing Permeability with Formation Testers. journal Schlumberger Oilfield Review : Autumn 2001.

[23] Ayan, C., Colley, N., Cowa, G., Ezekwe, E., Wannell, M., Goode, P., Halford, F., Joseph, J., Mongini, A., Obondoko, G., and Pop, J.. Measuring Permeability Anisotropy The Latest Approach. journal Schlumberger Oilfield Review : October 1994.

[24] McClain, D.. MDT Basic Tool String Training Manual: Schlumberger, July 31, 1996.

[25] Wireline Formation Testing and Sampling. Schlumberger Wireline & Testing. Schlumberger : 1996.

[26] Well Test Interpretation. Schlumberger : 2002.

[27] Warren, J.E., Skiba, F.F., and Price, H.S.. An Evaluation of the Significance of

Permeability Measurements. paper SPE 001641   presented at SPE Formation Evaluation Symposium, Houston, USA. : November 21-22, 1906.

[28] Darling, T.. Well Logging and Formation Evaluation. Gulf Professional Publishing : Elsevier Inc., 2005.

[29] Chassignol, V.. Dynamic Flow Analysis. v.4.10.01.KAPPA Company, 1988-2009.

[30] Palasarn, D.. Evaluation of Reservoir Properties from Wireline Formation Test in Multilayer Reservoir. Master's Thesis Department of Mining and Petroleum Engineering Faculty of Engineering Chulalongkorn University, 2006.

[31] Goode, P.A., and Thambynayagam, R.K.M.. Influence of an Invaded Zone on a Multiprobe Formation Tester. paper SPE 23030   presented at the 1991 SPE Asia-Pacific Conference held in Perth, Australia. : November 4-7, 1991.

[32] Morris, C.W., and Sonnier, B.. Evaluation of Reservoir Fluids Using Formation Tester Tool Samples. paper SPE 22129   presented at the International Arctic Technology Conference held in Anchorage, Alaska. : May 29-31, 1991.

[33] Smits, A.R., Fincher, D.V., Nishida, K., Mullins, O.C., Schroeder, R.J., and Yamate, T.. In-Situ Optical Fluid Analysis as an Aid to Wireline Formation Sampling. paper SPE 26496   presented at the 1993 SPE Anual Technical Conference and Exhibition held in Houston, USA. : October 3-6, 1993.

[34] MDT Overview general. Schlumberger Wireline. Schlumberger : 2009.

APPENDICES

APPENDIX A: Sample ECLIPSE data file:

Single probe – Case 2

File name: SP_case6++.DATA

```
-----------------------------------------------------------------
RUNSPEC
-----------------------------------------------------------------

TITLE
 Single probe

START
 1 'JAN' 1983 /

-- Unit
FIELD

-- Grid Type
RADIAL

-- Phases Present
OIL
WATER
--
MONITOR
RSSPEC

NOINSPEC

MSGFILE
 1 /
```

```
DIMENS
-- Grid dimension
-- NR          NTheta          NZ
   100          20              31 /


ENDSCALE
/


EQLDIMS
1 100 100 1 20 /


REGDIMS
 1 1 0 0 /


TABDIMS
 1 1 20 20 1 20 20 1 /


VFPPDIMS
 2 2 2 2 2 0 /


WELLDIMS
 2 2 2 2 /
```

GRID

-- IN THIS SECTION, THE GEOMETRY OF THE SIMULATION

-- GRID AND THE ROCK PERMEABILITIES AND POROSITIES

-- ARE DEFINED.


```
GRIDFILE
 2 /
```

INIT

ECHO

MAPAXES

     0   0   0   0   0   0 /

GRIDUNIT
 'FEET' /

COORDSYS
-- Coordinate system for each reservoir
--   Lower Block   Upper Block   Completion of circle
    1   31   'COMP' /
 NOECHO

DRV
-- Radial-direction grid block sizes (vector)
0.032274861   0.058770214   0.079305574   0.107016355   0.144409778
0.194869128   0.262959876   0.354842744   0.478831124   0.646143255
0.871917227   1.17658065   1.587698904   2.142469205   2.891086138
3.901283173   5.264461061   7.103957604   9.586207031   81*12.93579866
/

DTHETAV
-- Angular sizes of grid blocks (vector)
7.393877297 9.921386359 11.49270936 13.31289435 15.42135544
17.86374903 20.69296248 23.97025929 27.76660572 32.16420748
32.16420748 27.76660572 23.97025929 20.69296248 17.86374903
15.42135544 13.31289435 11.49270936 9.921386359 7.393877297
/

DZ

-- Z-direction grid block sizes

2000*2.39058764   2000*1.827430369   2000*1.396937598

2000*1.067857186   2000*0.816299147   2000*0.624001323

2000*0.477003624   2000*0.364634576   2000*0.278736611

2000*0.213073865   2000*0.162879472   2000*0.124509509

2000*0.095178463   2000*0.072757012   2000*0.055617444

2000*0.0325   2000*0.055617444   2000*0.072757012

2000*0.095178463   2000*0.124509509   2000*0.162879472

2000*0.213073865   2000*0.278736611   2000*0.364634576

2000*0.477003624   2000*0.624001323   2000*0.816299147

2000*1.067857186   2000*1.396937598   2000*1.827430369

2000*2.39058764

/

BOX

        1   100   1   20   1   1 /

TOPS

-- Depths of the top face of each grid block

2000*8100

/

ENDBOX

INRAD

-- Inner radius for radial geometry or radial local grid refinements

     0.25 /

-- PERMEABILITIES and POROSITY

EQUALS

PERMR 10 /

/

```
EQUALS
PORO 0.18 /
/


EQUALS
PERMK 1 /
/


EQUALS
PERMTHT 10 /
/


BOX
13  17  1  5  5  27  /


PORO
575*0.001
/


PERMI
575*0.001
/


COPY
PERMI  PERMJ  /
PERMI  PERMK  /
/


MULTIPLY
PERMK  0.1  /
/


ENDBOX
```

```
BOX

13  17  16  20  5  27  /


PORO

575*0.001

/


PERMI

575*0.001

/


COPY

PERMI   PERMJ  /

PERMI   PERMK  /

/


MULTIPLY

PERMK   0.1  /

/


ENDBOX

--------------------------------------------------------------

PROPS

--------------------------------------------------------------

-- THE PROPS SECTION DEFINES THE REL. PERMEABILITIES,

-- CAPILLARY PRESSURES, AND THE PVT PROPERTIES OF THE

-- RESERVOIR FLUIDS


ECHO
```

DENSITY

-- At Surface Condition

-- Oil Density	Water Density	Gas Density
51.457	63.029	0.0437

/

PVDO

-- PVT properties of dead oil (no dissolved gas)

-- Oil Phase Pressure	Bo	Oil Viscosity
1847.9	1.3129	0.34932
2005.6	1.3088	0.35453
2163.2	1.3053	0.36022
2320.8	1.3023	0.36636
2478.4	1.2997	0.37293
2636	1.2974	0.37992
2793.6	1.2954	0.3873
2951.2	1.2935	0.39507
3108.8	1.2919	0.40319
3266.4	1.2904	0.41167
3424	1.2891	0.42049
3581.6	1.2879	0.42964
3739.2	1.2868	0.43911
3896.8	1.2857	0.44888
4054.4	1.2848	0.45896
4212	1.2839	0.46932
4369.6	1.2831	0.47996
4527.2	1.2824	0.49088
4684.8	1.2816	0.50206
5000	1.2804	0.52515

/

RSCONSTT

-- Constant Rs value for each dead oil PVT Table

```
--      Rs              Bubble point pressure
        0               1847.9
/
```

PVTW
```
-- PVT Water Function
--   Pref Bw      cw         Water viscosity      Water viscosibility
     3450      1.0235    2.9111e-006   0.30286              1*
/
```

ROCK
```
-- Rock compressibility
--      Pref              rock compressibility
        3450              1.048e-006
/
```

SWOF
-- Water / oil saturation functions versus water saturation

-- Sw	Krw	Kro	Water-Oil Pc
0.16283	0	1	15947
0.2069	3.5397e-013	0.89751	5832.4
0.25096	3.0203e-010	0.80055	564.75
0.29502	1.5654e-008	0.70914	144.11
0.33908	2.5771e-007	0.62327	54.684
0.38314	2.2632e-006	0.54292	25.788
0.4272	1.3357e-005	0.46808	13.954
0.47126	5.9918e-005	0.39872	8.3024
0.51532	0.0002199	0.33476	5.295
0.55939	0.00069228	0.27615	3.5609
0.60345	0.0019311	0.22281	2.4971
0.64751	0.0048848	0.1747	1.8113
0.69157	0.011397	0.13186	1.3512
0.73563	0.024846	0.094431	1.0319

0.77969	0.051126	0.062731	0.80391
0.82375	0.10009	0.037204	0.6372
0.86782	0.18763	0.018335	0.5127
0.91188	0.33858	0.0063942	0.418
0.95594	0.59069	0.00094699	0.3448
1	1	0	0.28739

/

BOX

 1 100   1   20   1   31 /

SWCR

-- Scaled critical water saturations

 62000*0.5 /

ENDBOX

SOLUTION

-- THE SOLUTION SECTION DEFINES THE INITIAL STATE OF

-- THE SOLUTION VARIABLES (PHASE PRESSURES,

-- SATURATIONS AND GAS-OIL RATIOS).

RPTRST

  BASIC=2   PRESSURE   /

EQUIL

-- Equilibration data specification

-- Depth   Pressure   WOC

  8110   5000   15000   /

/

```
-----------------------------------------------------------------------
SUMMARY

-----------------------------------------------------------------------

-- THIS SECTION SPECIFIES DATA TO BE WRITTEN TO THE

-- SUMMARY FILES AND WHICH MAY LATER BE USED WITH

-- THE ECLIPSE GRAPHICS PACKAGE.


ALL
BOKR
1 1 16 /
 /
BWKR
1 1 16 /
 /
BOSAT
1 1 16 /
 /
BPR
1 1 16 /
 /
BWSAT
1 1 16 /
 /
CDBF
'T1'  1 1 16 /
 /
COPP
'T1'  1 1 16 /
 /
COPR
'T1'  1 1 16 /
 /
```

```
CPR
'T1'  1 1 16  /
 /
WBHP
 /
WBHPH
 /
WGOR
'WELL1' /
WGPR
'WELL1' /
WLPR
'WELL1' /
WWPR
'WELL1' /


----------------------------------------------------------------------
SCHEDULE
----------------------------------------------------------------------
-- THE SCHEDULE SECTION DEFINES THE OPERATIONS TO BE
-- SIMULATED

WELSPECS
-- General specification data for wells
'WELL1' '1' 1 1 8120 'OIL' 1* 'STD' 'SHUT' 'YES' 1* 'SEG' 3* 'STD' /
 /

COMPDAT
-- Well completion specification data
'WELL1' 1 1 16 16 'OPEN' 1 1* 0.5 3* 'Z' 1* /
 /

WCONPROD
```

-- Control data for production wells

'WELL1' 'OPEN' 'LRAT' 3* 0.5 1* 1847.9 3* 6* 1* /

 /

-- Advances simulator to new report time(s)

TSTEP

1e-010 /

TSTEP

1.19e-010 /

..

TSTEP

0.00331 /

WELOPEN

'WELL1'   SHUT /

 /

TSTEP

1E-10   /

TSTEP
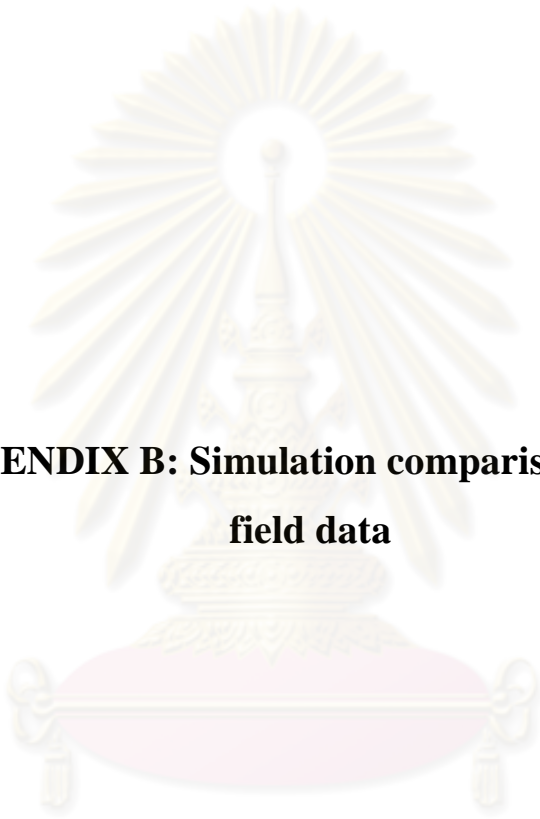
1.09658E-10   /

..

TSTEP

 0.01019411   /

END

APPENDIX B: Simulation comparison with actual field data

This section presents the real data of dual packer WFT conducted in Asia Pacific region. The pressure transient analysis of the real data is applied based on the concept and simulation results in previous chapters.

Figure B1 shows the pressure history of real data generated from dual packer WFT. Many draw downs and build ups have been conducted at initial times in order to pump out mud filtrate and later on test on formation fluid. The last buildup is taken for estimating reservoir permeability.
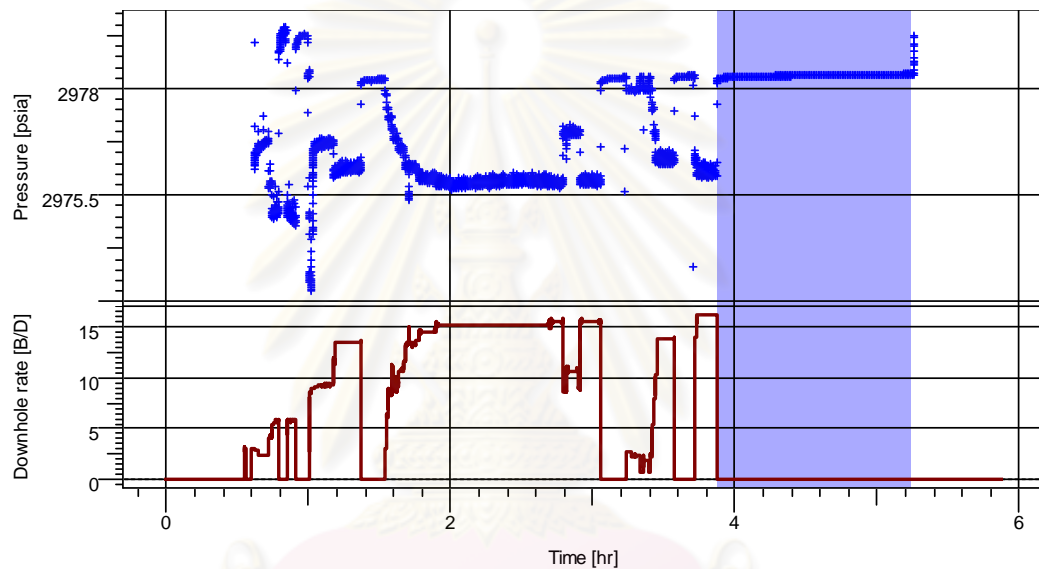
Figure B1: Pressure history of field data
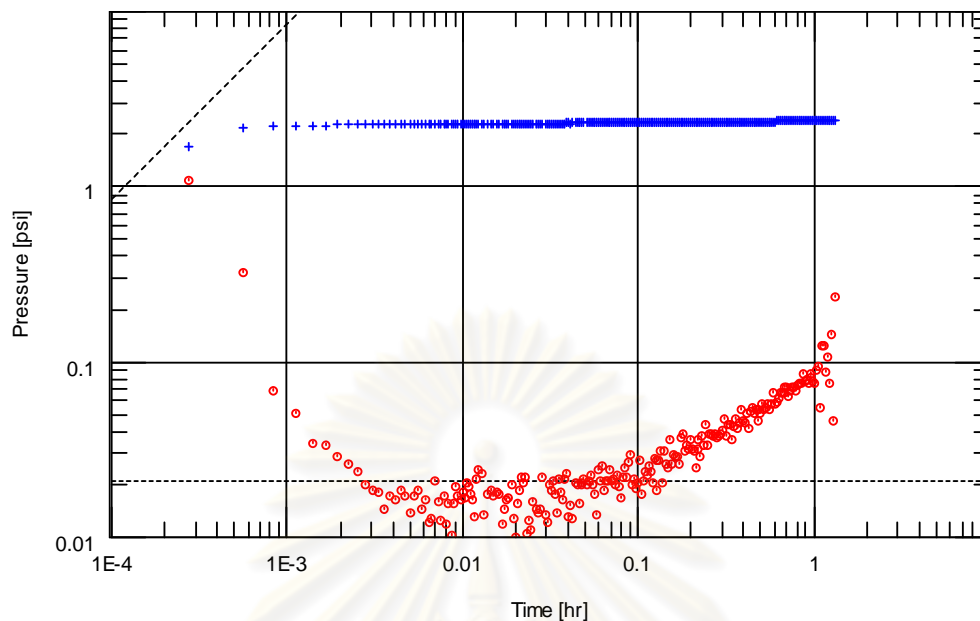
Figure B2: Derivative plot of last build up

The derivative of the last build up set of data is used for estimating permeability, as shown in Figure B2. From this set of data, 4 cases of simulated pressure response from dual packer WFT are designed as following:
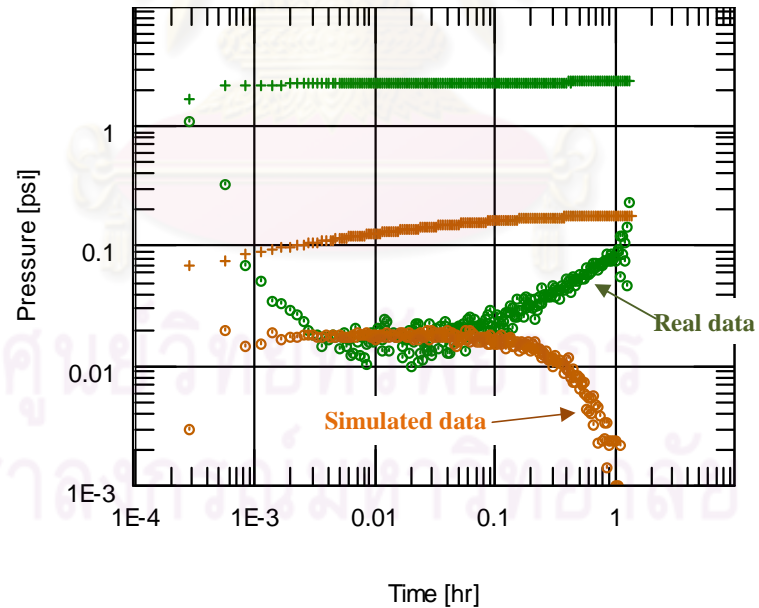
1. No shale barrier exists in the reservoir.
2. 2 parallel shale barriers located 300 ft away from well bore.
3. 2 parallel shale barriers located 600 ft away from well bore.
4. 2 parallel shale barriers located 1700 ft away from well bore.

After evaluating the best match among 4 cases, the pressure responses from single probe WFT and well test are simulated in order to compare derivative plot with the one from dual packer WFT.

162
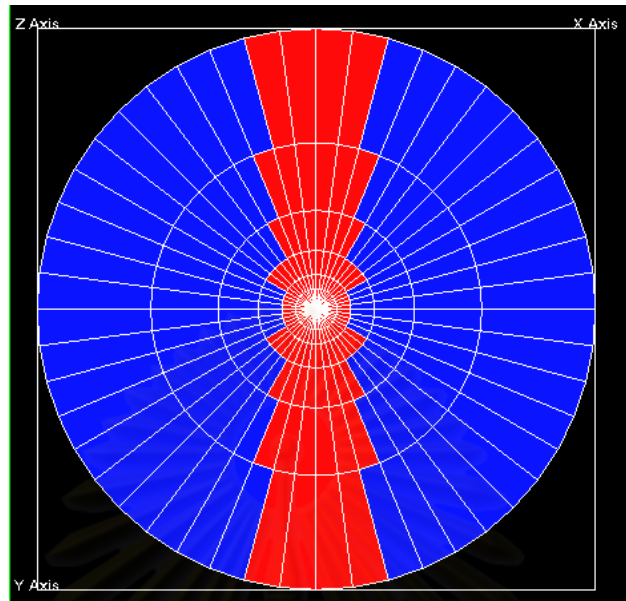
Figure B3: Example of shale configuration for 2 parallel shale barriers

Figures B4 - B7 show derivative plots as a result of 4 simulated pressure response cases compared with pressure response from real data.

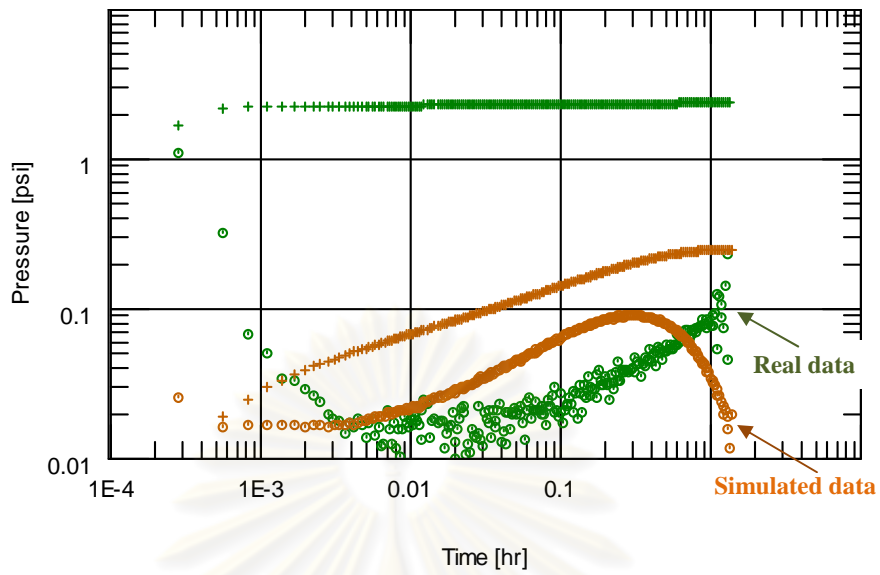Figure B4: No shale barrier exists in the reservoir

Figure B5: 2 parallel shale barriers located 300 ft away from well bore
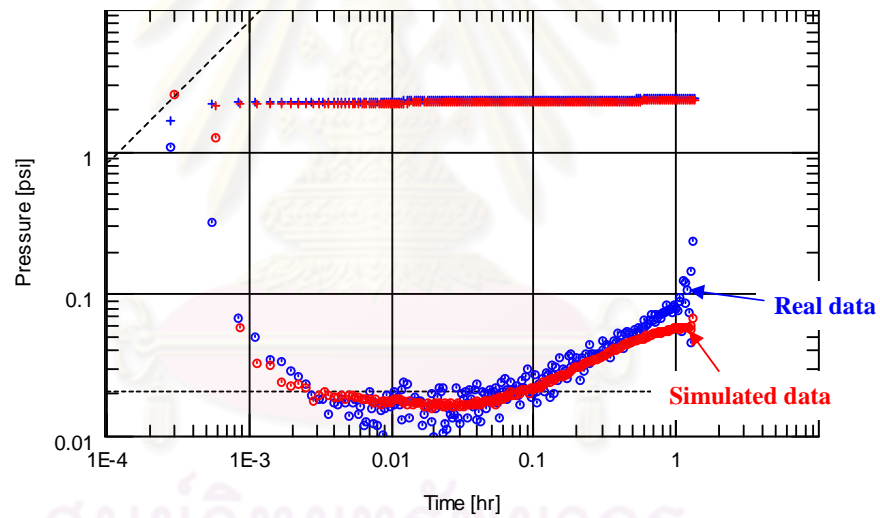

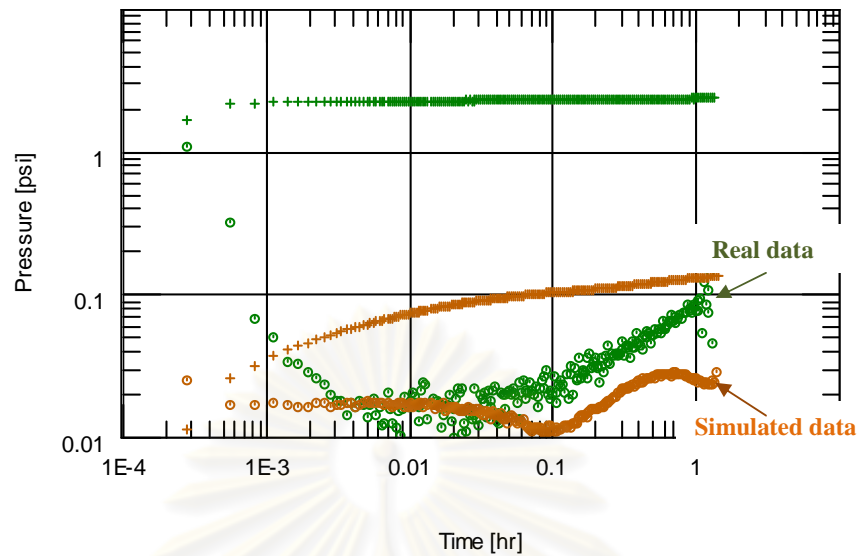Figure B6: 2 parallel shale barriers located 600 ft away from well bore

Figure B7: 2 parallel shale barriers located 1700 ft away from well bore

Among all derivative plots in Figures B4 - B7, the best match of pressure derivative is at the condition of 2 parallel shale barriers located 600 ft away from well bore. So, this shale configuration is used for generating pressure response from single probe WFT and well test in order to conduct a comparison.

Figure B8 compares the simulated pressure for dual packer WFT with actual pressure response corresponding to the draw down and buildup periods.
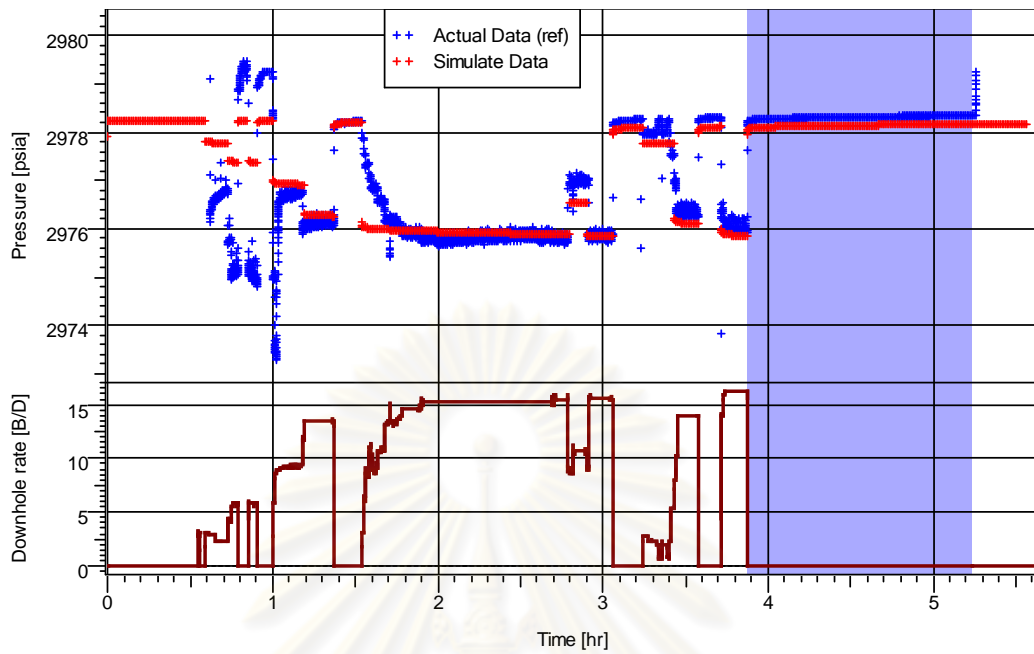
Figure B8: Simulated pressure for dual packer WFT vs. actual pressure response from real data

Figures B9 and B10 show derivative plots of simulated pressure response from single probe WFT and well test, orderly.
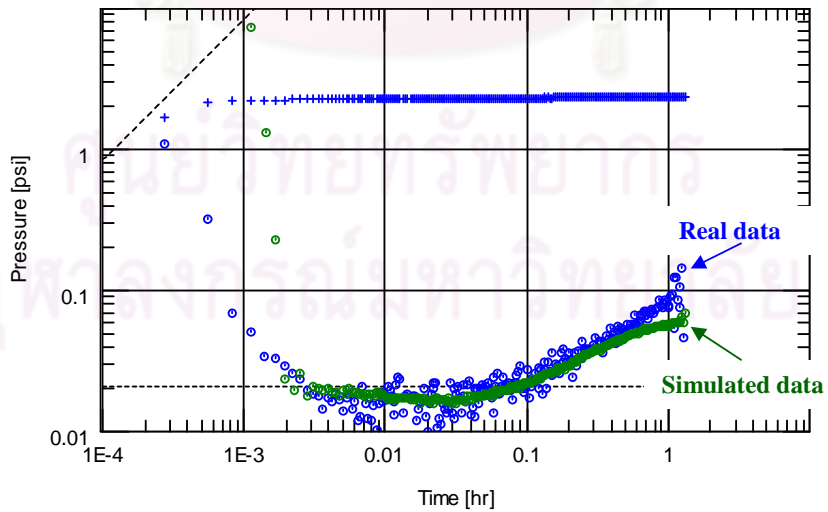

Figure B9: Derivative plots of simulated single probe WFT vs. actual data
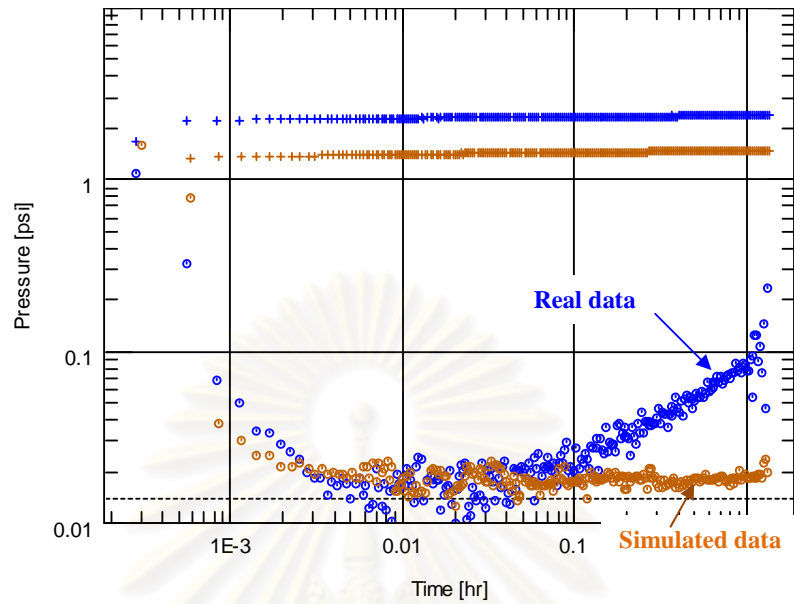
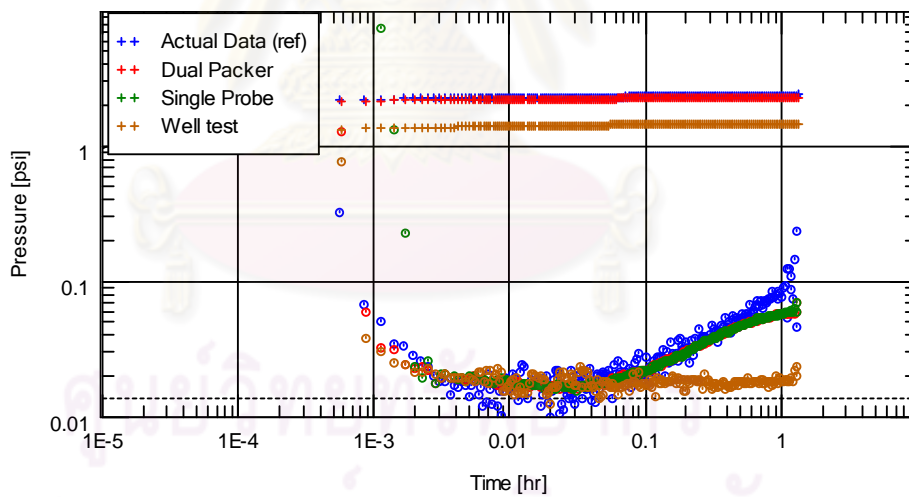Figure B10: Derivative plots of simulated well test vs. actual data

Figure B11: Comparison of all simulated pressure response with actual data

From Figure B11, the derivative of simulated pressure responses from single probe and dual packer WFT are matched to actual data. However, the pressure derivative from simulated well test response does not match.

VITAE

Wiriya Kiatpadungkul was born on July 17, 1980 in Nakhon Ratchasima, Thailand. She received her B.Eng. in Computer Engineering from the Faculty of Engineering, Chulalongkorn University in 2001. After graduating, she worked for the Stock Exchange of Thailand (SET) for 9 months. In year 2002, she joined Schlumberger Company as IT support engineer, and information management engineer, accordingly. In 2008, she started to work as production engineer and also studied in the Master of Petroleum Engineering program at the Department of Mining and Petroleum Engineering, Faculty of Engineering, Chulalongkorn University.